EFFECTS OF PREOXIDATION ON PYROLYSIS BEHAVIOR AND RESULTANT CHAR STRUCTURE OF CAKING COALS

D. J. Maloney and R. G. Jenkins

The Fuels and Combustion Laboratory
The Pennsylvania State University, University Park, PA 16802

INTRODUCTION

Coal gasification processes may be divided into two stages. They are, the initial rapid release of volatile matter and the relatively slow gasification of the residual char. These two processes are not, however, totally independent because the heat treatment conditions under which coal pyrolysis occurs determine, to a large extent, the structure and reactivity of the remaining char (1). The importance of understanding devolatilization kinetics has long been recognized (2-6). However, it is surprising to note that very little information is available in the literature regarding the structure and reactivity of the chars produced in these studies.

The work described here is concerned with the utilization of bituminous (caking) coals in dilute phase, rapid heating gasification and combustion systems. Two highly caking coals were pyrolyzed in an entrained flow tube furnace system and devolatilization kinetics determined for each coal at temperatures of 900 and 1000°C. Structural properties of the chars collected in this work were then analyzed. In addition, the effects of mild preoxidation of these coals upon their subsequent pyrolysis behavior were examined. Samples of each coal were oxidized to various levels prior to heat treatment. Devolatilization kinetics and structural properties of the chars produced were then analyzed. Results reported here follow the development of char structure with varying heat treatment conditions and examine changes in char morphology which occur on preoxidation of these coals. This work is of practical importance in future design considerations for dilute phase gasifiers and of particular interest in gasification schemes where agglomeration of caking coals can cause serious problems.

EXPERIMENTAL

Pyrolysis experiments were conducted in an entrained flow tube furnace somewhat similar to that described by Scaroni et al. (7,8) and Nsakala and coworkers (9). Briefly, a dilute-phase coal stream is entrained in a primary carrier gas, passed through a water cooled probe and then injected into the center of a preheated secondary gas stream. The secondary gas stream enters the reaction zone at a temperature slightly above the furnace wall temperature so that upon mixing the combined gas stream attains the desired reaction temperature (± 10°C). The primary modes of coal particle heating are conduction from the gas and radiation from the furnace walls. Heating rates in excess of 10,000°C/s are estimated. Coal particles travel in a pencil stream down the axis of the furnace tube. Samples are collected and rapidly quenched (> 10,000°C/s quench rate) using a water cooled probe which is inserted up the axis of the furnace. Reaction times are varied by changing the position of the sampling probe relative to the injector. The operating conditions at each temperature studied are given in Table 1. Helium is used as the primary carrier gas and is adjusted to maintain isokinetic sample injection. The secondary gas is nitrogen.

Weight loss due to pyrolysis was determined using ash as a tracer. The proximate analyses of the samples used in this work are presented in Table 2. The coals examined were PSOC-1133 a LV coal from the Lower Kittaning seam in Pennsylvania

TABLE 1. OPERATING CONDITIONS

Operating Temperature °C	900	1000
Coal Feed Rate g/min	0.5	0.5
Mean Gas Velocity cm/s	97	105
Secondary N_2/Primary He (Mole Basis)	26.4	24.2

TABLE 2. PROXIMATE ANALYSES OF SAMPLES (200x270 mesh fractions)

Sample	Moisture, %	Ash, %	Volatile Matter, %	Fixed Carbon, %
PSOC-1099 (Raw Coal)	1.6	9.0	33.7	56.7
PSOC-1099 (1% O_2 added)	0.9	12.6	32.5	64.0
PSOC-1133 (Raw Coal)	0.4	16.4	18.5	64.7
PSOC-1133 (o.5% O_2 added)	1.1	19.3	17.6	62.0
PSOC-1133 (1% O_2 added)	1.1	19.5	18.2	62.2

and PSOC-1099 a HVA coal from the Pittsburgh seam in Pennsylvania. All work was conducted on 200x270 mesh size fractions with mean particle diameter of 63 μm.

Preoxidized samples were prepared in a fluidized bed furnace. Samples of sized coal (200x270 mesh) were fluidized in nitrogen and brought to reaction temperature (175°C). The fluidizing gas was then switched to air and the samples were oxidized for various predetermined times. Oxidation times were determined based upon thermogravimetric studies of the air oxidation of each coal. It is assumed that oxidation rates in the thermobalance and fluidized bed systems are equivalent. This assumption is valid if one insures that the O_2 partial pressure in each system is the same and that there are no bed diffusion effects in the thermobalance system. Operating conditions were selected to meet these requirements. Oxidation levels reported here are given as % weight gain on oxidation (dry coal basis).

RESULTS AND DISCUSSION

Typical weight loss versus time curves for devolatilization of PSOC-1133 (LV coal) are presented in Figure 1. This plot shows weight loss is essentially complete within the first 100 msec of residence time. The same behavior was observed for the HVA coal examined in this study. These results are in good agreement with that of Badzioch and Hawksley (10). In similar experimental systems it is often assumed that pyrolysis occurs isothermally (7-10), however, this assumption cannot be made for the coals analyzed here.

Figure 1 also shows the maximum weight loss for devolatilization at 900°C is greater than at 1000°C. Similar observations have been reported by Menster et al. (11,12). These authors suggest a possible explanation for this behavior which involves a competition between bond breaking reactions (which result in volatile formation) and secondary recombination or polymerization (char forming) reactions,

Figures 2 and 3 demonstrate the effects of preoxidation on devolatilization behavior. Oxidation appears to have little effect on the rate of pyrolysis, however, devolatilization occurs so rapidly that the time resolution of this system may be inadequate to distinguish such effects. Preoxidation reduces the yield of volatile material in all cases examined. This corresponds with a sharp decrease

in the amount of condensible products (tars) collected.* Increases in the level of oxidation prior to pyrolysis result in a progressive reduction in the yield of volatile material. Devolatilization curves for preoxidized coals all have the same characteristic shape. Weight loss passes through a shallow minimum with residence time. Further study of this behavior is in progress.

Figure 4 shows an electron micrograph of PSOC-1133 char collected after 330 msec residence time at 1000°C. Coal structure has undergone extensive physical changes during the pyrolysis process. These chars are thin walled transparent structures commonly called cenospheres (13), the average diameter of which is three times that of the starting coal. This represents a > 20 fold increase in volume. Similar results are obtained at 900°C and for PSOC-1099 at each temperature studied. Under the pyrolysis conditions employed in this work cenospheres are fully developed during the early stages of pyrolysis (< 40 msec) after which no detectable changes in macroscopic properties are observed.

Figure 5 is a micrograph of a preoxidized coal char (PSOC-1133, 1% oxygen added) collected after 330 msec residence time at 1000°C. These chars do not form the cenosphere structures exhibited by the unoxidized coals. Char particles are rounded in shape indicating that the coal passes through a plastic transition during carbonization but no significant swelling is observed.

SUMMARY

The sharp contrast in macroscopic properties of the chars collected in this study give rise to several important questions regarding char gasification. Varying heat treatment conditions and coal feed stocks give rise to chars of widely varying structure. In order to understand the behavior of these materials in subsequent gasification steps a more detailed analysis of char structure is required. At present microstructural properties (surface areas, porosities) of the chars generated in this study are being examined in an effort to better understand the relationship between char structure and heat treatment conditions. Results of this work will be available shortly.

ACKNOWLEDGEMENTS

Financial support for this work was provided by the Cooperative Program in Coal Research at The Pennsylvania State University. Coal samples were obtained from the Penn State/DOE coal sample bank.

*Tar yields were not measured quantitatively in this work, however, the differences in the amounts of condensible materials collected in the filtering systems were substantial enough to warrant the above comment.

REFERENCES

1. Mahajan, O. P. and Walker, P. L., Jr., "Analytical Methods for Coal and Coal Products," Vol. 2, (C. Karr, Editor), Academic Press, New York, 1978, pp. 465-494.

2. Badzioch, S., B.C.U.R.A. Monthly Bull., 25, 285, 1961.

3. Jones, W. Idris, J. Inst. Ful, 37, 3, 1964.

4. Yellow, P. C., B.C.U.R.A. Monthly Bull., 29, 285, 1965.

5. Badzioch, S., Field, M. A., Gill, D. W., Morgan, B. B., and Hawksley, P. G. W., B.C.U.R.A. Monthly Bull., 31, 193, 1967.

6. Anthony, D. B. and Howard, J. B., A.I.Ch.E. Journal, 22, 625, 1976.

7. Scaroni, A. W., Walker, P. L., Jr., and Essenhigh, R. H., ACS Div. Fuel Chem., Preprints, 24, No. 2, 123, Sept. 1979.

8. Scaroni, A. W., Walker, P. L., Jr., and Essenhigh, R. H., Fuel, 60, 71, 1981.

9. Nsakala, N., Essenhigh, R. H., and Walker, P. L., Jr., Comb. Sci. and Tech., 16, 153, 1977.

10. Badzioch, S. and Hawksley, P. G. W., Ind. Eng. Chem. Process Des. Develop., 9, 521, 1970.

11. Menster, M., O'Donnell, H. J., Ergun, S., and Friedel, R. A., "Coal Gasification," Advances in Chemistry Series 131, Am. Chem. Soc., Washington, D. C., 1974.

12. Menster, M., O'Donnell, H. J., and Ergun, S., ACS Div. Fuel Chem., Preprints, 14, No. 5, 94, 1970.

13. Newall, H. E. and Sinnatt, F. S., Fuel, 3, 424, 1924.

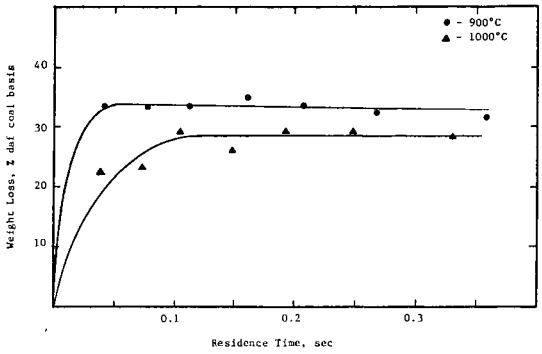

Figure 1. WEIGHT LOSS AS A FUNCTION OF RESIDENCE TIME FOR PSOC-1133

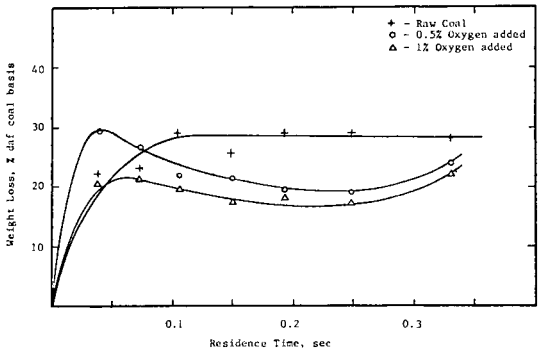

Figure 2. WEIGHT LOSS VERSUS RESIDENCE TIME AS A FUNCTION OF PREOXIDATION LEVEL FOR PSOC-1133

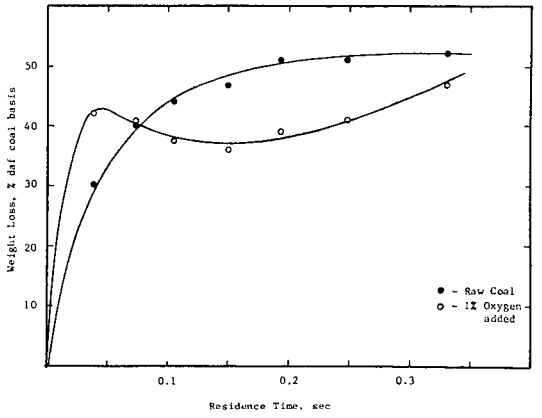

Figure 3. WEIGHT LOSS VERSUS RESIDENCE TIME AS A FUNCTION OF PREOXIDATION LEVEL FOR PSOC-1099

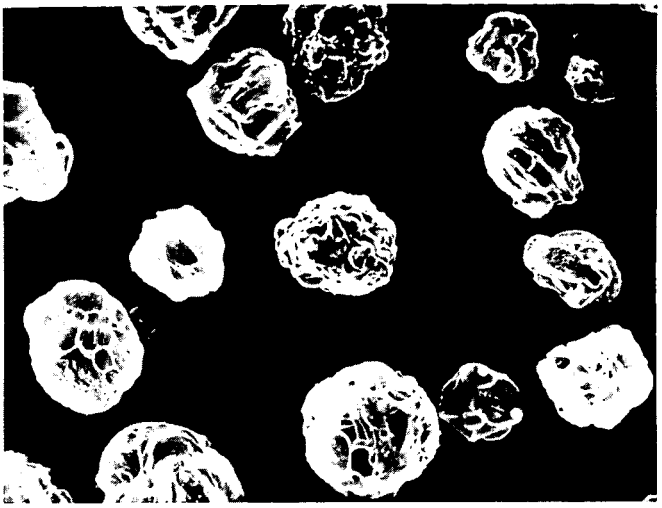

Figure 4. SCANNING ELECTRON MICROGRAPH OF PSOC-1133 CHAR 330 msec Residence Time at 1000°C

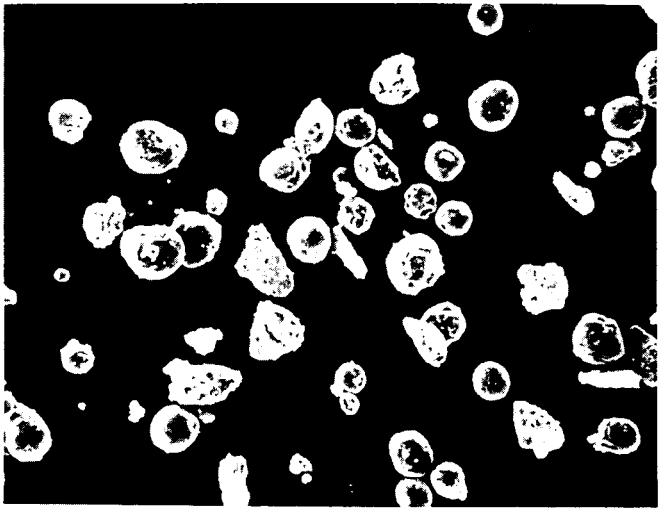

Figure 5. SCANNING ELECTRON MICROGRAPH OF A PREOXIDIZED COAL CHAR (PSOC-1133 1% Oxygen Added) 330 msec Residence Time at 1000°C

INFLUENCE OF PARTICLE STRUCTURE CHANGES ON THE RATE OF COAL CHAR REACTION WITH CO_2

K. A. Debelak, M. A. Clark and J. T. Malito

Department of Chemical Engineering
Vanderbilt University
Nashville, TN 37235

Introduction

A common feature of gas-solid reactions is that the overall process involves several steps: (1) mass transfer of reactants and products from bulk gas phase to the internal surface of the reacting solid particle; (2) diffusion of gaseous reactants or products through the pores of a solid reactant; (3) adsorption of gaseous reactants on solid reactant sites and desorption of reaction products from solid surfaces; (4) the actual chemical reaction between the adsorbed gas and solid.

In studying gas-solid reactants, we are concerned with these four phenomena and other phenomena which affect the overall rate of reaction and performance of industrial equipment in which these gas-solid reactions are carried out. These other phenomena include: heat transfer, flow of gases and solids through reactors, and changes in the solid structure, all of which affect the rate of diffusion and surface area available for reaction. The reaction to be studied is the reaction between carbon and carbon dioxide to form carbon monoxide. This reaction is of importance for it is one of the prime reactions occurring in coal gasifiers, and also it is a reaction on which there is data from other investigations (1-17). Considerable discrepancy has been found for activation energies which ranges from 48-86 kcal/mol and for reaction rate constants. This can be explained by the somewhat oversimplified view of the mechanism which was thought to be rate-controlling, and the simplification made in the corresponding reaction rate models.

Gulbransen and Andrew (2) showed that the internal surface area of graphite increased during reaction with carbon dioxide and oxygen. Walker et al. (3) studied graphite rods for the possible correlations existing between reaction rates and changes in surface area during reaction. They concluded that the reaction develops new surface, to some extent, by enlarging the micropores of the solid but principally by opening up pore volume not previously available to reactant gas either because the capillaries were too small or because existing pores were unconnected. Surface area increased up to a point where rate of production of new surface equalled the destruction of old surface, after which surface area then continued to decrease. For the graphite-carbon dioxide reaction, Petersen (4) found that observed rates were not simple functions of the total available surface area as determined by low-temperature adsorptions prior to reaction, as might be expected if the reaction was chemical-reaction controlled.

Turkgodan et al. (18) studied the pore characteristics of several carbons, graphite, coke and charcoal. They concluded that about 1/2 of the volume is located in micropores and therefore not available for reaction. Most of the internal surface area was located in pores in the micropore range. The pore volume, pore surface area, and effective diffusivity increased with conversion during internal oxidation.

Dutta and Wen (16, 17) studied the reactivities of several raw coals and chars. They noted a change in the actual pore structures of a few samples at different conversions from scanning electron micrographs. A rate equation was proposed that incorporated the change of the relative available surface area during reaction. No measurements of this change were made. A rate expression, which includes the influence of a chemical and diffusion reaction controlling mechanisms, is expressed

$$\frac{dX_c}{dt} = \eta S k C_{CO_2} (1-X_c) \qquad 1)$$

where:

X_c is the conversion of the solid
S is the surface area available for reaction
k is the reaction rate constant
η is the effectiveness factor
C_{CO_2} is the concentration of CO_2 in gas phase
t is time

The effectiveness factor η is equal to the ratio of the reaction rate under diffusion-controlled conditions to that which would occur if the concentration of reactants were equal to the surface concentration. For a first order diffusion-controlled reaction the influence of pore-diffusion is given by equation 2)

$$\eta = \frac{1}{\phi}\left[\frac{1}{\tanh 3\phi} - \frac{1}{3\phi}\right] \qquad 2)$$

$$\phi = \frac{1}{3} r_c \left(S k/D_e\right)^{1/2} \qquad 3)$$

where:

S is the specific surface
k is the reaction rate constant
r_c is the radius of the particle
D_e is the effective diffusivity

The effectiveness factor η is a function of the effective modulus, ϕ, which is dependent upon the effective diffusivity, D_e. The effective diffusivity and the surface area available for reaction change during the reaction.

This may be expressed as

$$S = S_o f(X_c) \quad 4)$$

$$D_e = D_{e_o} h(X_c) \quad 5)$$

where S_o and D_{e_o} are the available surface area and effective diffusivity at zero conversion, and $f(X_c)$ and $h(X_c)$ are functions of conversion, X_c. The determination of these changing parameters and their influence on the overall reaction rate is the objective of this research.

Effective Diffusivity

I. Theoretical Development of Model

Experimental determination of the effective diffusivity in coal is performed in a packed bed of coal particles with a carrier gas flowing through the bed. A pulse in the concentration of the adsorbate gas is introduced at the inlet of the packed bed. The mass transfer characteristics of the bed change the shape of the pulse as it passes through the bed. A theoretical model describing the mass transfer in the bed is used to relate the unsteady state concentration response in the bed effluent to the original pulse input. By applying the model to the experimental data, the parameters of the model are determined. The model describing the mass transfer in the packed bed consists of unsteady state material balances in the packed bed and the coal particles. Equations (6-14) describe the mass transfer in the packed bed of particles and the boundary conditions.

Material balance on coal particle

$$D_c \frac{\partial^2 q}{\partial r^2} + \frac{2}{r} \frac{\partial q}{\partial r} = \frac{\partial q}{\partial t} \quad 6)$$

Relation between adsorbed concentration and concentration of surface

$$q(r_c, t) = K_c C(r_c, t) \quad 7)$$

Boundary conditions

$$\frac{\partial q}{\partial r}(0, t) = 0 \quad 8)$$

$$\frac{3k}{r_c}\left[C(z, t) - C(r_c, t)\right] = \frac{\partial q}{\partial t} \quad 9)$$

$$\bar{q} = \frac{3}{r_c^3} \int_0^{r_c} r^2 q\, dr \quad 10)$$

Material balance on packed bed

$$\frac{D_L \partial^2 C}{\partial z^2} - v \frac{\partial C}{\partial z} - \frac{1 - \varepsilon}{\varepsilon} \frac{\partial \bar{q}}{\partial t} = \frac{\partial C}{\partial t} \qquad 11)$$

Boundary conditions

$$C(z, 0) = C(r_c, 0) = q(r_c, 0) = 0 \qquad 12)$$

$$C(0, t) = C_0 \delta(t) \qquad 13)$$

$$C(\infty, t) = 0 \qquad 14)$$

II. Solution of the Model

Three alternative techniques for solution and subsequent parameter estimation from the model are curve fitting in the time domain, curve fitting in the Laplace or Fourier domain, and the method of moments. Moments of the response curve resulting from a pulse input can be solved analytically for the solution to the model in the Laplace domain. Parameter estimation is achieved by matching the measured moments with the analytical expression for the moments. The method of moments was used in this work because it does not require a numerical solution to the model and because parameters estimation can be performed in the time domain. The Laplace transform is applied to the time variable in the equations and boundary conditions of the model. A system of coupled ordinary differential equations is obtained after applying this transform. A theorem relating the transformed solution to the absolute and central moments of time domain solution is

$$M_n = (-1)^n \lim_{s \to 0} \frac{d^n}{ds^n} \bar{C}(s, z) \qquad 15)$$

The n^{th} absolute moment is defined as:

$$\mu_1' = \frac{M_n}{M_0} \qquad 16)$$

$$M_n = \int_0^\infty t^n C(z, t) e^{-st} dt \qquad 17)$$

The n^{th} central moment is defined by:

$$\mu_n = \frac{1}{M_0} \int_0^\infty (t - \mu_1')^n C(z, t) dt, \qquad 18)$$

Applying equation 15) to the transformed solution of the model results in the following equations for the first absolute and second central moments:

$$\mu_1' = \frac{L}{v}\left[1 + \frac{(1-\varepsilon)}{\varepsilon} K_p\right] \qquad 19)$$

$$\mu_2 = \left[\frac{2D_L L}{v^3} + \frac{2L}{v}\frac{\varepsilon}{(1-\varepsilon)}\left(\frac{r_c}{3k} \frac{r_c^2}{15D_c K_p}\right)\right]\left[1 + K_p \frac{(1-\varepsilon)}{\varepsilon}\right] \qquad 20)$$

These two equations relate the model parameters to the moments which can be calculated from experimental data.

Experimental

WYODAK subbituminous coal, particle size 35 x 60, was used in the experimental study. The experimental system consisted of a pulse reactor, Figure 1, a flow type BET apparatus, Figure 2, and the chromatographic apparatus, Figure 3. This allowed determinations of surface area and effective diffusivity to be made in conjunction with reaction studies without removing the sample.

Measurements of surface area and effective diffusivity were made on raw coals. Surface area measurements were made by adsorbing carbon dioxide at 195 K for 30 minutes. The single point BET method was used for evaluation of the surface area. The raw coals were devolatilized by heating at 5^{o}C/min to a temperature of 800^{o}C to produce a coal char. Changes in surface area and effective diffusivity were again determined. The coal char was then partially reacted at a temperature of 800^{o}C by injecting a known volume of carbon dioxide. Changes in surface area and effective diffusivity were again determined. This procedure was repeated until the conversion of the carbon in the coal approached 1.0.

Results and Discussion

The devolatilization caused structural changes which are reflected in an average weight loss of 41% of the initial weight, a decrease in the diffusion coefficient, and an increase in total surface area. Table 1 gives these changes for three WYODAK samples. The increase in surface area represents the opening of pores which were not accessible before devolatilization. Walls closing off pores are devolatilized and small pores inaccessible to the initial CO_2 adsorption are enlarged because of the evolution of volatile material during the heating. This new pore structure has a greater resistance to diffusion, seen as a decrease in the diffusion coefficient. The small pores and enlarged pore form a more complex network of voids within the particles. The production of char by devolatilization causes an increase in total available surface area and a decrease in the diffusion coefficient.

The heterogeneous chemical reaction causes continuous changes in the pore structure due to the consumption of carbon. Pore walls are being gasified slowly as the reaction continues toward completion. The continually changing internal structure affects the diffusion of gaseous reactants and products to and from the active carbon sites within the particle.

These phenomena may be described by examining Figure 4 which is a plot of the diffusion coefficient data for the three WYODAK samples measured at various carbon conversions. The diffusion coefficient increases slowly at low conversion and is somewhat stable during the mid-range of conversion, but increases very quickly as the reaction nears completion. Overall the diffusion coefficient increases as carbon conversion inreases. These data can be correlated by

$$\frac{D_c}{r_c^2} = (0.06) \exp (1.7 \cdot X_c) \qquad 21)$$

which gave an index of determination of 0.88. Physically, the pore structure after devolatilization consists of a small amount of void, characteristic of the low diffusion coefficient which means that the resistance to diffusion is substantial. During reaction these pores gradually enlarge due to gasification of the carbon. Therefore as conversion increases the pore volume or void increases resulting in less resistance to diffusion, which is reflected by the increase in the diffusion coefficient.

The CO_2-char reaction occurs at active carbon sites upon the coal char surface. Thus the consumption of the reactant carbon will affect the total surface area. The total surface area decreases for these WYODAK samples as the carbon conversion increases, Figure 5. As conversion goes toward completion, pore walls which are measured as surface area are gasified or consumed by the reaction causing a decrease in total surface area.

Figure 5 shows the specific surface area versus the carbon conversion. The specific surface area first goes through a minimum at low carbon conversions and then a maximum as carbon conversion goes toward completion. Mahajan and Walker (19) predicted the maximum in their qualitative description of the reaction process. Dutta and Wen (16) found that the reaction rate reaches a maximum at a carbon conversion of approximately 0.2 for reactions carried out at low temperatures. In an attempt to correlate this data they assumed a reaction rate model, Equation 1), for the chemical controlled regime. They incorporated into the model a proposed function of conversion which describes changes in surface area.

$$a = 1 \pm 100\, X_c^{\nu\beta} \exp (-\beta X_c) \qquad 22)$$

where a equals the specific surface area divided by the initial specific surface area. Fitting the model to the reaction rate versus conversion data the parameters of the proposed function were estimated by Dutta and Wen (16). This function describing changes in specific surface area exhibits a maximum at approximately the same conversion as our data. At low temperatures where reaction rate is predominantly chemically controlled, the maximum in the reaction rate vs. conversion data can be

explained by the fact that the specific surface for chemical reaction also goes through a maximum and this behavior of the specific area has been experimentally confirmed. The problem with equation 22) is that it predicts either a maximum or minimum for the value of a, but not both. In a recent paper Bhatia and Perlmuter (20), using a random pore model, have derived an expression for surface area as a function of conversion

$$a = \frac{1 - X}{\left(1 - \frac{r_c}{kCt}\right)^3} \sqrt{1 - \frac{4\pi L_o (1-\varepsilon_o)}{S_o^2} \ln \frac{1 - X}{\left(1 - \frac{r_c}{kCt}\right)^3}} \qquad 23)$$

where L_o, S_o and ε_o are the initial total pore length, surface area to volume ratio, and porosity respectively. This equation correlates our data predicting both a minimum and maximum in values of specific surface area, Figure 6.

Acknowledgements

This work was supported by a National Science Foundation Research Institution Grant, Eng. 7907988.

References

(1) Gadsby, J., Long, F. J., Sleighthom, P., and Sykes, K. W., "The Mechanism of the Carbon Dioxide Reaction," Proc. Roy. Soc. London, Ser. A, 193, 377 (1948).

(2) Gulbransen, E. A., and Andrew, K. F., "Reaction of Carbon Dioxide with Pure Artificial Graphite at Temperatures of 500°C," Ind. Eng. Chem., 44, 1039 (1952).

(3) Walker, P. L., Foresti, R. J. and Wright, C. C., "Surface Area Studies of Carbon-Carbon Dioxide Reaction," Ind. Eng. Chem., 45, 8, 1703 (1953).

(4) Petersen, E. E., Walker, P. L. and Wright, C. C., "Surface Area Development Within Artificial Graphite Rods Reacted with Carbon Dioxide from 900°C to 1300°C," Ind. Eng. Chem., 47, 1629 (1955).

(5) Wicke, E., "Fifth Symposium on Combustion," p. 245, Reinhold, New York, New York (1955).

(6) Rossberg, V. M., and Wicke, E., "Transportvogage and Oberflachem-reaktionen bei der Verbrennung Graphitischen Kohlenstoff," Chem. Ing. Tech., 28, 191 (1956).

(7) Ergun, S., "Kinetics of the Reaction of Carbon Dioxide with Carbon," J. Phys. Chem., 60, 480 (1956).

(8) Walker, P. L., Rusinko, F., and Austin, L. G., "Gas Reactions Carbon," Advances in Catalysis, Vol. XI, 133-221 (1959).

(9) Austin, L. G. and Walker, P. L., "Effect of Carbon Monoxide in Causing Nonuniform Gasification of Graphite by Carbon Dioxide," AIChE Journal, 9, 303 (1963).

(10) Turkdogan, E. T., Kaoump, V., Vinters, J. V., "Rate of Oxidation of Graphite in Carbon Dioxide," Carbon, 6, 467 (1968).

(11) Turkdogan, E. T., Vinters, J. V., "Kinetics of Oxidation of Graphite and Charcoal in CO_2," Carbon, 7, 101 (1969).

(12) Yoshida, K., and Kinii, D., "Gasification of Porous Carbon by Carbon Dioxides," J. Chem. Engr., Japan, 2, 170 (1969).

(13) Wen, C. Y., and Wy, N. T., "An Analysis of Slow Reactions in a Porous Particle," AIChE Journal, 20, 5, 833-840 (1974).

(14) Walker, P. L, and Hippo, E., "Reactivity of Heat-Treated Coals in Carbon Dioxide at 900°C," Fuel, 54, 245 (1975).

(15) Fuchs, W., Yavarsky, P. M., "Am. Chem. Soc., Div. Fuel Chem.," 20 (3), 115, (1975).

(16) Dutta, S., Wen, C. Y., "Reactivity of Coal and Char. 2. In Oxygen-Nitrogen Atmosphere," Ind. Eng. Chem., Process Des. Dev., 16, No. 1, 20 (1977).

(17) Dutta, S., Wen, C. Y., "Reactivity of Coal and Char. 2. In Oxygen-Nitrogen Atmosphere," Ind. Eng. Chem., Process Des. Dev., 16, No. 1, 31 (1977).

(18) Turkdogan, E. T., Olsson, R. G., and Vinters, J. V., "Pore Characteristics of Carbon," Carbon, 8, 545-564 (1970).

(19) Mahajan, A. P., Yarzab, R., and Walker, P. L., Jr., "Unification of Coal-Char Gasification Reaction Mechanisms," Fuel, Vol. 57, pp. 643-646, October 1978.

(20) Bhatia, S. K. and Perlmutter, D. D., "A Random Pore Model for Fluid Solid Reactions: I. Isothernal, Kinetic Control", AIChE J., 26, No. 3, 379-385 (1980).

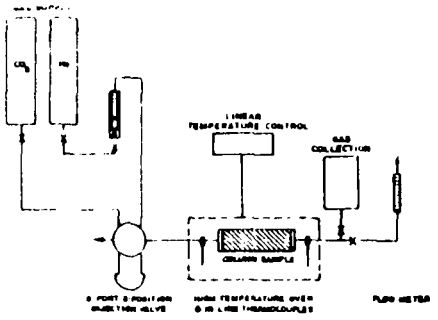

Figure 1 Schematic Diagram of the Apparatus for Reaction of Coal and CO_2 at High Temperatures

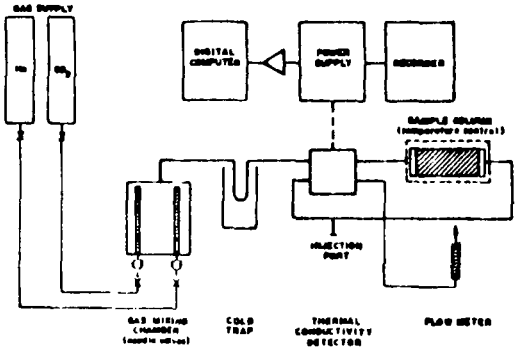

Figure 2 Schematic Diagram of the Experimental Apparatus for Determination of B.E.T. Surface Area

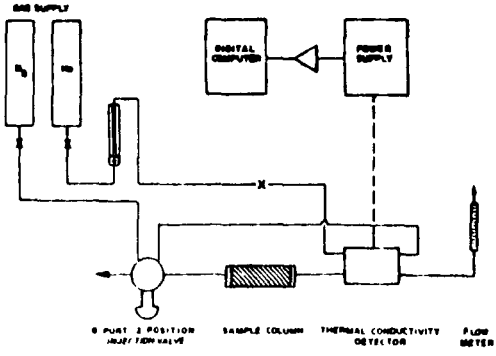

Figure 3 Schematic Diagram of Experimental Apparatus for Determination of Effective Diffusivity

Table 1

EFFECTS OF DEVOLATILIZATION

MTODAR	Weight (g) (coal)/(char)	Total Surface (m^2) (coal)/(char)	Specific Surface Area (m^2/g) (coal)/(char)	Diff. Co. (s^{-1}) (coal)/(char)
Sample 1	1.0094/0.6172	80.9/128.0	80.15/207.4	0.216/0.0630
Sample 2	0.9719/0.5712	70.9/104.5	72.9/182.9	1.150/0.0644
Sample 3	1.0169/0.5930	74.7/102.8	73.4/171.8	1.478/0.0719

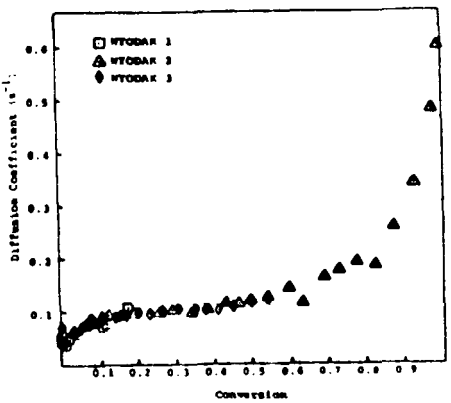

Figure 4 Diffusion Coefficient versus Conversion

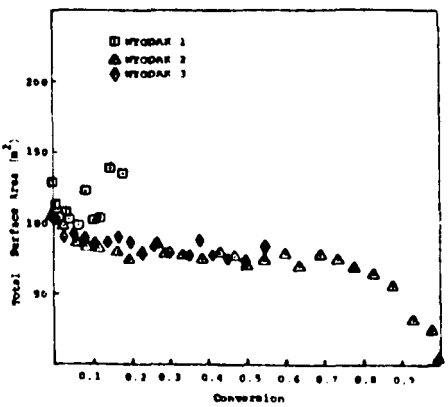

Figure 5 Total Surface Area Versus Conversion

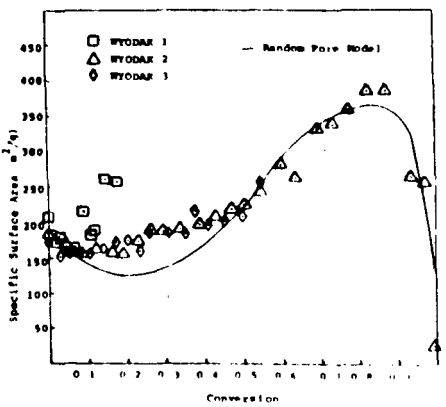

Figure 6 Comparison Between Experimental Specific Surface Area and Prediction of Random Pore Model

AN ENTRAINED FLOW REACTOR WITH IN SITU FTIR ANALYSIS*

Peter R. Solomon and David G. Hamblen

Advanced Fuel Research, Inc. 87 Church St., East Hartford, CT 06108

INTRODUCTION

A key element in predicting coal gasification behavior is pyrolysis. This is the initial step in gasification, the step which controls the amount and physical structure of the char and the step which is most dependent on the properties of the coal. Recent reviews of coal pyrolysis (1,2,3) conclude that the pyrolysis product distribution and apparent kinetic rates vary widely with the experimental measurement. It is clear that to establish a true predictive capability additional work is needed to understand pyrolysis reactions and define usable rates.

Among the experiments which have been useful in investigating pyrolysis have been the captive sample heated grid devices which have achieved good mass and elemental balances and have provided data on individual species evolution (4-16). However, the heating of the coal is slower than in practical devices so that the kinetic data is of limited value.

Entrained flow reactors which provide more realistic particle heating have been employed to study pyrolysis weight loss but have not provided much species evolution data (17-23). New visual data on pyrolysis behavior have been obtained in reactors with optical access (24, 25). These reactors employ flat flame burners into which coal may be injected.

This paper reports on a new apparatus which has been designed to combine the advantages of the reactors described above. The new reactor: 1) injects coal into a preheated gas stream in a hot furnace to provide rapid particle heating, 2) provides for optical access, 3) employs an FTIR for species concentration measurements, both in-situ and in an external cell and 4) has provisions for obtaining mass balances. The reactor will be used in a program to study pyrolysis and secondary reactions of interest in gasification. The results will be used to test the conclusions of a previously developed pyrolysis model (11-15, 26-29) and fill in needed kinetic data. The paper describes the reactor, reports preliminary results obtained with four coals at furnace temperatures from 700°C to 1200°C and assesses how these results compare to data obtained in other experiments.

EXPERIMENTAL

The reactor has been designed to study coal behavior under conditions of temperature and heating rate encountered in an entrained flow gasifier. The schematic of the experiment is presented in Fig. 1. A gas stream of predetermined composition is heated during transit through a bed of alumina chips maintained at furnace temperature. (Prior to heating, the gas composition can be analyzed by routing the stream through an infrared cell). The gas stream then enters a test section, maintained at the furnace temperature, where coal is introduced through a water cooled injector. The coal is fed using a modification of a MIT entrainment system (30). In the modified system, the feeder tube, which extends up through the coal bed, is slowly lowered as the entrainment gas (injected above the bed) exits through the tube. When the tube feeder entrance is at the level of the bed, coal is entrained in the gas and enters the tube. The rate for coal feeding is controlled by the rate at which the tube is lowered.

* This program was initiated under EPRI contract #RP 1654-8. The program scope is currently being expanded under contract #DE AC01-81FE05122 from the US Department of Energy.

After a variable residence time, the reacting stream passes optical access ports and immediately downstream is quenched in a water cooled collector. There are five optical access ports, two of which are presently employed for the FTIR beam. The other three ports are available for additional diagnostics. The quenched stream of char, tar and gases enters a cyclone designed to separate particles larger than 4 microns (31) and then enters a series of filters to remove and sample the tar and soot. The clean gas stream then enters the room temperature FTIR cell which provides a longer path length for higher sensitivity analysis. The particle residence time can be varied from 0 to 700 msec and the furnace has been designed to operate up to 1650°C.

The FTIR can quantitatively determine many gas species observed in coal pyrolysis including CO, CO_2, H_2O, CH_4, C_2H_2, C_2H_4, C_2H_6, C_3H_6, C_3H_8, C_4H_8, C_6H_6, NH_3, HCN, SO_2, COS, CS_2 and heavy paraffins and olefins. The instrument can take spectra every 80 msec to follow rapid changes in the reactor or co-add spectra for long periods of steady state flow to increase signal to noise. FTIR is well suited to in-situ furnace experiments since the FTIR system operates by coding the infrared source with an amplitude modulation which is unique to each infrared frequency. The detector is sensitive to the modulated radiation so that unmodulated stray radiation is eliminated from the experiment.

In the work described below, experiments were run for the four coals listed in Table I. The coals were sieved to produce a -200, +325 mesh size cut. The coal was fed at 2.4 grams/min. Helium was used for both the preheated gas and the entrainment gas. The preheated gas was fed at rates between 40 and 25 l/min depending on temperature to provide a gas velocity of 1 m/sec within the furnace. The entrainment gas was fed at 1.2 l/min. Infrared spectra were obtained with a Nicolet model 7199 FTIR using a globar source and a mercury-cadmium telluride detector. For obtaining the spectra within the furnace and within the cell, 100 scans at 0.5 wavenumber resolutions were accumulated in 140 seconds and transformed in under 2 minutes.

TABLE I

COALS USED IN THE ENTRAINED FLOW REACTOR STUDY

COAL	TYPE	WT% (DAF)					
		C	H	N	S	O	ASH (Dry)
Savage	Montana Lignite	71.2	4.6	1.1	1.3	21.8	10.6
Jacobs Ranch	Wyom. Subbituminous	74.3	5.2	1.1	.6	18.8	7.8
Illinois #6	Bituminous	73.9	5.1	1.4	4.2	15.4	11.0
Pittsburgh #8	Bituminous	83.5	5.5	1.6	3.3	6.1	9.2

Gas Analysis in the Furnace

Figure 2 shows the in-situ gas analysis. There is an acceptable noise level and no drastic effects from the particle scattering. The analyses are for the coal injector at positions from 5 to 66 cm above the optical port. The species which can easily be seen are CO, CO_2, H_2O, CH_4, C_2H_2, C_2H_4, and heavy paraffins. Additional species could be observed through the use of software signal enhancement techniques which can be used to detect species whose absorption lines are smaller than the noise (32). These techniques consider all of the absorption lines for a species, rather than a single line.

FTIR spectra obtained directly within the hot furnace allows the observation of heavy products such as tar which don't appear in the gas phase at room temperature and provide a means to determine whether reactions occur during the quenching and sampling of the gas stream. The in-situ observation also permits gas temperatures to be measured as described below.

Temperature Measurements by FTIR

It appears possible to use the ratios of lines from a given species to determine gas temperatures in the furnace. As the temperature of a gas changes, the populations in its higher energy levels increases. In terms of its absorption spectrum, this generally means that more absorption lines are visible. The effect is illustrated in Fig. 3 which compares CO spectra at a number of temperatures. The energy is clearly shifted from the central lines toward the wings as the temperature increases. Lines at 2250 and 2000 cm^{-1} which are too small to be observed at room temperature are clearly visible at the higher temperatures. The ratio of these lines to the lines at the center of the distribution can be used to determine temperature.

Gas Analysis in a Cell

Figure 4 shows the gas analysis from the room temperature cell. This cell was filled with the effluent gas stream from the furnace after passing through the cyclone and filter. The cell provides higher sensitivity detection because the path length is about 12 times longer than in the furnace. The spectra compare the pyrolysis gases from Jacobs Ranch coal injected at 66 cm above the optical port at furnace temperatures of 800 and 1200°C. Important differences in the product mix at these two temperatures can be observed. The top pair of spectra show the region between 3500 and 2800 cm^{-1}. At 1200°C there is HCN, C_2H_2 and CH_4. At 800°C there is less methane and little HCN or C_2H_2 but significant amounts of ethane and heavy paraffins (indicated by the broad background). This observation is consistent with the cracking of paraffins to form olefins, acetylene and soot which has been discussed previously (12,14). The region between 2600 and 1900 cm^{-1} shows the CO_2 and CO. The CO_2 increases by 50% but the CO increases by a factor of 3 in going from 800°C to 1200°C. This is consistent with previous observations of low temperature production of CO_2 and high temperature production of CO (11-15). The evolution of CO_2 and CO may be related to the early disappearance of carboxyl groups and the retention of ether lingages observed in the infrared spectra of chars discussed below. The region between 1800 and 1200 cm^{-1} shows water and methane. The region between 1200 and 500 cm^{-1} shows olefins, acetylene, HCN and CO_2. The ethylene and heavier olefins are lower and acetylene is higher at the higher temperature (consistent with cracking of olefins to form acetylene and soot).

A comparison of the pyrolysis gas composition from different coals is presented in Fig. 5. The coals were all injected at 66 cm above the optical window at a furnace temperature of 800°C. The spectra show the kind of variation with rank which has been discussed previously (11-15). The low rank coals, which are high in the oxygen functional groups, produce pyrolysis gases which are high in the oxygen containing species, CO, CO_2 and H_2O. The higher rank coals, which are higher in aliphatic functional groups, yield higher concentrations of hydrocarbons.

Data of the kind illustrated above were collected at several reaction distances at 800°C . Curves of concentration vs reaction distance differed among the species. On a normalized basis, however, these curves were similar for the various coals even though the concentration varied from coal to coal. This result is also in agreement with earlier work (11-15).

Changes in Char Chemistry

The infrared spectra of chars provide a convenient means of monitoring the chemical changes occurring during the pyrolysis process. The changes in functional group concentration can be correlated with the appearance of gas species to determine the sources for the species. FTIR spectra of chars from pyrolyzing Jacobs Ranch Coal at 800°C are shown in Fig. 6. The techniques for preparing, drying and making scattering corrections have been discussed previously (13, 33). The aliphatic groups (peak near 2900 cm^{-1}) and carboxyl groups (shoulder near 1650 cm^{-1}) are observed to decrease with reaction distance. The hydroxyl groups (broad peak between 3500 and 2500 cm-1) also decrease although not as rapidly. As the residence distance (and time) is increased, the char aromatic hydrogen peaks near 800 and 3100 cm^{-1} are observed to increase. The O-C bond concentration (peak near 1200 cm^{-1}) shows little change. These changes in the functional group concentrations during pyrolysis are in agreement with results from earlier experiments (14, 15, 21). The changes in char chemistry will be correlated with evolution of gas species and compared with the pyrolysis model predictions.

Conclusions

Preliminary results have been obtained in a newly constructed Entrained Flow reactor with on-line in-situ analysis by FTIR. These results indicate that:

1. Gas concentration measurements for CO, CO_2, water, methane, acetylene, ethylene and heavy paraffins can be routinely made in a hot furnace with an FTIR.

2. Gas temperature measurements appear feasible using ratios of CO lines.

3. On-line gas analysis in an external gas cell is also extremely effective,

Several observations which have previously been reported for other pyrolysis experiments appear to be supported by the preliminary data. These are:

1. Gas kinetics appear to be relatively insensitive to coal rank.

2. The gas composition varies sytematically with the functional group composition of the coal.

3. There is temperature dependent cracking of paraffins to form olefins and acetylene and olefins to form acetylene.

4. Functional groups in the chars disappear in the following order: First aliphatics, then hydroxyl, and then aromatic hydrogen and ether linkages. The present results show that carboxyl groups also disappear quickly.

ACKNOWLEDGEMENT

The authors would like to thank N. Y. Nsakala, G. J. Goetz, R. W. Seeker and R. C. Flagan for their advice on various details of the reactor and acknowledge the able technical assistance of R. M. Carangelo in running the experiments. The authors also express their appreciation for the encouragement given to this program by J. Yerushalmi, George Quentin and Leonard Naphtali.

REFERENCES

1. Howard, J. B., Fundamentals of Coal Pyrolysis and Hydropyrolysis, in Chemistry of Coal Utilization. Second supplementary volume. Martin A. Elliot, Editor, Wiley, pg. 665 (1981).

2. Howard, J. B., Peters, W. A. and Serio, M. A., Coal Devolatilization Information for Reactor Modeling. EPRI report AP-1803, April, (1981).

3. Anthony, D. B. and Howard, J. B., Am. Inst. Chem. Eng. J. 22, 625 (1976).

4. Anthony, D. B., Howard, J. B., Meissner, H. P. and Hottel, H. G., Rev. Sci. Instrum., 45, Pg. 992 (1974).

5. Anthony, D. B., Howard, J. B., Meissner, H. P. and Hottel, H. G., Fifteenth Symposium (International) on Combustion, p. 1303, The Combustion Institute, Pittsburgh, PA (1975).

6. Suuberg, E. M., Rapid Pyrolysis and Hydropyrolysis of Coal, Ph.D Thesis, MIT (1977).

7. Suuberg, E. M., Peters, W. A. and Howard, J. B., Ind. Eng. Process Des. Dev., 17, #1, p. 37 (1978).

8. Suuberg, E. M., Peters, W. A. and Howard, J. B., Seventeenth Symposium (International) on Combustion, p. 117, The Combustion Institute, Pittsburgh, PA, (1979).

9. Juntgen, H. and van Heek, K. H., Fuel Processing Technology, 2, 26 (1979.

10. Gavalas, G. R. and Oka, M., Fuel 51, 285 (1972).

11. Solomon, P. R. and Colket, M. B., 17th Symposium (International) on Combustion, p. 131, The Combustion Institute, Pittsburgh, PA (1979).

12. Solomon, P. R., ACS Div. Of Fuel Chemistry Preprints, 24, #3, 154 (1979).

13. Solomon, P. R., In Coal Structure, Advances in Chemistry Series, 192, page 95 (1981).

14. Solomon, P. R. and Hamblen, D. G., Understanding Coal Using Thermal Decomposition and Fourier Transform Infrared Spectroscopy, Proceedings of the Conference on the Chemistry and Physics of Coal Utilization, Morgantown, WV, June 2-4 (1980).

15. Solomon, P. R., Hamblen, D. G. and Carangelo, R. M., Coal Pyrolysis, AIChE, Symposium on Coal Pyrolysis (Nov., 1981).

16. Solomon, P. R. and Colket, M. B., Fuel, 57, 749 (1978).

17. Badzioch, S. and Hawksley, P. G. W., Ind. Eng. Chem. Process Des. Dev., 9, 521 (1970).

18. Nsakala, N. Y., Essenhigh, R. H. and Walker, P. L., Jr., Combustion Science Technol., 16, 153 (1977).

19. Kobayashi, H., Devolatilization of Pulverized Coal at High Temperatures, Ph.D. thesis, Dept. of Mechanical Eng., Mass. Institute of Technology, Cambridge, MA (1976).

20. Kobayashi, H., Howard, J. B. and Sarofim, A. F., Sixteenth Symposium (International) on Combustion, The Combustion Institute, Pittsburgh, PA, 411, (1977).

21. Solomon, P. R., Hamblen, D. G., Goetz, G. J. and Nsakala, N. Y., ACS Div. of Fuel Chemistry Preprints, 26, #3 (1981).

22. Ubhayaker, S. K., Stickler, D. B., von Rosenberg, Jr., C. W. and Gannon, R. E., 16th Symposium (International) Combustion, Combustion Inst., Pittsburgh, PA p. 427, (1977).

23. Scaroni, A. W., Walker, Jr., P. L. and Essenhigh, R. H., Fuel, 60 71 (1981)

24. McLean, W. J., Hardesty, D. R. and Pohl, J. H., 18th Symposium (International), on Combustion, The Combustion Institute, Pittsburgh, PA p. 1239 (1981).

25. Samuelson, G. S., Trolinger, J. D., Heap, M. P. and Seeker, W. R., Combust. Flame 38, #3 (1980).

26. Solomon, P. R., Fuel, 60, 3 (1981).

27. Solomon, P. R., Hobbs, R. H., Hamblen, D. G., Chen, W. Y., La Cava, A. and Graff, R. S., Fuel, 60, 342 (1981).

28. Solomon, P. R., Coal Structure and Thermal Decomposition, ACS Symposium Series, (In Press).

29. Solomon, P. R., Characterization of Coal and Coal Thermal Decomposition, Chapter III of EPA Monograph on Coal Combustion, (In Press).

30. Mims, C. A., Neville, M., Quann, R. and Sarofim, A., Laboratory Study of Trace Element Transformation During Coal Combustion, presented at the National 87th AIChE Meeting, Boston, MA, Aug. 19-22 (1979).

31. John, W. and Reischl, G., A Cyclone for Size-Selective Sampling of Ambient Air, Journal of the Air Pollution Control Assoc., 872 (1980).

32. Haaland, D. M., Easterling. R. G., Applied Spectroscopy, 34, #5, 539 (1980)

33. Solomon, P. R. and Carangelo, R. M., FTIR Analysis of Coal: I. Techniques and Determination of Hydroxyl Concentrations, submitted to Fuel (1981).

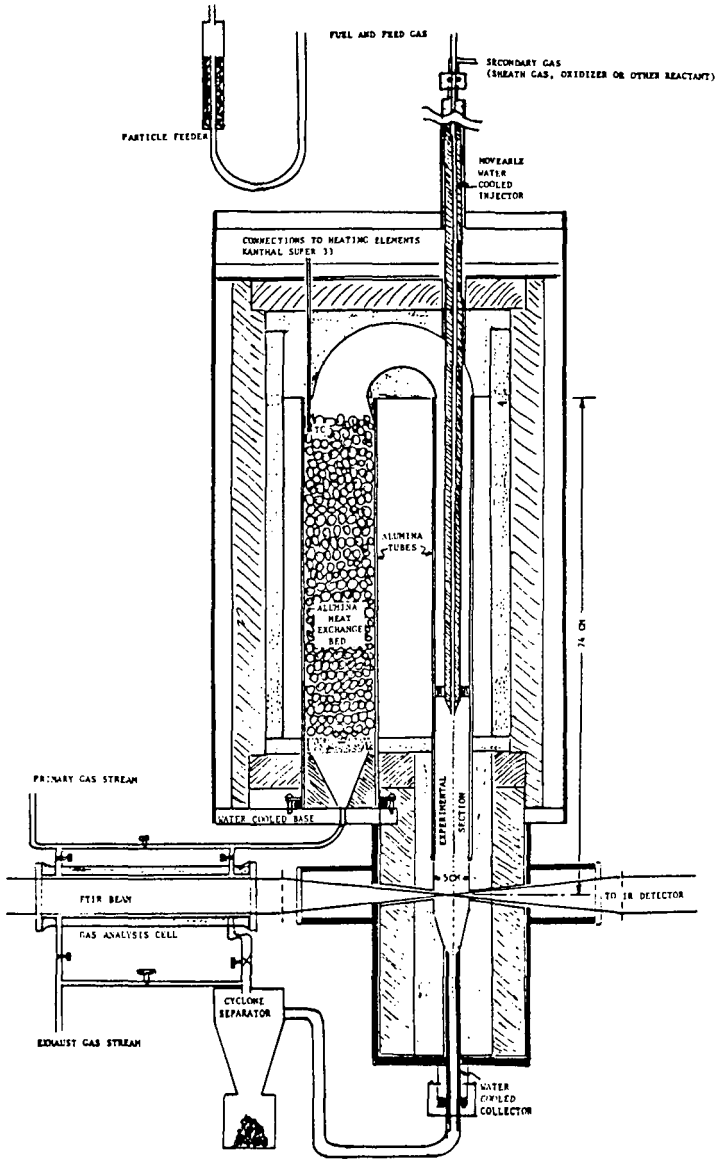

Figure 1. Entrained Flow Reactor.

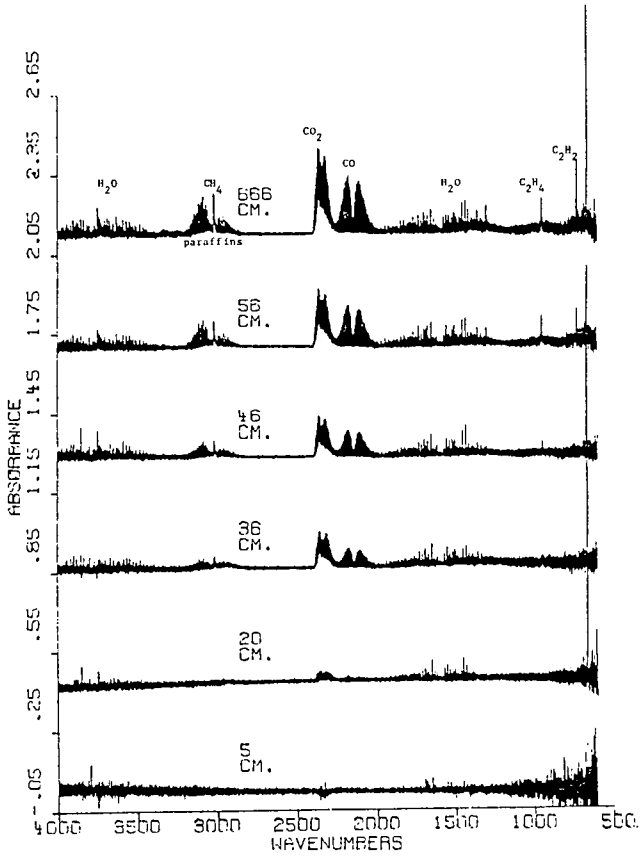

Figure 2. In-Situ FTIR Spectra of Pyrolysis Cases from Jacob's Ranch Coal at 1000°C.

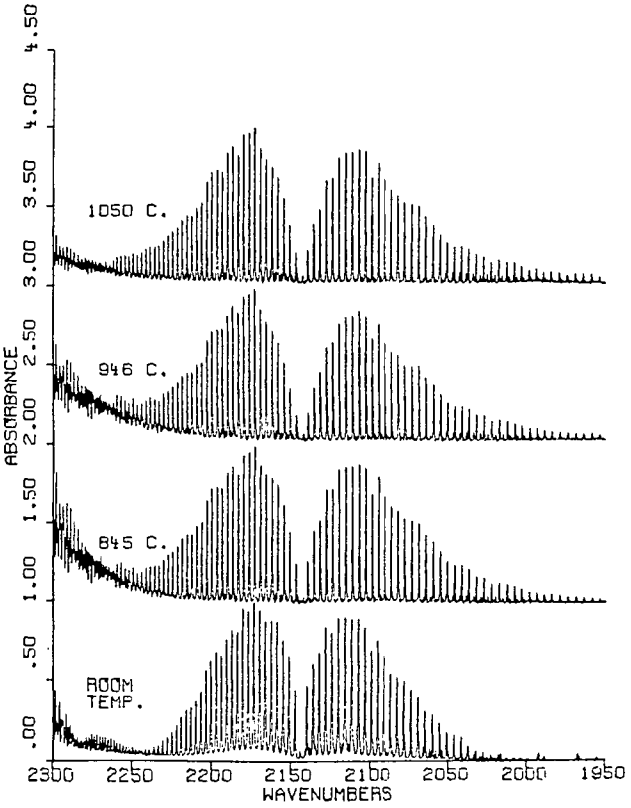

Figure 3. Spectra of CO at Elevated Temperatures.

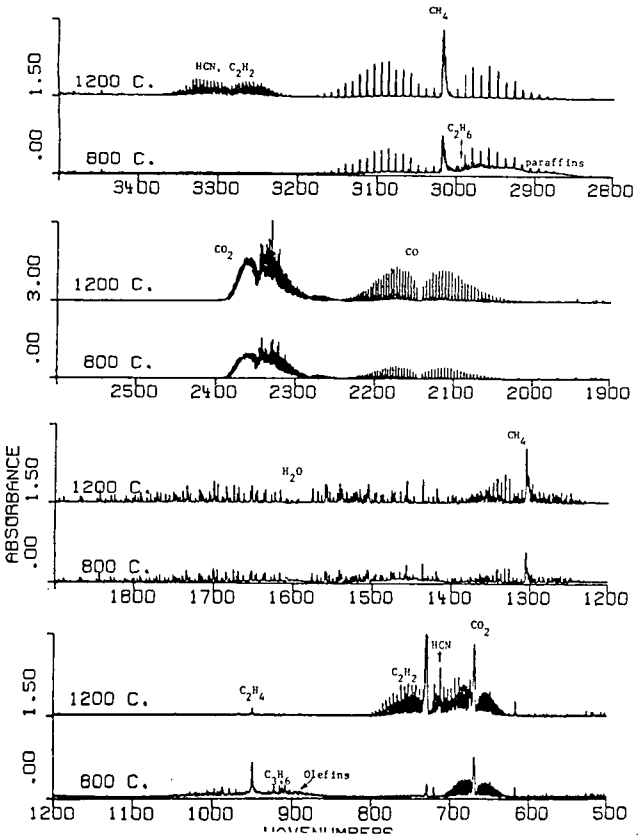

Figure 4. FTIR Spectra of Pyrolysis Cases from Jacob's Ranch Coal at 800°C and 1200°C in Room Temperature Cell. 66cm Residence Distance.

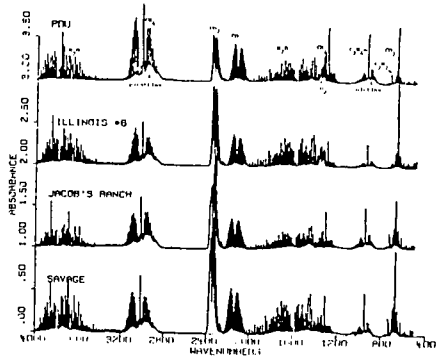

Figure 5. Comparison of FTIR Spectra from 4 Coals Pyrolized at 800°C at 66 cm Residence Distance.

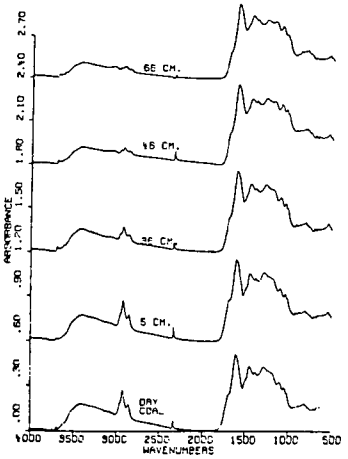

Figure 6. FTIR Spectra of Char from Jacob's Ranch Coal Pyrolized at 800°C.

COAL PYROLYSIS AT HIGH TEMPERATURES AND PRESSURES

S. S. Tamhankar, J. T. Sears and C. Y. Wen

Dept. of Chemical Engineering, West Virginia University, Morgantown, W.Va. 26506

INTRODUCTION

In coal conversion processes, such as combustion or high-temperature gasification, the extent of pyrolysis is an important parameter which is affected by temperature. Increasing amounts of coal converted directly to gaseous species would reduce the remaining material which must be converted by the relatively slow char-gas reactions. Studies on this aspect, particularly at pressure and high temperatures, are scarce.

ASTM standard methods obtain the amount of coal converted to volatile matter at low temperatures, slow heating rates and long exposure times. Other procedures have generally used either direct electric-resistance heating (1, 2) or a laminar-flow furnace (3, 4, 5, 6) to obtain high heating rates and high temperatures.

Menster et al. (1) and Kobayashi et at. (6) have indicated that the maximum temperature affects the extent of pyrolysis, with an apparent plateau or a peak in the weight loss curve at 900-1100°C, followed by an increase in the extent of pyrolysis. Scaroni, et al. (7) suggest that there is no direct heating rate effect on the extent of pyrolysis, but rather the preponderance of secondary char-forming reactions of the primary volatiles may yield an apparent heating rate effect as well as a sample-weight effect. There is evidence that the char formed by rapid heating at high temperatures is very reactive (3, 8). The previous work on pyrolysis at temperatures > 1000°C has been at 1 atm pressure.

To help fill in the data gaps, the present work has therefore been focused on the examination of pyrolysis at high temperatures (800-1600°C), pressures (1-15 atm) and in various reacting and nonreacting gases.

EXPERIMENTAL

A new design of a HPHT (high pressure, high temperature) TGA was utilized in this research. The details of the design and its performance have been discussed elsewhere (9). The system is depicted in Figure 1, which mainly consists of two chambers. The chambers are designed for 1200 psi, although supporting inlet lines limited the operating pressure to 450 psi. The small Grayloc flange was used as a port to introduce samples into the TGA. By raising the top chamber, attaching the sample, then lowering the chamber and securing the flange, a cumbersome, leaky port is avoided. A rugged electrobalance with a continuous weighing system, driven by an electric motor, is employed to lower the samples into the hot zone for weight-loss data. The heating system is a yttrium-stabilized ceramic "Kanthal" heating element. These elements are capable of 1800°C surface temperature, and work best in oxidizing gases. Temperatures were monitored throughout by Pt-Rh/Pt thermocouples. Steam can be introduced via a separate stainless steel flow system from gas lines, and condensation was avoided by maintaining the entire lower chamber at elevated temperatures.

This design has capability for quickly bringing the sample from a cold zone into the hot zone in less than 5 seconds, taking subsequent weight-loss data, and then removing the sample as quickly. The temperatures at various points in the system were calibrated at each reactor temperature and pressure. The temperature profile is such that the heating of the sample in the pyrolyzing-temperature region was achieved at a rate of 500-1500°K/sec depending on the reaction zone temperature. There is provision for several ports for gas input. Pyrolysis, external gas-

diffusion limitations, and char kinetic reactivity were analyzed from the weight-loss data by both varying time in the reaction zone and gas flow rate.

The coals studied included lignite (PSOC-246), bituminous (PSOC-309) and subbituminous (PSOC-240) samples. Samples of 50-100 mg were weighed, loaded and lowered in the sample holder into the heated chamber as described. Most runs used a platinum-mesh folded screen (52 mesh) as the sample holder. For some studies on particle size, the sample holder was a disked platinum foil. The results obtained on pyrolysis and gasification using the two different sample holders matched very well, indicating no effect of sample holder geometry.

The coal particle sizes used were 35-48, 48-60, 60-80, and 80-100 mesh ($\bar{d}_p$ = 358, 273, 213 and 163 μm, respectively). The gaseous environments were nitrogen, carbon dioxide, nitrogen-steam. Pyrolysis and subsequent in-situ reaction with gas following pyrolysis were run at 800-1600°C, 1-15 atm.

RESULTS AND DISCUSSION

Typical weight-loss data obtained at 1200°C in both nitrogen and nitrogen-steam for the lignite coal are shown in Figure 2. Note that the determination of percent pyrolysis in the inert nitrogen is straightforward, while in a reacting environment it is obscured by the rapid chemical reactions of the volatiles and char. If the break in the curve is identified by extrapolating the primary pyrolysis and reaction curve portions, respectively (p) and (r), this weight-loss can be called the apparent pyrolysis; and the apparent percent pyrolysis determined. The values thus obtained for the apparent percent pyrolysis as well as the pyrolysis time were found consistent and reproducible under a given set of conditions, as confirmed by repeated runs. It may be noticed from Figure 2 that the ultimate pyrolysis in nitrogen is greater than the apparent pyrolysis in the reacting gas, while in the same time period the amount pyrolyzed is more or less the same in the two cases.

In Figure 3 are presented the apparent percent pyrolysis of lignite as a function of temperature for different gases. Note that the apparent percent pyrolysis in CO_2 and N_2-H_2O is less than that in nitrogen, in agreement with the above discussion.

There is a plateau in the curve of percent apparent pyrolysis (devolatilization) versus temperature in the region 1200-1400°C. This type of phenomena can be found in the data of Menster et al. (1) and Kobayashi et al. (6). Suuberg et al. (10) observed two stages (or plateaus) in coal pyrolysis up to a temperature near 1100°C, and a third stage was envisaged above that temperature. This third stage was assumed to remove primarily CO and CO_2. The data of Kobayashi et al. (6) indicate percent weight-loss near 60 percent at temperatures above 1500°C. The present results are consistent with the results reported by these authors and confirm a third plateau stage.

Figure 4 presents devolatilization results at various temperatures for predried coal and for various particle sizes in a CO_2 gas. There appear to be significant effects of the moisture content in coal and various particle sizes. Although these results are inconclusive, they can be explained by either an effect of heating rate on pyrolysis or by secondary pyrolysis reactions which are influenced by available surface area, moisture and other gases which could result in internal volatile decomposition and coke formation.

Figure 5 presents the effect of pressure on the apparent pyrolysis in a steam environment. At lower temperatures (800-1100°C) the apparent pyrolysis increases slightly with pressure, while at higher temperatures (1200-1400°C) there is a decrease in apparent pyrolysis with pressure. One possible explaination is that at lower temperatures the increased gas concentration increases the gas-volatile re-

actions, decreasing the secondary char formation reactions; at higher temperatures the increased pressure prevents some volatiles from escaping the solid and thus participating in secondary char-formation reactions. Similar results have been reported earlier (8) in a hydrogen atmosphere, wherein the amount of pyrolysis was found to increase only beyond about 20 atm pressure. Notably, in steam this effect is observed at lower pressures. The present studies also bring out the effect of temperature on this behavior. Further work in this area is necessary to confirm the anomalous results.

Table 1 presents results of subsequent reactivity of chars formed by coal devolatilization. A comparison is shown of chars formed in-situ, as in the present mentod with chars formed separately and then reacted. Note that in-situ-formed char is a factor two to ten times more reactive than chars formed separately. Thus, keeping the char at high temperatures for longer times before reaction apparently renders the char less reactive, and can be interpreted as a morphological rearrangement. These results are in agreement with previous results at this laboratory (11), and extend these results to higher temperature regimes. It is suggested that the char preparation method dramatically affects subsequent char reactivity. These effects must be considered in models of char reactivity and in the use of char reactivity data in coal-conversion reactor models and in the interpretation of pilot-unit data.

CONCLUSIONS

Devolatilization generally increases with temperature in a manner consistent with the proposed three-stage mechanism for the evolution of volatiles. Results here show a plateau at 1200-1400°C and a maximum devolatilization above 1500°C. Reactive gases can interact with the freshly formed volatiles and affect the secondary char-forming reactions which can cause changes in the apparent percent pyrolysis. This was evident from the effects of moisture content, particle size, pressure and gaseous environment on the extent of pyrolysis. Reactivity of char formed in-situ and immediately reacted was found to be higher than reactivity of chars formed separately and then brought into the reactive environment. It is suggested that morphological rearrangements may be important in pyrolysis and subsequent char reactions.

ACKNOWLEDGMENT

This work was made possible by a grant from the Department of Energy, Contract No. ET-78-S-01-3253.

REFERENCES

1. Menster, M., O'Donnell, H. J. and Ergun, S., "Rapid Thermal Decomposition of Bituminous Coals," Am. Chem. Soc., Div. of Fuel Chem. Preprints 14 (5) 94 (1970).

2. Menster, M., O'Donnell, J. J., Ergun, S. and Friedel, R. A., "Devolatilization of Coal by Rapid Heating, " in Coal Gasification, p. 1, Advances in Chemistry Series No. 131, Am. Chem. Soc., Washington, D.C. (1974).

3. Nsakala, N.Y., Essenhigh, R. H. and Walker, P. L., Jr., Fuel 57 605 (1978).

4. Nsakala, N.Y., Essenhigh, R. H. and Walker, P. L., Jr., Comb. Sci. & Technol. 16 153 (1977).

5. Badzioch, S. and Hawksley, P. G. W., Ind. Eng. Chem. Process Des. & Dev. 9 (4) 521 (1970).

6. Kobayashi, H., Howard, J. B. and Sarofim, A. F., "Coal Devolatilization at High Temperatures," 16th Intern. Symp. on Combustion, p. 411, The Combustion Institute, Pittsburgh, Pa. (1977).

7. Scaroni, A. W., Walker, P. L., Jr. and Essenhigh, R. H., Fuel 60 71 (1981).

8. Anthony, D. B., Howard, J. B., Hottel, H. C. and Meissner, H. P., Fuel 55 121 (1976).

9. Sears, J. T., Maxfield, E. A. and Tamhankar, S. S., "A Pressurized Themobalance Appartus for Use in Oxidizing Atmospheres at High Temperatures," Ind. Eng. Chem. Fundamentals (submitted 1981).

10. Suubert, E. M., Peters, W. A. and Howard, J. B., Ind. Eng. Chem. Process Des. & Dev. 17 37 (1978).

11. Agarwal, A. K. and Sears, J. T., Ind. Eng. Chem. Process Des. & Dev. 19 364 (1980).

12. Linares-Solano, A., Mahajan, O. P. and Walker, P. L., Jr., Fuel 58 327 (1979).

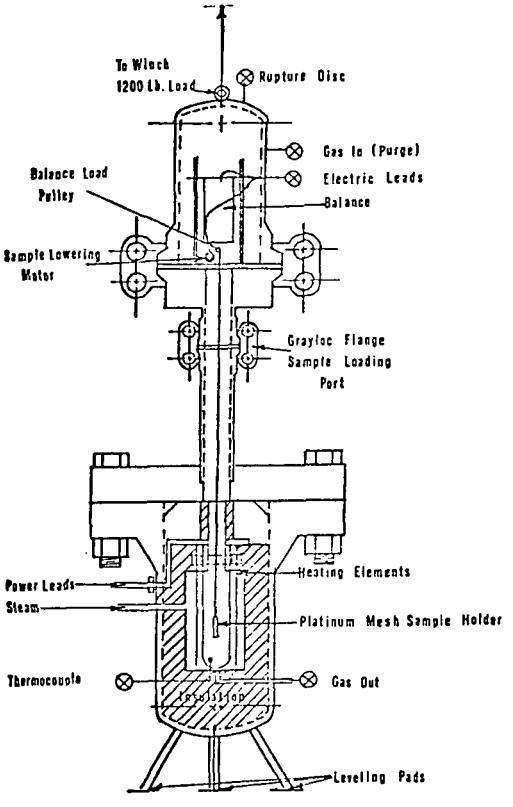

FIG. 1. SCHEMATIC OF HIGH PRESSURE/TEMPERATURE THERMOBALANCE APPARATUS.

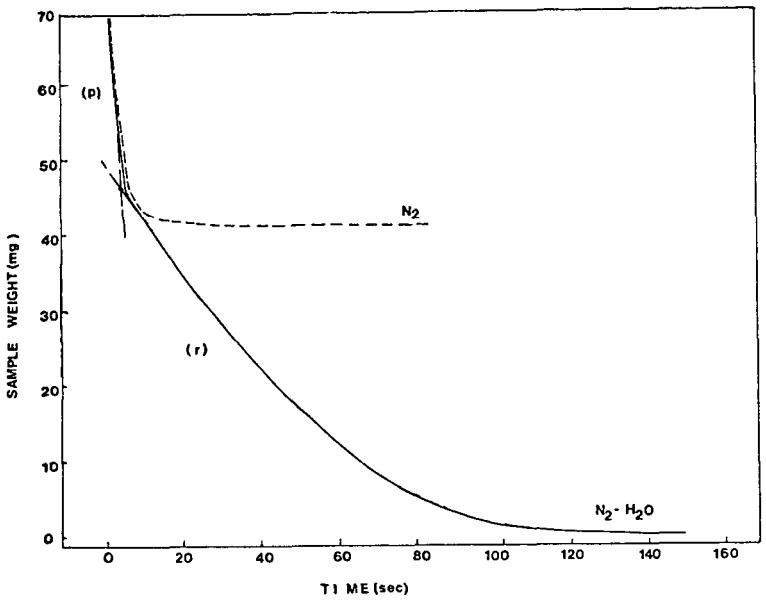

FIG. 2. REPRESENTATIVE WEIGHT LOSS CURVES OBTAINED AT 1200°C WITH PSOC-246 LIGNITE.

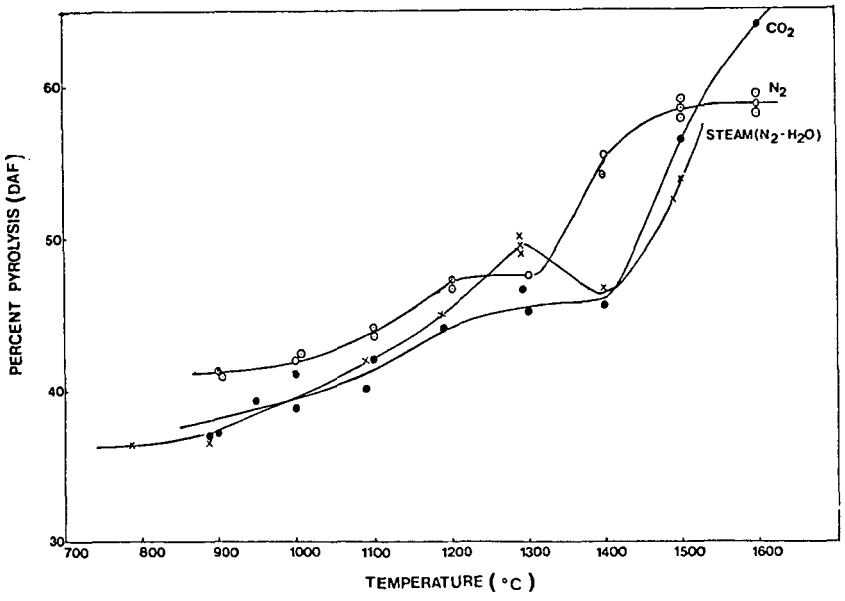

FIG. 3. EXTENT OF PYROLYSIS AS A FUNCTION OF TEMPERATURE FOR PSOC-246 LIGNITE.

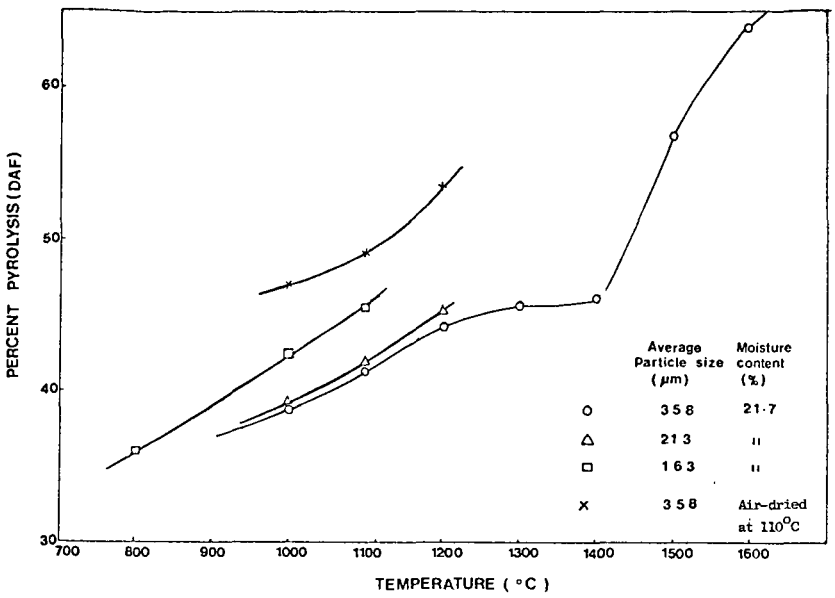

FIG. 4. EFFECTS OF PARTICLE SIZE AND MOISTURE CONTENT ON THE EXTENT OF PYROLYSIS IN CO_2 ATMOSPHERE.

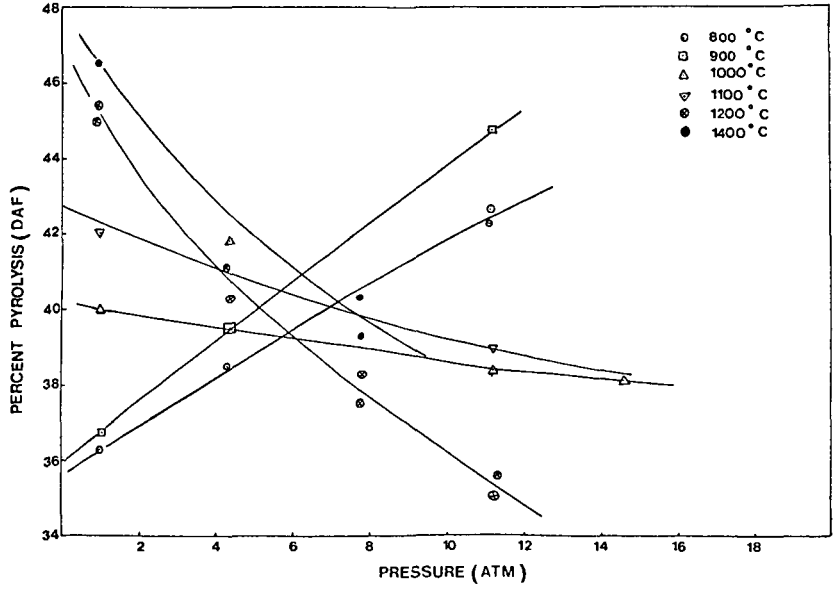

FIG. 5. VARIATION OF PERCENT PYROLYSIS WITH TEMPERATURE AND PRESSURE IN N_2-H_2O.

Table 1

REACTIVITY OF CHARS AS A FUNCTION OF PREPARATION CONDITIONS

(A) Reactivity of N.D. Lignite (PSOC-246) in CO_2

Reaction Temperature °C		900	950	1000	1050	1200	1250	1300
Initial Reactivity mg/mg Min.	In-situ	0.30	0.40	0.69	0.80	2.14	2.15	2.15
	Preformed Char*	0.26	0.32	0.57	0.62	0.88	0.89	1.02

(B) Reactivity of a Subbituminous Coal (PSOC-314) in CO_2

Reaction Temperature °C		1250	1300	1350	1400
Initial Reactivity mg/mg Min.	In-situ	0.54	0.67	1.13	1.30
	Preformed Char*	0.50	0.60	0.76	0.79

(C) Comparison of In-situ Reactivities with Other Reported Results

Coal Type	Method/Treatment	Reaction Temp. °C	Gas	Maximum Reactivity mg/mg Min.	Ref.
N.D. lignite (PSOC-246)	In-situ	910	N_2-H_2O (excess H_2O)	0.48	Present study
N.D. lignite (PSOC-87)	Coal heated in N_2 at 10°C/min to 1000°C, kept for 2 hrs, cooled. Reheated in N_2 at 20°C/min to 1000°C, cooled to 910°C, held for 20 min, reacted.	910	N_2-H_2O (excess H_2O)	0.0467	12
HVC bituminous (PSOC-309)	In-situ at ~ 600°C/sec	920	CO_2	0.20	Present study
HVC bituminous (PSOC-309)	In-situ at ~ 200°C/min.	920	CO_2	0.088	11

*Char prepared by pyrolyzing coal in N_2 at 1100°C for 2 min.

SIMULATION OF ENTRAINED FLOW HYDROPYROLYSIS REACTORS

A. Goyal
Institute of Gas Technology
Chicago, Illinois 60616

D. Gidaspow
Chemical Engineering Department
Illinois Institute of Technology
Chicago, Illinois 60616

The phenomena of coal pyrolysis and hydropyrolysis have become of considerable interest in recent years because of their significance in the efficient conversion of coals to clean fuels. The proposed hydropyrolysis commercial reactors are usually based on the entrained flow concept in which coal particles are rapidly heated in a dilute phase by mixing with hot hydrogen (or a gas mixture rich in hydrogen). A wide variation in the product distribution can be obtained in such reactors by manipulating temperature, residence time, and other operating parameters. Mathematical models incorporating hydrodynamics, coal kinetics, heat transfer characteristics, etc. are needed for understanding the influence of design variables, feed materials, and process conditions on the reactor performance. The literature is lacking in coal hydropyrolysis entrained flow reactor models. Such a model has been developed in this study.

Mathematical Formulation

A one-dimensional mathematical model has been formulated here. The physical system considered is an entrained flow hydropyrolysis reactor. Pulverized coal mixes with the hot gas feed at the reactor entrance. As coal particles are carried by the gas, their temperature increases and hydropyrolysis takes place.

The single coal particle hydropyrolysis kinetic model used in this study is described by Goyal (1). The model is primarily based on Johnson's kinetic model (2, 3, 4) supplemented by Suuberg's kinetic model (5) for rapid reactions. In this model, the coal is assumed to consist of eleven solid species while the gas of nine species (Table 1). Gaseous species $(CH_z)_a$ represents gaseous heavy hydrocarbons while $(CH_M)_b$ represents vaporized oils and tars.

The kinetic model has been combined here with reactor flow model and heat and mass transfer characteristics of the multiparticle system to derive a reactor model. Because of the significant amount of coal weight loss and gas generation in such systems, hydrodynamics may also be very important. The equations describing the system are given in Table 2. In this formulation, it is assumed that the heat of reaction of the solid-gas phase reaction affects the solid temperature only while that of occurring solely in the gas phase affects the gas phase temperature only. Also, the extent of swelling of the coal particles is directly proportional to the extent of devolatilization. Furthermore, the expression giving the gasification rate of the solid species CH_x (semichar) is somewhat complex. This rate is dependent on the time-temperature history of the particle and involves a double integration. The mathematical manipulation performed to simplify the complexity resulted into several additional differential equations, the details of which are given by Goyal (1).

The solid species production rate (S_i) is given by equation (18). The gas species production rates can be related to the solid species production rates (1).

Furthermore, coal hydrogenation experiments in the laboratory are often carried out in helical reactors (4, 6). The relationship between the particle

and the gas velocity is often represented in terms of a slip velocity factor (ϕ_s). In such reactor, the centrifugal forces are often more important than gravitational force. This slip velocity factor depends on the tube diameter, helix diameter, solids to gas ratio, particle size, gas velocity, etc. Thus for helical reactors:

$$D(v_s) = \phi_s D(v_g) \qquad 24)$$

This equation replaces equation (5) in Table 2.

This set of equations (Table 2) also requires a large number of auxiliary, algebric equations as component model parts; for example relationships for f_s, f_w, h_{gp}, h_{gw}, ε_{app} etc. These relationships are taken from the literature and the details are given by Goyal (1).

Furthermore, the model has been developed here for coal hydropyrolysis. Nevertheless, the formulations and the method of solution are flexible and can be easily manipulated for other entrained flow gasifiers, for example, peat gasification.

Solution Methodology

The entrained flow hydropyrolysis reactor has been modeled in the preceding section by a set of fifty three simultaneous nonlinear first order ordinary differential equations. The solutions to the formulations are sought in the form of time histories of quantities such as particle and gas temperature, their compositions, velocities, densities, and other derived quantities such as conversion etc. This system of equations is very stiff primarily due to the high temperature dependence of various hydropyrolysis reactor rates (1). A computer program based on implicit backward differentiation formulas of orders one through five (Gear's method) has successfully been used here in solving this set of stiff equations.

Comparison With Experimental Data

Cities Service Research and Development Company has performed studies on the hydropyrolysis of Montana Rosebud subbituminous coal, Western Kentucky No. 9/14 bituminous coal, and North Dakota lignite. Experiments were conducted in a bench-scale system of 2-4 lb/hr nominal capacity entrained-downflow tubular reactor. Different types of reactors (free fall, vertically-entrained, helically-entrained) were used in this study. The reactor was mounted inside an electric furnace designed for isothermal operation. Preheated hydrogen and coal were mixed inside a high-velocity coaxial injector nozzle located near the entrance to produce very high heating rates. The coal-hydrogen mixture moved to the reactor outlet where it was quenched to below 1000°F directly by a stream of cryogenically-cooled hydrogen, which terminated reactions. A more detailed description of the reactor system has been given by Hamshar et al. (7).

The reactor and coal types, flow rates, and operating conditions used in different test runs have been summarized along with experimental results by Cities Service Research and Development Co. (6). Operating conditions were varied in the nominal ranges of 1400°-1700°F reactor temperature, 34-170 atm reactor pressure, 0.18-1.3 hydrogen/coal weight ratio, and 0.3-25 sec vapor residence time. A few runs utilized a 78/22 (vol.) mixture of hydrogen/methane feed gas; the remainder used high purity hydrogen. The reactor temperature was measured by a series of removable skin thermocouples tacked along the wall of the reactor. However, these measured temperature profiles have not been reported. Instead, the mix temperature, maximum gas temperature and equivalent isothermal temperature for each run have been reported.

A total of twenty-one runs having good carbon and ash balance closures have been simulated in this study. The operating conditions for these runs are given by Goyal (1). The coal feed in these runs was dry. Also, several of their tests were conducted in helical coil reactors. Oko et al. (8) from Cities Service have recently reported the results of a helical glass cold-flow study. In this apparatus, average particle velocities were measured in the same flow regimes that were experienced in the bench-scale hydropyrolysis apparatus. The following empirical equation was derived to estimate the slip velocity factor:

$$\bar{\phi}_s = \bar{v}_s/\bar{v}_g = 1 - k_o \, Reg^p R_c^q \, (D_H/D_t)^r \qquad 25)$$

where k_o, p, q, and r are empirical constants.

Several important reactor performance parameters have been compared here in Figures 1 through 4. Figure 1 shows a comparison of calculated and experimental carbon conversion for different types of coals. As seen from this figure, the computer model calculations agreed quite closely with the actual experimental results. Figure 2 compares the predicted moisture-ash-free (MAF) coal conversions with the experimental values of these conversions. The comparison is quite good; however, the model somewhat underpredicts this coal conversion. This is primarily due to the fact that Johnson's model allows for only 89% of coal oxygen evolution whereas the experimental oxygen evolution is approximately 97%. If this additional oxygen were allowed to evolve, then the predicted coal conversion would increase by approximately 1.5%. This would result in an excellent comparison.

Figure 3 compares the predicted carbon conversion to light hydrocarbons methane + ethane with experimental values. The predicted methane + ethane yield is somewhat higher. The comparison of carbon oxides yield is shown in Figure 4. The model underpredicts this yield. Again, it is probably because Johnson's model allows for only 89% coal oxygen removal while reported coal oxygen removal is in the range of 95% to 100%.

As mentioned earlier, the model is capable of predicting time histories of quantities such as conversions, particle and gas temperatures, their flow rates, compositions, velocities, etc. As an example, some of the important reactor variables have been summarized (as a function of reactor length) in Figures 5 to 7 for Run No. KB-5 with Western Kentucky bituminous coal feed. In this test, a 17.7 ft long and 0.26 inch ID reactor was operated at 1557°F (EIT) and 1500 psia hydrogen pressure. The superficial gas velocity, vapor residence time and hydrogen/coal weight ratio were 12.3 ft/sec, 1.44 sec, and 1.17 respectively. The wall temperature was assumed to be 1581°F which is the average of reported maximum reactor temperature and EIT. The data points shown in these figures are the actual experimental results at the reactor's exit.

Figure 5 shows carbon and MAF coal conversions as a function of reactor length. As seen from the figure, a significant conversion (12% to 14%) takes place within 0.1 ft reactor length. Note that the reactor length has been shown on a log scale, which allows to show the significant conversions occurring in the extremely short distance near the entrance. The particle residence time is also calculated by the model and is shown at the top of the graph.

Figure 6 shows the carbon conversion to different species over the length of the reactor. It shows that oil is evolved first and very rapidly. Again, log scale has been used to represent the reactor length. The change in the gas composition over the reactor length is shown in Figure 7. Pure hydrogen feed gas was used in this test and 96% of the exit product gas was hydrogen. This is so because excess amount of hydrogen was used in this run.

The mathematical model developed here has been used successfully to describe these hydropyrolysis reactors. Reasons for small discrepancies in experimental and predicted reactor performances are attributable to inadequacies in model formulation, unavailability of experimental data particularly reactor wall temperature profiles, and uncertainties in the experimental data.

A detailed parametric study has been performed using this model to identify important reactor parameters for the design of commercial entrained flow hydropyrolysis reactors. The results are given elsewhere (1).

Acknowledgement

The authors are grateful to Dr. S. Weil for providing many helpful suggestions and criticisms throughout this entire study.

Nomenclature

a	Contact area between solids and gas per unit reactor volume
a	Number of carbon atoms per mole of gas species $(CH_z)_a$
A	Reactor cross-sectional area
b	Number of carbon atoms per mole of gas species $(CH_M)_b$
B_j	Rate of gas species j going from solid phase to gas phase (i.e. crossing boundary) per unit reactor volume
C	Fractional coal conversion (moisture-free)
C_{af}	Fractional coal conversion (moisture-ash-free)
C_{pgj}	Heat capacity of gas species j
C_{psi}	Heat capacity of solid species i
D	Derivative with respect to distance along reactor (x)
D_H	Helix diameter
D_p	Particle diameter
D_t	Reactor diameter
f_s	Drag force exerted by fluid on the particles per unit volume of particles
f_w	Frictional force between the gas and the wall of the reactor
F	Solids flow rate per unit reactor cross-sectional area
g	Gravitational acceleration
g_c	Conversion factor (32.2 lbm-ft/sec^2/lbf)
G	Gas flow rate per unit reactor cross-sectional area
h_{gj}	Total enthalpy of gas species j
h_{gp}	Overall heat transfer coefficient between gas and solid particle
h_{gw}	Overall heat transfer coefficient between gas and wall
h_{si}	Total enthalpy of solid species i
H_{2gs}	Rate of gaseous hydrogen reacting with solid phase per unit reactor volume
H_{ls}	Wall heat losses from reactor per unit reactor length (due to convection between gas and wall)

H_{lsa} Total wall heat losses from reactor per unit reactor length per unit reactor cross-sectional area

M Atomic ratio of hydrogen to carbon in oils and tars (also in species CH_M)

M_j Molecular weight of gas species j

P Total reactor pressure

Q_{ash} Ash flow rate per unit reactor cross-sectional area

R Universal gas constant

R_c Char to gas weight ratio

Reg Gas Reynolds number

R_i Reaction rate ($d\xi_i/dt$) for i^{th} reaction

$(S_i)_s$ Mass rate of solid species i produced per unit reactor volume

$(S_j)_g$ Mass rate of gas species j produced per unit reactor volume

t Time

T_g Gas temperature

T_s Solids temperature

T_w Wall temperature

v_g Gas velocity

v_s Solids velocity

V_R Ratio of particle volume at anytime to its initial volume

x Distance along reactor

x Atmoic ratio of hydrogen to carbon in species CH_x (semichar)

y Atmoic ratio of hydrogen to carbon in species CH_y (final product char)

y_j Mass fraction of gas species j

z Atmoic ratio of hydrogen to carbon in hydrocarbon gases other than CH_4 and C_2H_6 (also in solid species CH_z)

θ Angle between horizontal line and the reactor axis

θ_g Gas residence time

θ_s Solids residence time

ρ_{ash} Ash density

ρ°_{ash} Ash density of raw coal

ρ_g Gas density

ρ_s Solids density

ϵ Voidage

ϵ_{app} Effective emmissivity

σ_B Stephen-boltzman constant

γ_s Swelling parameter

ξ_i Fraction of solid species i not yet gasified ($i \neq CH_y$)

ξ_i° = 1 for $i \neq CH_y$

$\omega^\circ_{CH_y}$ Maximum lbs of CH_y that can be formed per lb of ash (equation 21)

ω_i° Lbs of solid species i in raw coal per lb of ash ($i \neq CH_y$)

ϕ_s Slip velocity factor defined as the ratio of solids velocity to gas velocity

Subscript

i Refers to solid species

j Refers to gas species

References

(1) Goyal, A., Mathematical Modeling of Entrained-Flow Coal Gasification Reactors, Ph.D. Thesis, Illinois Institute of Technology, Chicago, IL, May (1980).

(2) Johnson, J. L., ACS, Div. of Fuel Chem. Preprints, 20, No. 3, 61 (1975).

(3) Johnson, J. L., ACS, Div. of Fuel Chem. Preprints, 22, No. 1, 17 (1977).

(4) Johnson, J. L. and D. Q. Tran, "Kinetics of Devolatilization and Rapid-Rate Methane Formation," Final Report, AGA Project IU-4-11, GRI Contract No. 5010-322-0025, Report No. GRI-78/0049, Institute of Gas Technology, Chicago, IL, Nov. (1980).

(5) Suuberg, E. M., W. A. Peters and J. B. Howard, Ind. Eng. Chem. Process Design Develop., 17, No. 1, 37 (1978).

(6) Cities Service Research and Development Company, "Hydrogasifier Development for the Hydrane Process," Final Technical Progress Report, Feb. 1977 to July 1978, Subcontract to Rocketdyne Division of Rockwell International Corporation of DOE Contract No. EX-77-C-01-2518, Cranbury, NJ, July 31 (1978).

(7) Hamshar, J. A., S. J. Bivacca and M. I. Greene, Paper presented at 71st Annual AIChE Meeting, Miami Beach, FL, Nov. (1978).

(8) Oko, U. M., J. A. Hamshar, G. Cuneo and S. Kim, ACS, Div. of Fuel Chem. Preprints, 24, No. 3, 82 (1979).

(9) Gidaspow, D., "Hyperbolic Compressible Two-Phase Flow Equations Based on Stationary Principles and the Fick's Law," in Two Phase Transport and Reactor Safety, edited by S. Kakac and T. N. Veziroglu, 1, p. 283, Hemisphere Publishing Corp., Washington, D. C. (1978).

Table 1. Solid and Gas Species

Solid Species	Gas Species
1. HOH	1. CO
2. O·O	2. CO_2
3. OH	3. H_2
4. CO	4. H_2O
5. COO	5. CH_4
6. CHH	6. C_2H_6
7. CH_z	7. $(CH_z)_a$
8. CH_M	8. $(CH_M)_b$
9. CH_x	9. Inert gas
10. CH_y	
11. Ash	

Table 2. Differential Equations Model

Total Solids Mass Balance: $D[(1-\varepsilon)\rho_s v_s] = \Sigma(S_i)_s = D(F)$ 1)

Total Gas Mass Balance: $D(\varepsilon \rho_g v_g) = \Sigma(S_j)_g = D(G)$ 2)

Solids Species Balance: $D(Q_{ash}\omega_i^{\circ}\xi_i) = (S_i)_s$ 3)

Gas Species Balance: $D(\varepsilon \rho_g v_g y_j) = (S_j)_g$ 4)

Constitutive Equation for the Mixture: (Ref. 9)

$$-(1/2)D\left[|v_g - v_s|(v_g - v_s)\right] = f_s/\rho_s - g \sin\theta \quad 5)$$

Mixture Momentum Balance:

$$g_c D(P) = (v_g - v_s)\Sigma(S_i)_s - (1-\varepsilon)\rho_s v_s D(v_s) - \varepsilon \rho_g v_g D(v_g) - f_w - [\rho_s(1-\varepsilon)+\rho_g\varepsilon]\, g \sin\theta \quad 6)$$

Solids Density: $D(\rho_s) = D[\Sigma(\omega_i^{\circ}\xi_i)\rho_{ash}^{\circ}/V_R]$ 7)

Gas Density: $D(\rho_g) = D[(P/RT_g)(\Sigma y_j/M_j)^{-1}]$ 8)

Table 2. Differential Equations Model (Cont.)

Solids Phase Energy Balance:

$$D(T_s) = -[\{(-H_{2gs})(h_{gH_2})_{T_g} + \Sigma(B_j)(h_{gj})_{T_s} + h_{gp}a(T_s - T_g) - 4\sigma_B\varepsilon_{app}(T_w^4 - T_s^4)/D_t\}/Q_{ash} + \Sigma(\omega_i^\circ(h_{si})_{T_s} D(\xi_i)]/[\Sigma(\omega_i^\circ\xi_i C_{psi})] \quad 9)$$

Gas Phase Energy Balance:

$$D(T_g) = [(-H_{2gs})(h_{gH_2})_{T_g} + \Sigma(B_j)(h_{gj})_{T_s} + h_{gp}a(T_s - T_g) - H_{ls}/A - \Sigma(h_{gj})_{T_g}(S_j)_g]/[\Sigma(Gy_j C_{pgj})] \quad 10)$$

Fractional Coal Conversion:

$$D(C) = D[1 - \Sigma(\omega_i^\circ\xi_i)/\Sigma(\omega_i^\circ\xi_i^\circ)] = D[-\Sigma(S_i)_s/\{Q_{ash}\Sigma(\omega_i^\circ\xi_i^\circ)\}] \quad 11)$$

Particle Relative Volume:

$$D(V_R) = D[(1 + \gamma_s C_{af})^3] \quad 12)$$

Average Particle Diameter:

$$D(D_p) = (D_p/3V_R)D(V_R) \quad 13)$$

Gas Residence Time:

$$D(\theta_g) = 1/v_g \quad 14)$$

Particle Residence Time:

$$D(\theta_s) = 1/v_s \quad 15)$$

Total Heat Loss:

$$D(H_{lsa}) = H_{ls}/A - 4\sigma_B\varepsilon_{app}(T_w^4 - T_s^4)/D_t \quad 16)$$

Useful Algebric Equations:

$$\Sigma(S_i)_s = -\Sigma(S_j)_g \quad 17)$$

$$(S_i)_s = (1-\varepsilon)\rho_{ash}\omega_i^\circ\dot{R}_i \quad 18)$$

$$Q_{ash} = (1-\varepsilon)v_s\rho_{ash} \quad 19)$$

$$G = \varepsilon\rho_g v_g \quad 20)$$

$$\omega_{CH_y}^\circ = (M_{CH_y}/M_{CH_x})\omega_{CH_x}^\circ \quad 21)$$

$$H_{ls} = \pi D_t h_{gw}(T_g - T_w) \quad 22)$$

$$C_{af} = C[\Sigma(\omega_i^\circ\xi_i^\circ)/\Sigma\{(\omega_i^\circ\xi_i^\circ)-1\}] \quad 23)$$

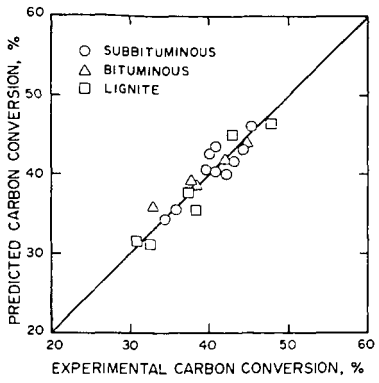

Figure 1. Comparison of Experimental and Predicted Carbon Conversion

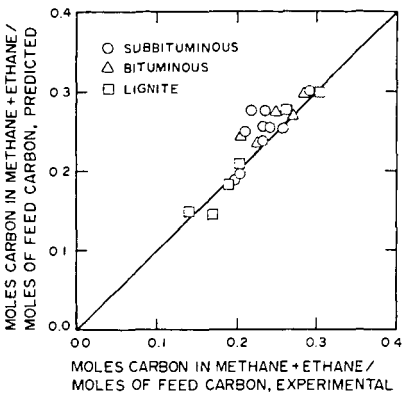

Figure 3. Comparison of Experimental and Predicted Methane + Ethane Yields

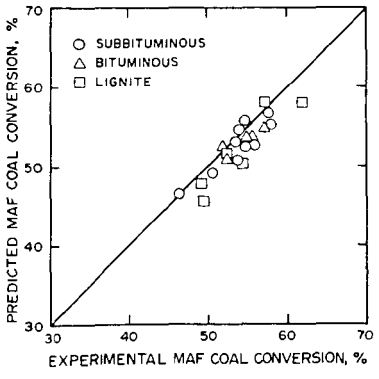

Figure 2. Comparison of Experimental and Predicted Moisture-Ash-Free Coal Conversion

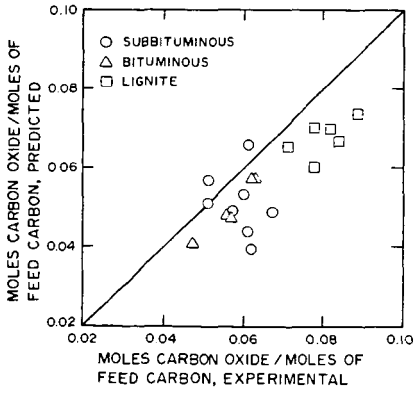

Figure 4. Comparison of Experimental and Predicted Carbon Oxides ($CO + CO_2$) Yields

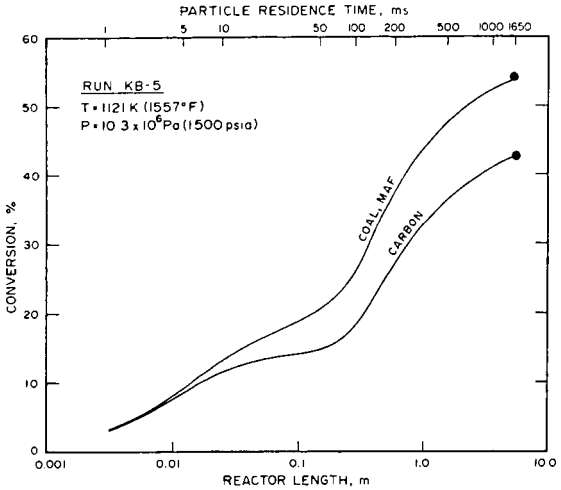

Figure 5. Carbon and Moisture-Ash-Free Coal Conversions along Reactor Length

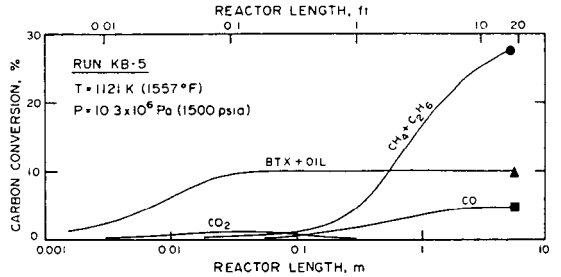

Figure 6. Distribution of Total Carbon Conversion to Different Species along Reactor Length

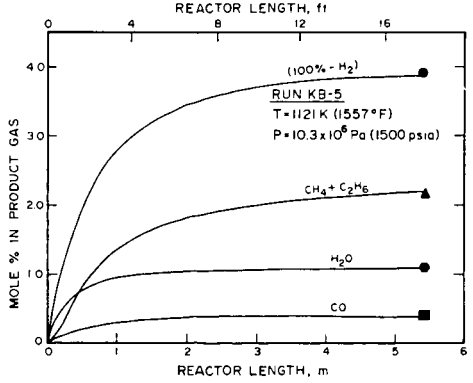

Figure 7. Gas Composition along Reactor Length

The Effect of Potassium Carbonate on the Gasification of Illinois No. 6 Coal

A.H. Pulsifer and J.F. McGehee, Department of Chemical Engineering and Engineering Research Institute, Iowa State University, Ames, Iowa 50011.

L. Saroff, U.S. Department of Energy, Pittsburgh Energy Technology Center, Pittsburgh, Pennsylvania 15213.

Catalyzed coal gasification can lead to reduced gasifier size and lower gasification temperatures which give greater thermal efficiencies. Therefore, an investigation of the steam gasification of a bituminous coal under moderately high pressures was conducted. The primary objective of the study was to determine the influence of an alkali metal carbonate catalyst on the kinetic parameters of the gasification reaction.

The coal chosen for the study was an Illinois No. 6 coal and this material was gasified both with and without the addition of potassium carbonate. Experiments were carried out at temperatures between 700 and 900°C and at a pressure of 2.17 MPa (21.4 atm). The partial pressures of steam, carbon dioxide and hydrogen were also varied during the investigation. The carbon gasification rate was modeled using an unreacted, shrinking-core model and kinetic constants and activation energies were determined.

Experimental Methods

The apparatus used to gasify the coal was a high-pressure, tubular, fixed bed reactor with an external heat supply. One of the unique features of this apparatus was its charging system. A 10 g sample of coal was held at a temperature near ambient in a pressurized vessel located above the reactor. Actuation of a ball valve allowed the sample to fall into the reactor, commencing the experimental run.

The apparatus was able to gasify a sample of coal with steam, or mixtures of steam and H_2,N_2, or CO_2. Carbon gasification rates were determined from the product gas flowrate and composition. The essential features of the apparatus are shown in Fig. 1.

The reactor and coal charging vessel were constructed from type 316 stainless steel. The reactor body was a 21-inch (53.3 cm) long, 3/4-inch schedule 160 tube with an outside diameter of 1.050 in. (26.7 mm) and an inside diameter of 0.614 in. (15.6 mm). A 0.125-in. (3.2 mm) thick porous stainless steel disc was located inside the tube, 6.5 in. (16.5 cm) from the bottom. This disc supported the bed of coal inside the reactor.

The coal charging vessel, a cylindrical funnel-shaped container with a volume of approximately 50 cm^3, was connected to the top of the reactor by a vertical 3/4-inch schedule 160 tube with an inside diameter of 0.464 in. (11.8 mm). At the bottom of this vessel was a ball valve. Charging the reactor was accomplished by opening the valve by means of a pneumatic actuator. The coal then fell a distance of 11 in. (27.9 cm) into the reactor.

The heat necessary to generate steam and gasify the coal was supplied externally through electric resistance heaters. There were three separate electrical heating circuits. These supplied the gas preheater and steam vaporizer, the reactor furnace, and the bottom flange heater.

Water for steam generation was delivered to the system by a high-precision

metering pump. The water used was high purity, liquid chromatography solvent grade material. The flowrate of the other gases supplied to the reactor were controlled by means of two electronic thermal-type mass flow controllers.

After exiting the reactor, the hot product gases and unreacted steam were filtered using glass wool to remove tar and liquid products. The gases were then cooled to condense excess steam, the pressure of the cooled gases was reduced to atmospheric, and they were then analyzed. A quadrapole mass spectrometer was used to determine the product gas compositions. The flowrate of product gas was determined with a wet test meter.

All of the material used in this study was Illinois No. 6 coal. Its proximate and ultimate analyses, free swelling index, and heating value are listed in Table 1. The coal had been previously pulverized, and particles with sizes between 0.297 mm and 0.149 mm(50 x 100 U.S. mesh) were retained.

The catalyst used in this investigation was anhydrous reagent quality potassium carbonate. The catalyzed samples used in the gasification experiments were produced by solution impregnation of the raw coal with K_2CO_3 in an autoclave at 285°C and 7.0 MPa with the product being dried by flash evaporation. The uncatalyzed samples were subjected to mild oxidative pretreatment. This was necessary to prevent agglomeration of coal in the fixed-bed reactor.

An experimental run was carried out in the following manner. Appropriate conditions of reaction temperature and reactant gas partial pressure were selected. The flowrates of nitrogen and carbon dioxide or hydrogen were adjusted to meet these specifications as measured by timed readings of the wet test meter. Steam flow was commenced by adjusting the water metering pump. Finally the ball valve was opened and the coal entered the reaction zone.

During the first five minutes of the run, the flow of products was rapid due

Table 1. Analyses of Illinois No. 6 coal.

	Moisture free coal	Moisture and ash free coal
Proximate analysis (wt. %)		
Volatile matter	40.5	46.5
Fixed carbon	46.5	53.5
Ash	13.0	- -
Ultimate analysis (wt.%)		
Hydrogen	4.7	5.4
Carbon	67.7	77.8
Nitrogen	1.1	1.3
Sulfur	3.8	4.3
Oxygen	9.8	11.2
Ash	13.0	- -
Heating Value	12307 Btu/lb (28619 kJ/kg)	14148 Btu/lb (32900 kJ/kg)
Free swelling index	3.5	3.5

to the devolatilization of the coal and the time at every one-quarter revolution of the wet test meter (0.0125 cu ft, 354 cm^3) was recorded. After five minutes, the volume reading of the wet test meter was recorded at 3-minute intervals. Discrete values of the concentration of each gas were also read from a digital display and recorded by the operator at intervals of 2.5 minutes, beginning at 5 minutes.

The length of time of each experiment varied. In the experiments conducted at 800°C and 900°C, the 10 g coal sample was usually allowed to react until 80-90% conversion of carbon had been achieved. At 700°C, the experiments were terminated after approximately two hours.

At the end of the experiment, flow of water to the steam vaporizer and flow of gases were terminated. All heaters were shut down, and the reactor furnace was opened. When the apparatus was cool, the reactor was depressurized and opened. The char and ash were withdrawn and weighed. All condensate was drained from the trap and the volume of water recorded. The tar filter was removed and weighed immediately.

Results

In this study, the influence of the following parameters on the steam gasification rate of Illinois No. 6 coal was investigated: the presence of K_2CO_3 as a catalyst; the partial pressures of steam, CO_2 and H_2; and reaction temperature. The total pressure of the system was held at a constant value of 2.17 MPa (21.4 atm) throughout the study. The total flowrate of gases into the reaction zone was also kept fixed in each experiment at some value between 980 and 1020 sccm. Variation of the reactant gas composition was accomplished by increasing the mass flowrate of steam, CO_2 or H_2 and simultaneously decreasing the mass flowrate of the inert carrier gas, nitrogen. Nitrogen was both a diluent and a carrier gas for product removal.

Runs were made at 700, 800 and 900°C with the pretreated coal and coal impregnated with 10 wt.% K_2CO_3. The effect of CO_2 concentration on the gasification rate of K_2CO_3-impregnated coal was studied at a constant steam partial pressure in a series of 6 runs. An additional 6 runs were made with a mixture of steam, N_2, and H_2 of constant composition to evaluate the magnitude of hydrogen inhibition of the steam gasification rates. Runs were made at each of the three temperatures, 700, 800 and 900°C, with both the pretreated coal and coal impregnated with 10 wt.% K_2CO_3.

Using the data of each experiment, a number of calculations were performed. The gasification rate and carbon conversion were calculated from a balance of carbon-containing reaction products. The extent of reaction of the steam was determined from a balance of hydrogen-containing or oxygen-containing products. Reactant and product gas partial pressures were computed at the reactor inlet and outlet. From these partial pressures, the apparent equilibrium constants of the water-gas shift, carbon-steam, and carbon-H_2 reactions were calculated. Finally, product gas sums and overall material balances were determined for each experiment.

Gasification rate

The carbon gasification rate was generally high initially, decreased rapidly and then slowly decreased throughout the remainder of the run. Fig. 2 shows typical results obtained at 700°C with a catalyzed coal sample. The initial peak in the curve seemed to be caused by devolatilization of the coal, which was followed by gasification of the base carbon in the sample.

To obtain a quantitative measure of the reaction rate, the shrinking, unreacted-core model for the case of complete gasification of a spherical, solid particle under conditions of chemical reaction rate control was used to describe the carbon

conversion-time data.* The integrated form of the equation based on this model is

$$1 - (1 - X_c)^{1/3} = \frac{kC_s^n t}{\rho_p R}$$

where X_c = carbon conversion
k = reaction rate constant
C_s = concentration of gaseous reactant at particle surface
n = reaction order
ρ_p = molar density of particle
R = initial radius of particle
t = time

In general, the model did not fit the initial data where devolatilization was occurring, but a good fit was obtained over the range of carbon conversions from 0.3 to 0.8. Applying the model to data from all the runs over the range of conversions from 0.3 to 0.7 using linear regression analysis gave correlation coefficients of 0.98 or larger except for two runs where the coefficients were 0.95 and 0.91.

To determine the reaction order with respect to steam concentration, n, a multiple linear regression analysis was performed on the data from the gasification experiments where only steam and nitrogen were used. Within the standard error of the estimate, the overall reaction order was one for both K_2CO_3-catalyzed and uncatalyzed steam gasification.

Assuming first order kinetics and using the Arrhenius expression, the frequency factor and activation energy were calculated for both catalyzed and uncatalyzed steam gasification of Illinois No. 6 coal. The derived reaction rate parameters are summarized in Table 2. As expected, the overall activation energy was somewhat lower for catalyzed gasification.

Apparent Equilibrium Constants

The value of the apparent water-gas shift equilibrium constant, $K_S = (pCO_2)(pH_2)/(pH_2O)(pCO)$, tended to decrease from the time of peak gasification rate until devolatilization was complete. From the time devolatilization was complete until the carbon had completely gasified, the value observed was approximately constant. The value of K_S for each experiment, over the time for which it was approximately constant, is compared in Fig. 3 with a literature value of K_S over the range of temperatures from 700°C to 900°C.

Table 2. Arrhenius parameters for steam gasification of Illinois No. 6 coal.

Material Gasified	Parameter	Estimate	Standard error of estimate	Correlation Coefficient
10% K_2CO_3-impregnated coal	Activation energy	133.7 kJ/mol (31.7 kcal/mol)	13.8 kJ/mol (3.3 kcal/mol)	0.931
	Frequency factor, min^{-1}	1.32×10^8	4.5	
Oxygen-pretreated coal (uncatalyzed)	Activation energy	151.5 kJ/mol (36.2 kcal/mol)	6.3 kJ/mol (1.5 kcal/mol)	0.986
	Frequency factor, min^{-1}	2.94×10^8	2.1	

*For a derivation of the model, see Levenspiel, O. 1972. Chemical Reaction Engineering. 2nd ed. Wiley, New York.

The values of K_S fall both above and below the theoretical curve. Some deviation is due to the sensitivity of K_S to errors in calculation of product gas partial pressures. At 700°C, the gasification rate was slow and steam conversion was slight. Therefore, equilibrium of the water-gas shift reaction may not have been reached. At 800°C and 900°C apparent values of K_S for both catalyzed and uncatalyzed gasification are closer to the theoretical curve than were the values at 700°C. If a 20% margin of uncertainty is assumed, the K_S values of most experiments at 900°C indicate the attainment of water-gas shift equilibrium.

In contrast, the carbon-steam and carbon-H_2 reactions did not appear to be in thermodynamic equilibrium. Neither equilibrium constants reached a consistent value at any time during the burnoff of the carbon and both values were at least an order of magnitude smaller than their theoretical value during the char gasification period.

Influence of CO_2 on the gasification rate

To determine the effect of CO_2 partial pressure, a series of 5 runs was made at constant steam flowrate while varying the CO_2 concentration. These runs were carried out with 10 wt.% K_2CO_3-impregnated coal at 800°C and the CO_2 partial pressure was varied from 97 kPa (0.96 atm) to 576 kPa (5.68 atm) using a constant steam pressure of 1.35 MPa (13.3 atm).

The calculated kinetic constants for these runs were generally somewhat lower than the value determined with pure steam. However, the deviation was within the expected range introduced by experimental errors. Therefore, the only conclusion that may be drawn from this set of experiments is that CO_2 concentration, over the range used, exerted a relatively small effect on the steam gasification rate of K_2CO_3-impregnated coal when compared with the effects of steam concentration and temperature.

Influence of H_2 on the reaction rate

Runs were made at 700, 800 and 900°C with both 10 wt.% K_2CO_3-impregnated coal and untreated coal. All 6 runs were done with the same hydrogen and steam partial pressures, namely 428 kPa (4.22 atm) and 1.69 MPa (16.7 atm), respectively.

Hydrogen inhibited the steam gasification rate of both coal samples. The results of the experiments with the K_2CO_3-impregnated coal showed that the magnitude of this inhibition decreased with increasing temperature for the catalyzed reaction. Comparison of the k values obtained with and without H_2 present show that the ratio of $k_{H_2O/H_2}/k_{H_2O}$ increased from 0.13 at 700°C to 0.38 at 900°C. The ratio of the k values was higher for uncatalyzed coal and did not change systematically. This ratio was 0.51 at 700°C, 0.27 at 800°C and 0.47 at 900°C. At atmospheric pressure, the inhibition of the carbon-steam reaction by hydrogen is expected to decrease with increasing temperature because of the relative magnitudes of the elementary activation energies. At higher pressures, the trend is probably more complicated, since the reaction steps leading to CH_4 production are significant. CH_4 generation rates were approximately the same in the char gasification periods for reactions both in pure steam and in the steam/H_2 mixture. CH_4 represented a greater percentage of the total product gas in the experiments with the steam/H_2 mixture than in those with pure steam.

Conclusions

The overall gasification reaction was found to be first order with respect to steam concentration, with the rate being unaffected by CO_2 and inhibited by hydrogen. The variation of gasification rate with carbon conversion was described by the unreacted, shrinking-core model, with the rate constants for runs catalyzed by K_2CO_3 being about four times those for uncatalyzed runs. The activation energies for the

catalyzed and uncatalyzed runs were 134 and 152 kJ/mol, respectively. The principal products of both catalyzed and uncatalyzed steam gasification were H_2 and CO_2. The water-gas shift reaction reached equilibrium for most experiments at 900°C and some at 800°C, with the presence of K_2CO_3 having little effect on the approach to equilibrium.

Acknowledgement

The experimental portion of the study was carried out with the cooperation and financial support of the United States Department of Energy, using the facilities of the Pittsburgh Energy Technology Center in Bruceton, Pa. Mr. John W. Courts assisted in the operation of the experimental apparatus.

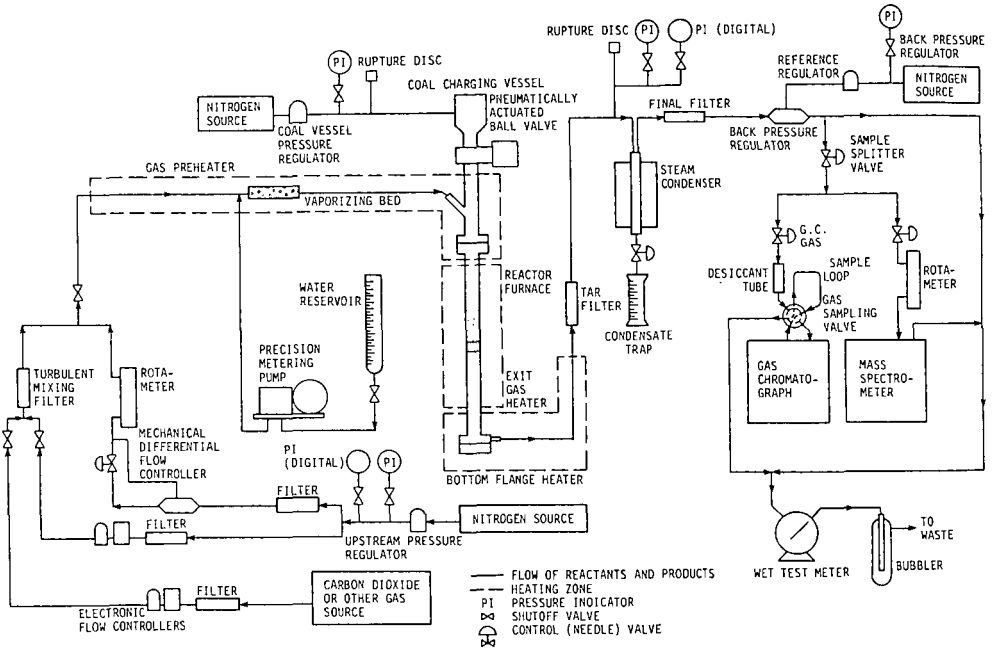

Figure 1. Flow diagram for experimental apparatus

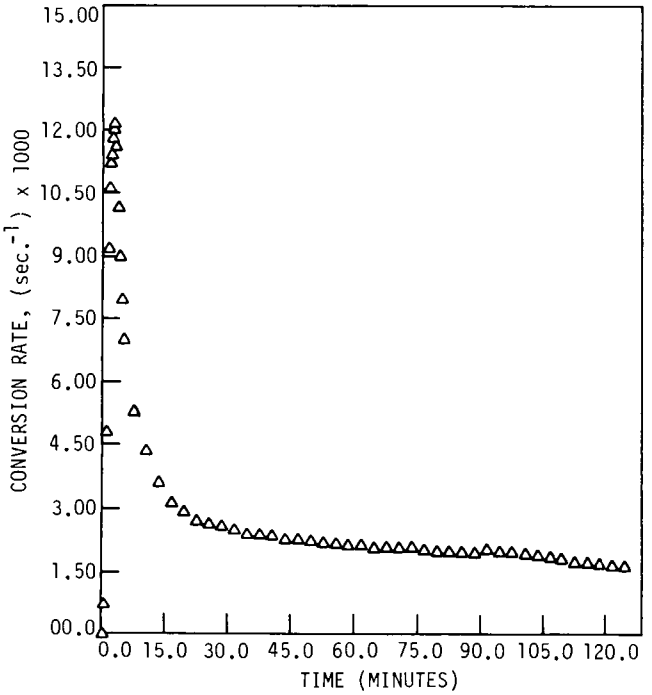

Figure 2. Rate of carbon conversion versus time; conditions = 700°C, 10 wt.% K_2CO_3-impregnated coal, and N_2-steam as reactant gas

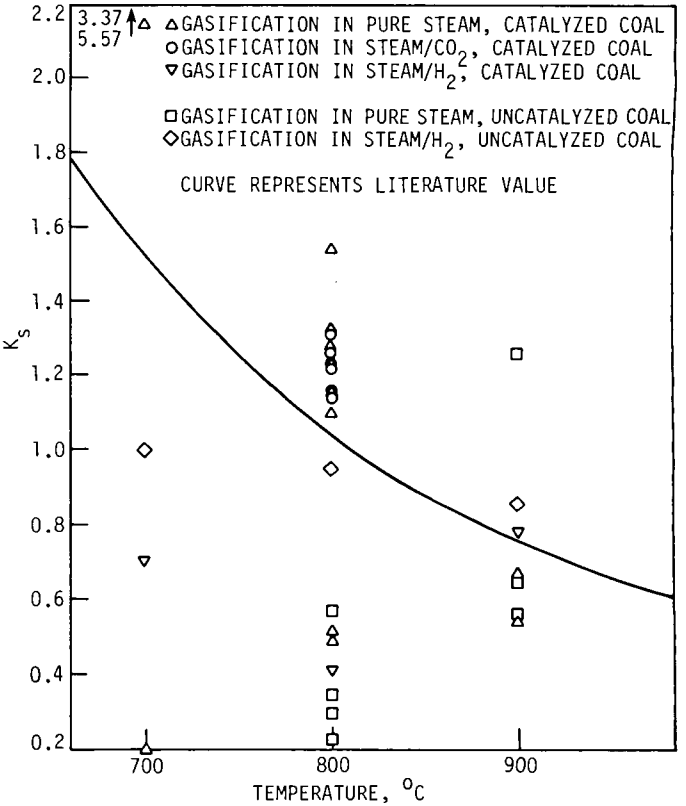

Figure 3. Approach of product gases CO, CO_2, H_2, and H_2O to thermodynamic equilibrium of the system: $CO + H_2O \rightarrow CO_2 + H_2$

CATALYTIC EFFECTS OF ALKALI METAL SALTS IN THE GASIFICATION OF COAL CHAR

D. W. McKee, C. L. Spiro, P. G. Kosky and E. J. Lamby

General Electric Corporate Research & Development
Schenectady, NY 12301

INTRODUCTION

Coal is a complex and variable carbonaceous rock which is composed basically of two types of materials. The macerals or carbonaceous remains of plants constitute the organic fraction of coal, with the remainder comprising minerals or inorganic impurities present in the parent vegetation or deposited subsequently. The major mineral components of coal include clays, alkaline carbonates, metallic sulfides, oxides and quartz,[1] but the minor and trace impurities may include most of the elements of the Periodic Table.

The reactivity and properties of coal can be profoundly influenced by these inorganic impurities.[2-4] Currently, there is interest not only in the effects of mineral matter on the chemical behavior of coal but also in the possibility of adding catalysts to coal in order to lower the temperature required for gasification processes. For example, it has been known for over one hundred years that the reactivity of coal and char towards steam is promoted by the addition of alkalis, such as caustic soda or lime.[5] There are a number of processes under development today which utilize the catalytic properties of alkali carbonates to improve the reactivity of coal in the gasifier.[6-8] Earlier work has shown that the carbonates and oxides of the alkali and alkaline earth metals are among the most active catalysts for the gasification of carbonaceous materials in steam and carbon dioxide.[9-11] However, there is still no generally accepted explanation for these catalytic effects.[12]

This paper describes the results of a continuing study of the catalytic behavior of salts of the alkali metals in the gasification of coal char by steam and CO_2. The main purpose of this work is to investigate possible mechanisms of the catalysis and to elucidate the effects of mineral impurities on the reactivity of coal char. For this purpose the behavior of a typical char and a pure graphite powder have been compared in the presence and absence of added alkali catalysts. In a companion paper (13), the effects of char pyrolysis temperature, surface area and mode of catalyst addition are described.

EXPERIMENTAL

Materials

The char used in this work was prepared from a large sample of Illinois #6 HVB bituminous coal from Inland Mine #1, Sessor, Illinois. Proximate and ultimate analyses of this coal sample are given in Table I. The results of x-ray diffraction on ash residues after low temperature ashing (LTA) showed major amounts of kaolinite and minor amounts of quartz and pyrite.

Initially the coal was coarse ground, homogenized, vacuum dried at 105°C and then stored in a vacuum desiccator. In some cases salt catalysts were added to coal samples before pyrolysis. Thus, about 15 g. of the dried coal was micronized in a nitrogen-driven fluid grinding mill to give a particle size of the order of several microns. A known amount, generally 5 percent, of the dried powder salt, e.g., K_2CO_3, CH_3COOK, was then added to the coal and the mixture rolled for four hours in a rolling mill. The doped samples were then placed in alumina crucibles and pyrolyzed in nitrogen at 700°C for 2 hours. Observed weight losses of the coal

samples during this pyrolysis were of the order of 30 percent. In other cases the catalysts were added after charring at 700°C by mixing weighed amounts of salts and char together in a Fisher Minimill. The char samples had surface areas of approximately 280 $m^2/g.$, as determined by CO_2 adsorption at 195°K.

Spectroscopic grade graphite powder (-325 mesh, Type UCP-2^R, highest purity) was obtained from Ultra Carbon Corp. This material had an initial surface area of 7.5 $m^2/g.$, as determined by nitrogen adsorption at -195°C.

The salt additives were Analytical Reagent or Certified ACS Grade materials and were used without further treatment. The gaseous atmospheres used included Linde Instrument Grade carbon dioxide and Linde Ultra-High Purity Grade helium. For experiments in steam (water vapor), the helium was passed through a distilled water bubbler at 25°C to give a water vapor pressure of 23 mm. (3.1 kPa) in the gas stream.

Proximate Analysis

	% Moisture	% Ash	% Volatiles	% Fixed C	BTU/lb
As Received	0.72	9.68	39.45	50.15	12979
Dry Basis	-	9.75	39.74	50.51	13073

Free Swelling Index = 5

Ultimate Analysis

	% Moisture	% C	% H	% N	% Cl	% S	% O (diff.)
As Received	0.72	73.06	5.04	1.68	0.39	1.20	8.23
Dry Basis	-	73.59	5.08	1.69	0.39	1.21	8.29

Table I: Analyses of Illinois #6 Coal Sample

Procedure

Thermogravimetric studies and measurements of the isothermal kinetics of the catalyzed gasification of char and graphite in CO_2 and water vapor were carried out in the Mettler Thermoanalyzer-2 automatically recording balance as previously described.[14] Kinetic measurements at a series of constant temperatures between 600 and 1000°C were made on 200 mg. samples of the doped carbons, using flowing CO_2 at 1 atm. (1.02×10^2 kPa) and a flow rate of 200 $ml.min^{-1}$. Gasification in water vapor was accomplished in a water vapor-saturated helium stream (23 mm. H_2O, 3.1 kPa) at a flow rate of 300 $ml.min^{-1}$. Kinetic data were generally plotted in the form of Arrhenius plots (rates vs. $1/T°K$), the gasification rates at each temperature being derived experimentally from the relation,

$$\text{Rate } (min^{-1}) = \frac{dW/dt}{W_o}$$

where W_o is the initial weight of the sample. In all cases, in order to minimize the effects of changing surface area and catalyst concentration, the total weight loss during gasification of each sample was kept below 15 percent.

Some thermogravimetric measurements of the reactions between the salts and the carbons and between the salts and selected minerals were carried out by heating appropriate mixtures in the thermobalance at a linearly increasing temperature of $10^{o}Cmin^{-1}$ using flowing atmospheres of pure dry helium or carbon dioxide.

RESULTS

Catalyzed Gasification in Steam

As expected, the carbonates of the alkali metals proved to be effective catalysts for the gasification of both char and graphite in steam. In the case of the char, the addition of 5 percent by weight of the salts resulted in slightly more active chars when the catalysts were introduced prior to charring at 700°C rather than physically mixed with the char after charring (13). In general, the reactivity of the doped chars in steam decreased on successive thermal cycles and with time at a constant gasification temperature. This effect will be discussed in more detail below. Figure 1 shows Arrhenius plots (gasification rates vs. $1/T^{o}K$) for the 700°C char doped with 5 percent by weight of alkali carbonates after charring. These data were obtained during the second thermal cycle in each case. A similar order of catalytic activity was observed previously for graphite,[15] although in this case Na_2CO_3 was slightly less active than K_2CO_3. Pure graphite was considerably less reactive than the uncatalyzed char sample, however the catalytic effects of the added salts were more marked in the former case, so that the catalyzed gasification rates in steam were quite similar for both graphite and char over the 600-900°C temperature range. Gasification rates for graphite doped with 1 and 5 wt. percent of the alkali salts were about the same, whereas with the char a progressive increase in rate was observed with increasing carbonate concentration up to 20 weight percent, as shown in Figure 2. This marked difference in behavior between graphite and char was probably related to the large difference in surface area between the two materials although the active site area was not known in either case. However, with a series of chars, prepared in the presence and absence of added catalysts, there was no significant correlation between reactivity and surface area. In fact, surface areas were generally somewhat smaller for catalyst-doped samples than for uncatalyzed chars. Also there was little difference in gasification rates when the char particles were ground from ca. 1 mm. size to ca. 1 μm.[13] These results indicate that surface areas and particle size are not important parameters in determining char reactivity, at least for chars of the same type and the same heat treatment history. In the steam environment, Li_2CO_3 was clearly the most active catalyst, with Na_2CO_3 and K_2CO_3 exhibiting somewhat lower activity. Other additives, such as KNO_3 and K_2SO_4, also showed substantial catalytic activity, whereas KCl was somewhat less active.

As noted above, the catalyzed char samples showed a progressive loss in reactivity towards steam during the experiments. This phenomenon, which was not observed with graphite, was studied in some detail. Figure 3 shows kinetic data obtained with a char sample doped with 5 weight percent K_2CO_3 during three successive thermal cycles. The initially high gasification rates in steam fell by a factor of about two on the second cycle with progressively smaller deactivation effects on subsequent cycles. Figure 4 shows the results of isothermal rate measurements obtained at 800°C for char samples initially doped with 2, 5 and 10 percent K_2CO_3. In all three cases a rapid drop in gasification rate occurred during the first hour with more gradual decreases during the subsequent four hours of the experiments. In the case of the sample containing 10% K_2CO_3, the gasification rate was so high that the rate began to decrease after about 3 hours because of loss of contact between the catalyst phase and the residual char substrate.

In steam (water vapor) catalyst deactivation was observed for every catalyst additive tested, regardless of whether the salt was added before or after charring. Figure 5 shows data obtained from a char sample to which 5 wt. % potassium acetate had been added before

charring at 700°C. Again a marked progressive loss in activity was found on successive thermal cycles, accompanied by an increase in the apparent activation energy from 18 to 51 Kcal/mole during the four cycles shown.

As it was found that this progressive deactivation did not occur during the catalyzed steam gasification of graphite, it appeared unlikely that the effect was due to sintering, agglomeration or vaporization of the salt catalyst. It seemed more probable that catalyst deactivation was related to reaction of the alkali salts with minerals such as quartz, clay, kaolin, and pyrite present in the char samples. Some experiments were therefore carried out in the thermobalance, using mixtures of K_2CO_3 with these mineral species, to determine if solid state reactions might occur at temperatures in the gasification range (600-1000°C).

Figure 6 shows thermograms (weight change vs. temperature) for 200 mg. pure K_2CO_3 (dashed curve) and for a mixture of 200 mg. K_2CO_3 and 200 mg. powdered quartz (solid curve) on heating in a stream of dry helium during a linear temperature rise of 10°C/min. Following an initial dehydration at 100-150°C, the pure salt showed no further weight loss on heating to 980°C and a slight loss at higher temperatures due to vaporization above the melting point. On the other hand, the mixture of salt and quartz lost weight rapidly at temperatures above 750°C, probably as a result of evolution of CO_2 by reactions of the type

$$K_2CO_3 + SiO_2 = K_2SiO_3 + CO_2$$

A variety of silicate-forming reactions are in fact possible. The extent of these reactions at a given temperature and the temperature of inception of the solid state reactions would be expected to depend on the particle size and interfacial contact area between the solid phases. Also the presence of CO_2 in the gas phase would tend to suppress these reactions. Similar thermogravimetric data for (A) 200 mg. pure K_2CO_3, (B) 200 mg. of powdered illite clay, and a mixture of 200 mg. K_2CO_3 and 200 mg. illite, are shown in Figure 7. The curve labelled (A+B) is the sum of curves (A) and (B) and represents the weight changes expected for a salt-illite mixture if no reaction occurred between the two phases. It is evident from the lower solid curve in Figure 7 that a reaction between the clay and the salt took place above 700°C with a continuous loss in weight of the sample, probably as a result of liberation of CO_2. The composition of the mineral illite, a complex aluminosilicate, is, however, indefinite, so no equation can be written for this reaction. Illite, however, is an important major mineral constituent in many coals. Similar data for kaolin-K_2CO_3 mixtures are shown in Figure 8. A comparison of curve (A+B) for kaolin + K_2CO_3 with no reaction and curve C, the experimental thermogram for the mixture, indicates that a reaction between the mineral and the salt took place at temperatures above 700°C with the loss of a volatile product, most likely CO_2. In a CO_2 atmosphere, this reaction was inhibited (curve D), but even in this case a marked loss in weight occurred above 900°C. A possible reaction between the salt and the kaolin is

$$Al_2Si_2O_5(OH)_4 + K_2CO_3 = 2KAlSiO_4 + 2H_2O + CO_2$$

The expected weight loss for the completion of this reaction is 60 mg, which corresponds closely to the experimental loss in weight of the kaolin-salt mixture between 650 and 1100°C. The reaction of potassium salts with the mineral constituents of fly ash to produce the water-insoluble mineral kalsilite ($KAlSiO_4$) has been reported by Karr et. al. to occur in the presence of steam at 850°C.[16]

Catalyzed Gasification in CO_2

As expected, the alkali metal carbonates were found to be active catalysts for gasification of coal char in CO_2. Results for the catalyzed gasification of graphite have been reported previously.[14] With coal char the kinetic data were much more reproducible in CO_2

than in steam. Figure 9 shows data obtained for a char-5% K_2CO_3 (the same sample as that used in Figure 3) on gasification in 1 atm. CO_2 between 600 and 900°C. In this case, during four successive thermal cycles the kinetic data were remarkably constant, with only a slight decrease in rates between the first and second cycles. The apparent activation energy for this series of experiments was 49.3 Kcal/mole. Similar data for a char sample to which 5 % K_2CO_3 had been added before the 700°C charring step are shown in Figure 10. Again, following a small reduction in gasification rates between the first and second cycles, the reactivity on further cycling was reproducible, with an apparent activation energy of 53.8 Kcal/mole. Comparison with Figure 9 indicates that the catalytic effect of the K_2CO_3 was similar regardless of whether the salt was added before or after charring. Similar data for a CH_3COOK-doped char sample are shown in Figure 11. In this case also, following a slight reduction in reactivity between cycles 1 and 2, subsequent kinetic data were quite reproducible. Comparison with Figure 5 shows the marked difference in behavior of this doped char sample in the two gaseous environments.

Gasification data in CO_2 for char doped with 5% Li_2CO_3, Na_2CO_3 and K_2CO_3 (added prior to charring) are shown in Figure 12. In this environment there was no significant difference in activity between the three salts when compared on a weight % basis. The effect of increasing concentration of K_2CO_3 (added prior to charring) on the CO_2 gasification kinetics is illustrated in Figure 13. Reactivity generally increased with K_2CO_3 concentration, at least up to the 20% level, however, the effect on apparent activation energy was small.

Reaction between Alkali Carbonates and Carbon

When K_2CO_3 is heated with carbon in an inert atmosphere, a solid state reaction takes place between 600 and 900°C, depending on the particle size and extent of physical contact between the two phases. The products of this reaction are CO and potassium vapor which sublimes into the cooler parts of the apparatus.[15] Figure 14 shows thermograms (weight changes vs. temperature) for K_2CO_3-char and K_2CO_3-graphite mixtures on heating in dry helium in the thermobalance at an increasing temperature of 10°C/min. In the case of graphite, loss in weight became marked above 800°C and the reaction was essentially completed at 1000°C. The char had a much larger surface area than the graphite and reaction with the salt began at about 600°C. This solid state reaction, which takes place in the gasification range, is believed to play an important role in the gasification of carbon with CO_2 or steam in the presence of the K_2CO_3[10,14] as discussed in the next section.

DISCUSSION

The reactivities of coal chars are obviously strongly influenced by a number of factors such as charring temperature and thermal history, pore size distribution and the presence of ubiquitous mineral impurities. However, the catalytic behavior of additives such as the alkali metal carbonates is similar for char and graphite and the same mechanisms probably operate in both cases.

The main effect of the salt catalysts (Figures 1,2,12,13) in both gasification reactions is to increase the pre-exponential factor of the rate equation. Changes in the apparent activation energy are small from catalyst to catalyst and on increasing the salt concentration. The most likely explanation of this effect is that the salt reacts with the char substrate to produce active sites on the surface where gasification can proceed. Increasing the amount of salt present increases the effective concentration of these active sites up to the point at which the surface becomes saturated.

A plausible mechanism which has been proposed previously[10,14,15] to account for the catalytic effects of Na_2CO_3 and K_2CO_3 in these reactions is shown in Table II. A common first

step, reaction (1) is suggested for both reactions, with the subsequent steps being different for CO_2 and H_2O as the gaseous oxidant.

C - CO_2 REACTION

$$M_2CO_3 + 2C = 2M + 3CO \quad (1)$$
$$2M + CO_2 = M_2O + CO \quad (2)$$
$$M_2O + CO_2 = M_2CO_3 \quad (3)$$
$$C + CO_2 = 2CO$$

C - H_2O REACTION

$$M_2CO_3 + 2C = 2M + 3CO \quad (1)$$
$$2M + 2H_2O = 2MOH + H_2 \quad (4)$$
$$2MOH + CO = M_2CO_3 + H_2 \quad (5)$$
$$C + H_2O = CO + H_2$$

Table II: Carbon Gasification Catalyzed by Na_2CO_3 or K_2CO_3

Although reaction (1) possesses a positive free energy change at temperatures in the 600-1000°C range, at low partial pressures of CO the reaction can proceed rapidly, as shown by the TGA data in Figure 15. Figure 15 shows the equilibrium stability regions of K_2CO_3 and K(g) for reaction (1), calculated from free energy data, as functions of temperature and the partial pressures (in atmospheres) of K(g) and CO. The sloping lines at each temperature separate the region of stability of K_2CO_3 (upper left) from that of K(g) (lower right). An overall gasification rate of 5×10^{-3} min^{-1} (about the maximum attained in this study at 900°C) would give an ambient partial pressure of CO of about 10^{-3} atm. above the gasifying char sample. At this value of P_{CO}, and with a similar value of P_K, Figure 15 indicates that reaction (1) would be thermodynamically possible for all temperatures above about 800°C. At a temperature of 600°C the measured gasification rate, and the ambient value of P_{CO}, are about two orders of magnitude less than at 900°C and Figure 15 shows that reaction (1) is again possible for $P_K = P_{CO} = 10^{-5}$ atm. The steady state values of P_K reaction will in fact be much less than P_{CO} because of the occurrence of reactions (2) and (4). Direct evidence that reaction (3) does occur has recently been obtained by Wood et al.,[16] using high temperature Knudsen cell mass spectrometry. On heating K_2CO_3 and carbon together at temperatures of 500°C and above, the evolution of K vapor and CO could be measured. Thus, reaction (1), which is inhibited by increasing amounts of CO in the gas phase, is probably the rate determining step in the case of the gasification reactions catalyzed by Na_2CO_3 and K_2CO_3. Reactions (2) and (3) and also (4) and (5) have large negative free energy values at gasification temperatures and are thus favored thermodynamically, although little is known about their kinetics.

A somewhat different pathway probably operates in the case of the reactions catalyzed by Li_2CO_3 as Li_2O is more stable than the oxides of Na and K, also Li_2CO_3 is more easily hydrolyzed to hydroxide than the carbonates of Na and K. A possible sequence of reactions that might be involved in the catalysis process in the case of Li_2CO_3 is shown in Table III below. Evidence for the occurrence of these individual reactions is still, however, indirect and future efforts will be directed to exploring the catalytic process by the aid of isotopic tracers and in determining the relative rates of the elementary steps involved in the catalyzed gasification process.

C - CO_2 REACTION

$$Li_2CO_3 + C = Li_2O + 2CO \quad \text{(i)}$$

$$Li_2O + CO_2 = Li_2CO_3 \quad \text{(ii)}$$

$$C + CO_2 = 2CO$$

C - H_2O REACTION

$$Li_2CO_3 + H_2O = 2LiOH + CO_2 \quad \text{(iii)}$$

$$2LiOH + C = Li_2O + CO + H_2 \quad \text{(iv)}$$

$$Li_2O + H_2O = 2LiOH \quad \text{(v)}$$

$$C + H_2O = CO + H_2$$

Table III: Carbon Gasification Catalyzed by Li_2CO_3

The above mechanistic schemes, although feasible for the alkali carbonates, cannot readily explain the observed catalytic activity of the alkali halides in these reactions. Such salts as KF, NaF and LiCl have been found to be moderately active catalysts for the gasification of both char and graphite in steam and CO_2. The route by which the alkali halides function as catalysts in these reactions is not clear at this point. Direct reduction of these salts to alkali metal by reaction with the carbon substrate seems unlikely on thermodynamic grounds. However, although the direct hydrolysis reaction

$$KF + H_2O = KOH + HF \quad \Delta G^{\circ}_{1100K} = +24 \text{ Kcal/mole}$$

has a positive free energy change at gasification temperatures, appreciable and catalytically active concentrations of KOH might be formed in a flowing gas in which the partial pressure of HF is low. KF-char mixtures have, in fact, been observed to evolve appreciable amounts of HF during steam gasification,[18] hence dissociation and hydrolysis of the KF salt evidently does occur in the presence of carbon and steam. In CO_2 the mechanism of catalysis by KF cannot be interpreted on this basis. It is interesting, however, that the alkali halide salts are also moderately active catalysts for the oxidation of carbon by molecular oxygen.[19] On heating a mixture of graphite powder and pure KF in air at 900°C until the carbon was completely gasified, the residue was found by analysis to contain appreciable amounts of K_2O (2.4% by weight). A similar experiment with pure NaCl produced lower (0.4%) amounts of Na_2O. As no oxides could be detected in the original halide salts, the catalytically active alkali oxides may have resulted from the oxidation of the halides during the gasification of the carbon, possibly by a reaction of the type

$$2NaCl + C + 3/2\, O_2 = Na_2O + CO_2 + Cl_2 \quad \Delta G^{\circ}_{1100K} = -11 \text{ Kcal/mole}$$

though other halogenated species, such as HX, COX_2, HOX and the like could be formed in low concentrations.

CONCLUSIONS

The catalytic effects of alkali carbonates and other salts in the gasification of coal char and graphite in steam and CO_2 have been studied. Although the patterns of catalytic activity for the various additives were similar for both char and graphite, the reactivity of the char was influenced by factors such as charring temperature, porosity and the presence of mineral impurities.

On increasing the charring temperatures from 700°C to 900°C, there was a marked decreased in reactivity towards both steam and CO_2, presumably due to loss in porosity of the

char or annealing of active sites at the higher temperature. Non-porous graphite had a much lower surface area than the char and a lower reactivity, in the absence of catalysts. However, within a series of char samples prepared at the same temperature, there was no significant correlation between reactivity and surface area. In fact, surface areas were slightly reduced when salt catalysts were added to char samples, even though the reactivity was increased considerably. Also, the reactivity of the catalyzed samples proved not to be strongly dependent on the mode of addition of the catalyst and physical mixing of the salt with the pre-carbonized char was almost as effective as adding the catalyst prior to charring.

An observation of important practical implication was the progressive and rapid initial loss in catalytic activity during gasification at constant temperature and on thermal cycling between gasification temperatures and ambient. This effect, which was much more marked in steam than in CO_2, appeared to be the result of reaction of the salt additives with mineral matter in the char to form stable inert silicates and aluminosilicates.

Thermodynamically feasible mechanisms for the alkali carbonate catalysts which involve sequences of oxidation/reduction reactions with the intermediate formation of alkali metal or oxides have been discussed. The moderate catalytic activity of certain alkali halide salts is however difficult to explain on this basis.

ACKNOWLEDGEMENT

Support of this work by the US Department of Energy (Contract No. DE-AC21-80MC 14591) is gratefully acknowledged.

References

1. N. Berkowitz, "An Introduction to Coal Technology," Chapt. 2, Academic Press, NY (1979).
2. K. Otto, L. Bartosiewicz and M. Shelef, Fuel 58, 85 (1979).
3. A. Linares-Solano, O. P. Mahajan and P. L. Walker, Jr., Fuel 58, 327 (1979).
4. K. J. Huttinger and W. Krauss, Fuel 60, 93 (1981).
5. T. du Motay, British Patent 2458 (1967).
6. J. E. Gallagher, Jr., and C. A. Euker, Jr., Energy Research 4, 137 (1980).
7. A. L. Kohl, R. B. Harty, J. G. Johanson and L. M. Naphtali, Chem. Eng. Prog., 74, 73 (1978).
8. A. E. Cover, W. C. Schreiner and G. T. Skaperdas, Chem. Eng. Prog., 69, 31 (1973).
9. N. Kayembe and A. H. Pulsifer, Fuel 55, 211 (1976).
10. M. J. Veraa and A. T. Bell, Fuel 57, 194 (1978).
11. D. W. McKee, Carbon 17, 419 (1979).
12. D. W. McKee, "Chemistry and Physics of Carbon," P. L. Walker and P. A. Thrower, Eds., Vol. 16, p. 1, Marcel Dekker, NY 1981.
13. C. Spiro, D. McKee, P. Kosky, E. Lamby, and D. Maylotte, to be published.
14. D. W. McKee and D. Chatterji, Carbon 13, 381 (1975).
15. D. W. McKee and D. Chatterji, Carbon 16, 53 (1978).
16. C. Karr, P. Waldstein and J. Kovach, J. Inst. Fuel 47, 177 (1974).
17. B. J. Wood, K. M. Sancier, J. G. McCarty and H. Wise, "The Mechanism of the Catalytic Gasification of Coal Char," Technical Progress Report, SRI International, January 1981, DoE Contract No. DE-AC21-14593.
18. R. Lang, Exxon Research and Engineering Co., unpublished observations.
19. D. W. McKee, unpublished observations.

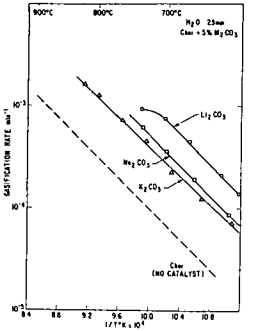

Figure 1 Catalytic effects of alkali metal carbonates on the gasification of coal char in water vapor. 5% salt added after charring at 700°C. Second cycle rate data vs. $1/T°K$.

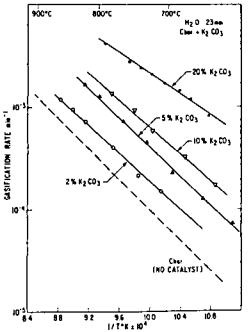

Figure 2 Effect of K_2CO_3 concentration on the rate of gasification of coal char in water vapor. Salt catalyst added after 700°C charring. Second cycle rate data vs. $1/T°K$.

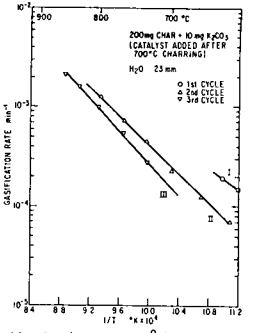

Figure 3 Gasification kinetics (rate vs. $1/T°K$) in water vapor for a 5% K_2CO_3-doped char (salt added after charring), for three successive thermal cycles.

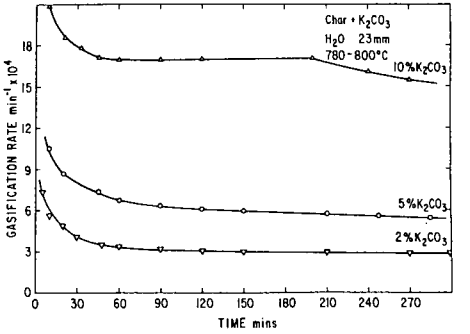

Figure 4 Gasification rates in water vapor vs. time at 800°C for a char with various concentrations of added K_2CO_3.

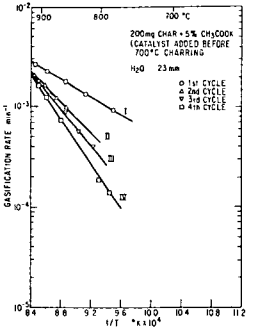

Figure 5 Gasification kinetics (rate vs. $1/T^{0}K$) in water vapor for a char containing initially 5% CH_3COOK (salt added before 700°C charring). Rates measured during four successive thermal cycles.

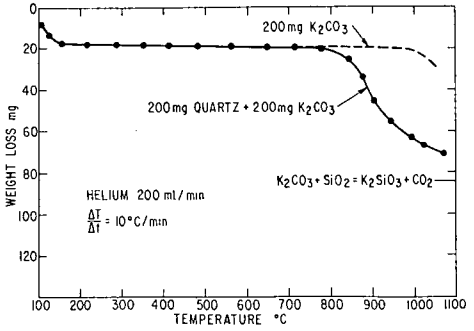

Figure 6 Thermograms (weight loss vs. temperature) for K_2CO_3 and a 1:1 quartz-K_2CO_3 mixture on heating in helium at 10°C/min.

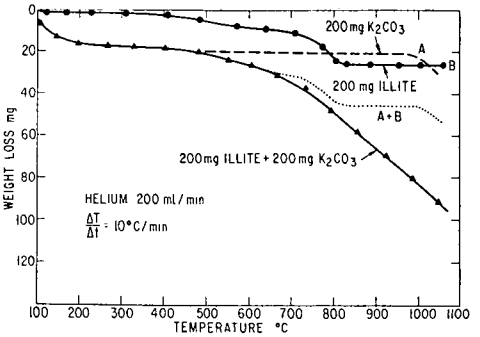

Figure 7 Thermograms (weight loss vs. temperature) for (A) K_2CO_3, (B) Illite and an illite-K_2CO_3 mixture on heating in helium at 10°C/min.

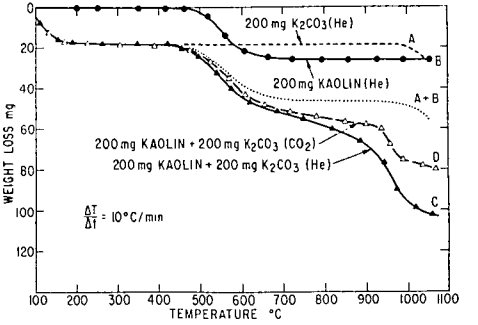

Figure 8 Thermograms (weight loss vs. temperature) for (A) K_2CO_3, (B) Kaolin and a kaolin-K_2CO_3 mixture on heating in helium (C) and CO_2 (D) at 10°C/min.

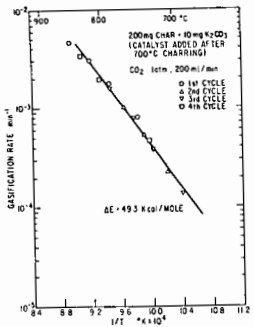

Figure 9 Gasification kinetics (rate vs. $1/T^{o}K$) in CO_2 for a char with 5% K_2CO_3 added after charring. Rates shown for four successive thermal cycles.

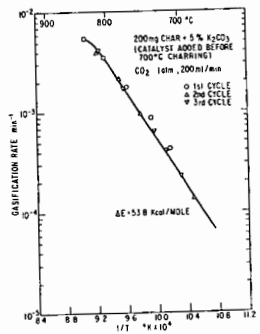

Figure 10 Gasification kinetics (rate vs. $1/T^{o}K$) in CO_2 for a char containing initially 5% K_2CO_3 (salt added before 700°C charring). Rates shown for three successive thermal cycles.

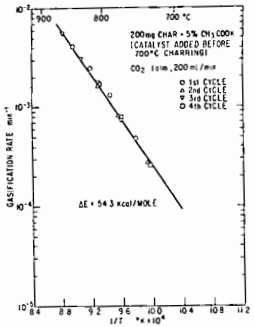

Figure 11 Gasification kinetics (rate vs. $1/T^{o}K$) in CO_2 for a char containing initially 5% CH_3COOK (salt added before 700°C charring). Rates shown for four successive thermal cycles.

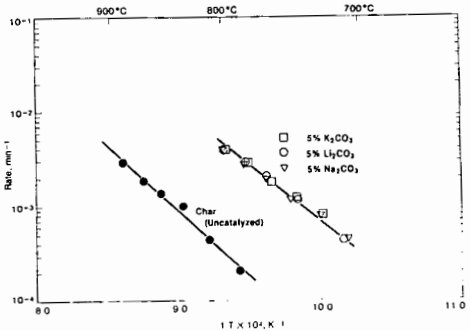

Figure 12 Gasification kinetics (rate vs. $1/T^{o}K$) in CO_2 for chars doped with 5% Li, Na and K carbonates (added prior to 700°C charring).

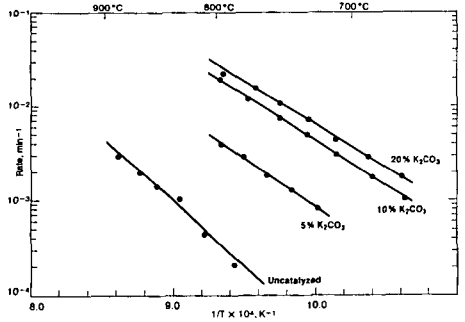

Figure 13 Gasification kinetics (rate vs. $1/T^{o}K$) in CO_2 for chars doped with 5%, 10%, and 20% K_2CO_3 (added prior to 700°C charring).

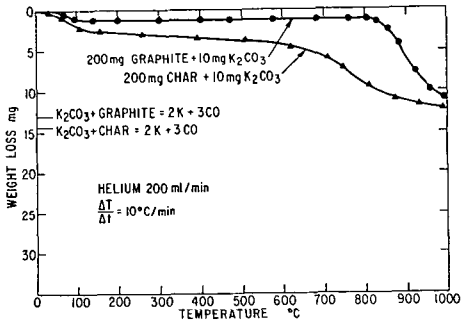

Figure 14 Thermograms (weight loss vs. temperature) for graphite-5% K_2CO_3 and char-5% K_2CO_3, on heating in helium at 10°C/min.

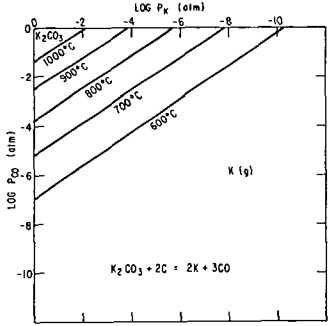

Figure 15 Equilibrium stability regions of K(g) and K_2CO_3 for the reaction $K_2CO_3 + 2C = 2K + 3CO$, as functions of temperature, P_{CO} and P_K.

5360-096bw

KINETICS OF POTASSIUM CATALYZED GASIFICATION

P. Knoer and H. W. Wong. Exxon Research and Engineering Co., Baytown Research and Development Division, P. O. Box 4255, Baytown, Texas 77520.

Commercial applications of the potassium catalyzed coal gasification reaction (CCG) are envisioned to include high pressure (2000 to 4000 kPa) and high concentrations of hydrogen in the gasification reactor (1, 2, 3). Published literature regarding CCG, however, report studies conducted at low pressure or with low concentrations of hydrogen or both (4, 5, 6). The present study was conducted to investigate the gasification reaction under commercially representative conditions. Thus, pressure was varied from 100 to 3500 kPa and hydrogen concentration was varied from 0 to 60%. Other reaction conditions, such as temperature and catalyst loading, were also varied in this study to check published results at these more representative conditions. The data from this study were combined with mechanistic information from the literature (6). Only one kinetic model was found which fit both the data and the literature mechanism. The two adjustable constants for this model were regressed using over 1200 pieces of data. The overall fit between the model and the data is very good.

Experimental Apparatus

This experimental program was carried out using a one atmosphere mini-fluid bed reactor and a fixed bed reactor capable of operating at high pressure. The atmospheric pressure unit was used to study variations in catalyst loading and temperature. These studies were conducted using both H_2O only and H_2O/H_2 mixtures, using chars from steady state pilot plant operations and chars prepared by devolatilization in the laboratory.

A schematic diagram of the mini-fluid bed reactor unit is shown in Figure 1. The reactor portion of the unit consists of a 0.6 cm I.D. quartz U-tube inside a hot steel block. Water is fed to the U-tube using a small syringe pump and is vaporized in the reactor. Argon or hydrogen gas is also fed to the unit. Ceramic beads are placed in the inlet leg of the U-tube to enhance the vaporization of water and to help disperse the gas flow. The exit gases from the reactor flow into an oxidizer where all carbon species are converted to carbon dioxide. After condensing any unreacted steam, the gas stream is bubbled through a sodium hydroxide solution where the amount of total carbon converted is automatically monitored by measuring the conductivity of the solution.

The argon or hydrogen gas fed to the mini-fluid bed serves to fluidize the char particles. The gas rate is typically about 40 cc/min STP which is equivalent to about 7 cm/sec linear superficial velocity in the reactor at 700°C. The minimum fluidizing velocity of the char particles is 3-4 cm/sec. Char sample sizes varied from 0.25 grams to 1.00 gram in the minifluid bed. The water feed rate ranged from 0.2 to 2.5 ml/hour.

The fixed bed reactor was used primarily to study pressure effects. All runs in the fixed bed were made at 700°C using laboratory prepared char. Variations were made in feed gas composition and flow rate. A simplified flow diagram of the fixed bed unit is shown in Figure 2. The unit consists of a high pressure water pump, steam generator, fixed bed reactor, condenser for unreacted steam, gas chromatographs, and dry gas flow measurement system.

The reactor itself is a one-inch Schedule 80 type 316 stainless steel pipe. The pipe holds a char sample inside a split tube furnace.

Effect of Varying Potassium-to-Carbon Ratio

If the overall carbon conversion is altered in the CCG reactor, the ratio of potassium-to-carbon (K/C) in the reactor will change as well. Therefore, the effect of catalyst loading on kinetics must be known in order to be able to optimize initial catalyst loading as well as overall carbon conversion for the CCG process. Experiments were conducted in the atmospheric mini-fluid bed reactor to determine the effect of carbon conversion and catalyst loading on the gasification rate.

Plotting the initial gasification rates against the water soluble K/C ratio reveals an approximately linear relationship between the two as shown in Figures 3 and 4. This is consistent with the earlier findings by others (6).

This suggests that the rate of gasification is proportional to the concentration of a (C-K) species rather than carbon or potassium concentrations per se. At high carbon concentrations and low K/C ratios, the concentration of the (C-K) species is proportional to the concentration of (K) since there is an overabundance of (C). The gasification rate thus appears to be independent of carbon concentration (i.e., zero order kinetics). At low carbon concentrations and high K/C ratios, there is an overabundance of (K). The gasification rate will then appear to be first order with respect to carbon. From studies of pilot plant chars, the demarcation between high and low K/C ratios appears to be about 0.2 mole C/mole water soluble potassium.

Variation of Reaction Temperature

The dependence of gasification rate on temperature was studied in the mini-gasifier, both with and without H_2 in the feed gas.

Figure 5 shows the measured reaction rates as a function of temperature for experiments both with and without H_2 in the reactor. The apparent temperature dependence changes as the composition of the gas fed to the reactor changes. From Figure 4 it is seen that for $H_2O + H_2$ in the feed gas, gasification rate is very sensitive to temperature changes. Gasification rate approximately halves for each 25°C drop in reactor temperature below 700°C.

There is an interaction between feed gas composition and apparent temperature dependence because the mini-reactor is an integral reactor. For example, when pure steam is introduced at the bottom of the bed of char, a mixture of $H_2O + H_2$ issues from the top of the bed. As the rate of reaction changes, the gas composition at various locations in the reactor changes even though the feed gas remains the same. Therefore, as temperature changes, some of the change in rate is due to activation energy, but some of the change is due to gas composition. A reactor model which performs an integration over the bed is required to account for both effects. Our modeling work discussed in the next section of this report has identified the true activation energy as about 50 kcal/g mole.

Gasification Rate Expression

During an earlier phase of research on the CCG process, a screening of gasification reaction rate models was reported by Vadovic and Eakman (5). In this screening, all combinations of from one to four inhibition terms involving the partial pressures of H_2, CO, H_2O, and the cross products of the partial pressures of $H_2$and CO, and H_2 and H_2O were tested in the denominator of the gasification rate expression. In all, they tested thirty models. Those models which gave negative coefficients on regression were discarded as being physically unreal. Four additional models were discarded because they gave an infinite rate for a pure steam environment. Of the thirty models tested, three models remained which gave good fit to their data. These three are listed below.

$$(A) \quad r_G = \frac{k(P_{H_2O} - P_{CO}P_{H_2}/2K_G)}{P_{H_2} + 0.1775\ P_{H_2O}}$$

$$(B) \quad r_G = \frac{k(P_{H_2O} - P_{CO}P_{H_2}/2K_G)}{P_{H_2} + 0.210\ P_{H_2}P_{CO} + 0.0595\ P_{H_2O}}$$

$$(C) \quad r_G = \frac{k(P_{H_2O} - P_{CO}P_{H_2}/2K_G)}{P_{H_2} + 1.26\ P_{CO} + 0.349\ P_{H_2O}}$$

For their screening of gasification rate models, Vadovic and Eakman used data from runs in which only pure steam was fed to the bed of coal char. Mixtures of H_2O and H_2 or H_2O, H_2, and CO were introduced and studied in the present program.

In addition to the empirical data, mechanistic considerations were used to discriminate among the three models for catalytic gasification kinetics. Several mechanisms have been proposed for the steam-carbon reaction in the past (7). Recent work by Mims and Pabst (6) indicated that the overall gasification kinetics are consistent with a simple surface oxide mechanism:

$$H_2O + \text{C} \underset{k_{-1}}{\overset{k_1}{\rightleftharpoons}} \text{C(O)} + H_2 \qquad \text{oxygen exchange}$$

$$\text{C(O)} \xrightarrow{k_2} CO + \text{C} \qquad \text{surface oxide decomposition}$$

With the larger data base and the proposed mechanism, it was possible to better distinguish among the three rate models identified earlier. Only Model A was found to be consistent with both the mechanism studies and the new data. This model is shown in general form below:

$$r_G = \frac{k(P_{H_2O} - P_{H_2}P_{CO}/2K_G)}{P_{H_2} + b\,P_{H_2O}} \qquad (1)$$

r_G = the rate of gasification in moles per hour per ft^3 of reactor

K_G = the equilibrium constant for steam and β-graphite

P_i = the partial pressure of component i in the reactor

k = the rate constant; it contains the catalyst loading and temperature dependence.

Parameter Estimation for the Gasification Reaction

A total of 28 successful fixed bed runs were made at pressures ranging from 100 to 3500 kPa, H_2 flows ranging from 0 to 1.0 moles per hour, CO flows ranging from 0 to 0.17 moles per hour and steam flows ranging from 0.3 to 1.3 moles per hour. It was observed that the total gas make and gas composition changed during the runs as carbon was depleted from the bed. It was also observed that the methane and carbon dioxide were nearly in chemical equilibrium with the other gas phase components for the conditions studied.

A combination of kinetic constants k and b in Equation 1 were sought which would make the predictions of the fixed bed model best fit the fixed

bed data. Best fit is defined by a small deviation between predicted and observed molar flow rates. Thus, one expression of the objective function would be as follows:

$$\text{minimize } s^2 = \sum_k \sum_j \sum_i (\tilde{N}_{ijk} - Nijk)^2 \qquad (2)$$

where,

S = the sum of the squares of the deviations

$\tilde{N}_{ijk}$ = a predicted molar flow rate
N_{ijk} = an observed molar flow rate
i = a particular gas component (H_2, CO, CO_2, CH_4, or H_2O)
j = a particular level of carbon in the fixed bed reactor
k = a particular fixed bed reactor run

Hunter (8) has shown that use of this objective function will yield the maximum likelihood estimates for k and b only if the following three criteria are met:

(1) The measurement errors on each of the five gas species are normally distributed and these errors are independent.

(2) The variances on the measurement errors of all of the five gas species are identical.

(3) There is no correlation between the measurement errors for any two gas species.

From the design of the experiment we know that the measurements on the four fixed gases were related in that they were all sampled simultaneously by the gas chromatograph and the composition was normalized. Therefore, an error in the measurement of any one of the four fixed gases would be distributed among the other three fixed gases as well. Furthermore, any error in the measurement of CO or CO_2 would result in an error in the measurement of H_2O as well since H_2O yield was calculated by oxygen balance. As a result of these considerations, equation 2 was not used as the objective function for this study.

Box and Draper (9) have derived the following objective function for use in cases where unquantified covariance exists in the experimental measurements:

$$\text{minimize} \qquad \Delta = \det \mid S_{nm} \mid$$

where,

Δ = the determinant of the 5 x 5 matrix composed of elements S_{nm}

and,

$$S_{nm} = \sum_k \sum_j (\tilde{N}_{njk} - N_{njk})(\tilde{N}_{mjk} - N_{mjk})$$

where,

n,m = particular gas components
j,k = as above.

Hunter (8) recommends the use of this objective function when covariance might exist in the experimental measurements.

Rosenbrock's hill climbing method (10) was used to search for the optimum values of k and b in equation 1. For each set of k and b, the fixed bed reactor model equations were numerically integrated 28 times; i.e., once for each fixed bed reactor run being estimated. For each of the 28 fixed bed reactor runs, comparisons between calculated and observed molar flow rates were made for 8 to 10 different levels of carbon in bed. With five different gas species being estimated, there were over 1200 comparisons made for each guess of a k,b pair. For each guess, the appropriate cross products of deviations were calculated and accumulated to form the 5 X 5 matrix of elements S_{nm}. The determinant of this matrix was calculated and used by the Rosenbrock routine to make a new guess at k and b.

Results of the Regression

The initial guesses for k and b were taken from the results of Vadovic and Eakman (5). For 700°C and the K/C ratio used these were as follows:

k = 0.0204
b = 0.1775

The routine returned the following values:

k = 0.0173
b = 0.2080

Figures 6 through 10 are parity plots of the predicted and observed values of the molar flow rates of H_2, CO, CO_2, CH_4, and H_2O. The parity plots show that the fixed bed reactor model does a good job of predicting all of the gas species from the fixed bed reactor runs over a wide variety of conditions with the exception of CH_4. A slight overprediction of CH_4 yield is observed.

Conclusions

The potassium catalyzed gasification of Illinois No. 6 bituminous coal was found to fit a Langmuir-Hinshelwood type kinetic model. This model provides a good fit to fixed bed and miniature fluid bed data over pressures

ranging from atmospheric to 3500 kPa and over broad ranges of gas composition. The model closely predicted the observed flow rates of each specie in the product gas over a range of an order of magnitude or more. This model is consistent with the surface oxide mechanism for the steam-carbon reaction which was proposed in earlier literature. A sophisticated statistical regression technique was used to choose the two adjustable constants for this model by comparison with over 1200 pieces of data.

The kinetic constants were regressed from data taken over the range of practical commercial interest. This kinetic model may be combined with independently verified correlations for bubble growth and mass transfer in a fluidized bed and used directly to study larger pilot plant data or scale-up issues.

ACKNOWLEDGEMENT

This work was supported by the United States Department of Energy under Contract No. ET-78-C-01-2777 and by the Gas Research Institute.

REFERENCES

1. N. C. Nahas and J. E. Gallagher, Jr., "Catalytic Gasification Predevelopment Research," Proceedings of the Thirteenth Intersociety Energy Conversion Engineering Conference, (August 1978).

2. B. T. Fant and C. A. Euker, Jr., "Exxon's Catalytic Coal Gasification Process," Presented to The First International Research Conference, (June 9-12, 1980).

3. D. Hebden and H. J. F. Stroud, "Coal Gasification Processes," in Chemistry of Coal Utilization Second Supplementary Volume, M. A. Elliot ed., (1981), pp. 1649-1650.

4. H. G. Hipkin, Carbon-Steam System at Low Temperatures and Under Pressure, PhD Thesis, M.I.T. (1951).

5. C. J. Vadovic and J. M. Eakman, "Kinetics of Potassium Catalyzed Gasification," presented at the meeting of the American Chemical Society (September, 1978).

6. C. A. Mims and J. K. Pabst, "Alkali Catalyzed Carbon Gasification II. Kinetics and Mechanism," presented at the meeting of the American Chemical Society (August, 1980).

7. P. L. Walker, Jr., F. Rusinko, Jr., and L. G. Austin, Advances in Catalysis XI, (1959).

8. W. G. Hunter, "Estimation of Unknown Constants From Multi-response Data," I & E C Fundamentals, Vol. 6, (1967), pp. 461-463.

9. G.E.P. Box and N. R. Draper, Biometrika, V52, (1965), p. 355.

10. H. H. Rosenbrock, "An Automatic Method for Finding the Greatest or Least Value of a Function," Computer J., 3 (1960).

81B-10-88

FIGURE 1

SCHEMATIC OF MINI-FLUID BED REACTOR UNIT

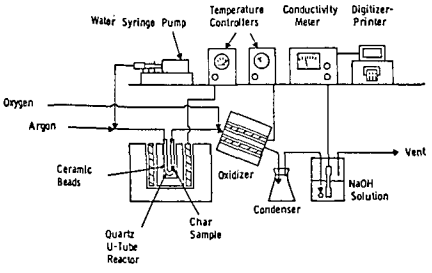

80B-12-1259

FIGURE 2

SIMPLIFIED FLOW DIAGRAM OF BENCH SCALE GASIFICATION UNIT

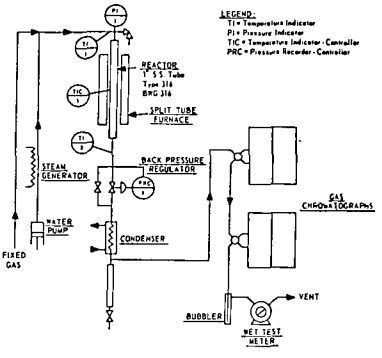

81B-3-37

80B-9-204

FIGURE 3

GASIFICATION RATE INCREASES LINEARLY WITH (K/C) RATIO

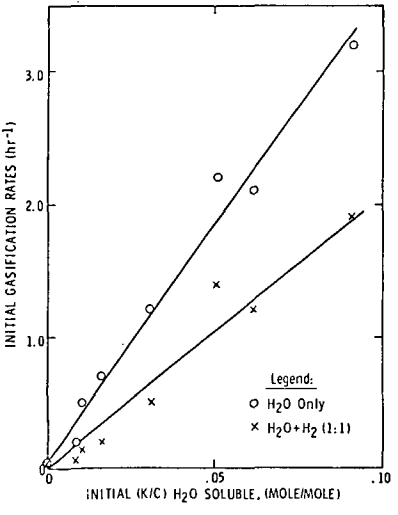

FIGURE 4

EFFECT OF CATALYST LOADING ON GASIFICATION

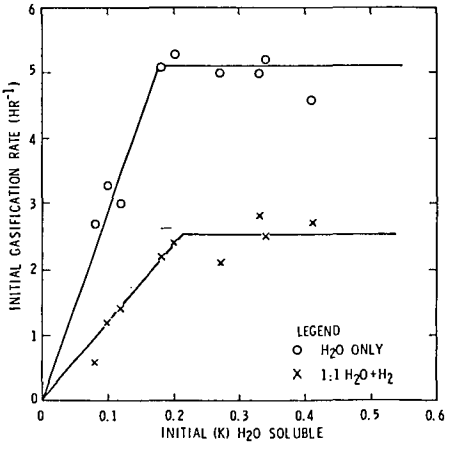

818-3-38

FIGURE 5

APPARENT ACTIVATION ENERGY DEPENDS ON FEED GAS COMPOSITION

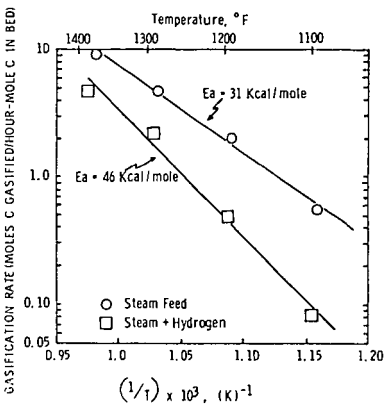

808-6-5-22

808-12-1130

FIGURE 6

CALCULATED AND OBSERVED FLOW RATES OF HYDROGEN

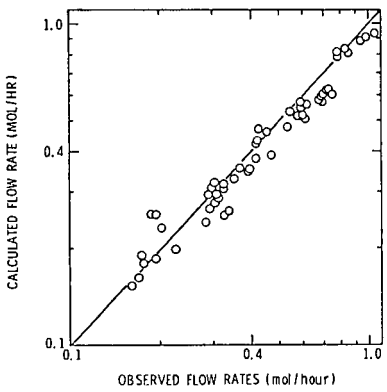

808-12-1131

FIGURE 7

CALCULATED AND OBSERVED FLOW RATES OF CARBON MONOXIDE

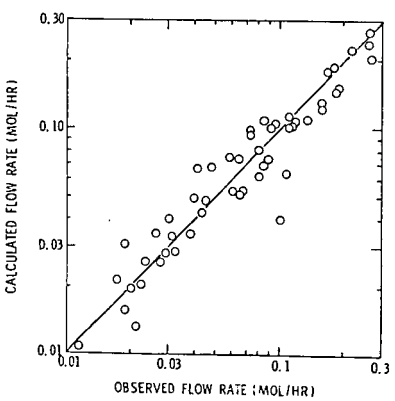

808-12-1132

FIGURE 8

CALCULATED AND OBSERVED FLOW RATES OF CARBON DIOXIDE

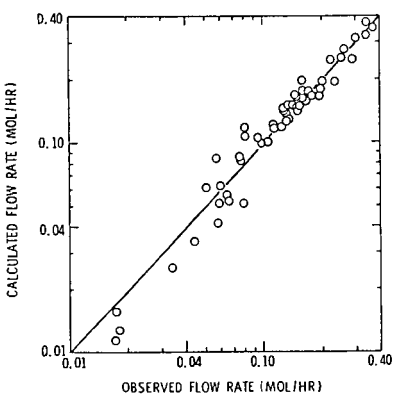

808-12-1133

FIGURE 9

CALCULATED AND OBSERVED FLOW RATES FOR METHANE

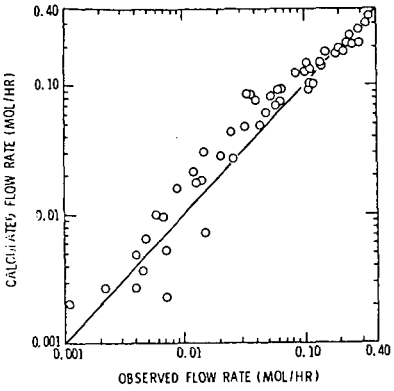

808-12-1134

FIGURE 10

CALCULATED AND OBSERVED FLOW RATES FOR STEAM

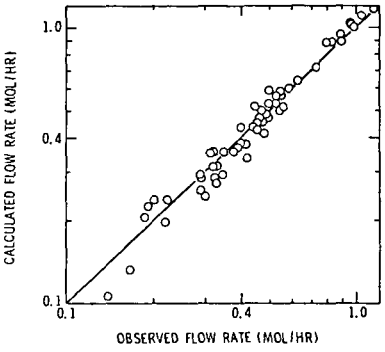

EVOLUTION AND REMOVAL OF POLLUTANTS FROM THE GASIFICATION OF A SUBBITUMINOUS COAL IN A FLUIDIZED BED REACTOR

R.M.Felder, J.K.Ferrell, R.W.Rousseau, M.J.Purdy, and R.M.Kelly

Department of Chemical Engineering
North Carolina State University
Raleigh, North Carolina 27650

INTRODUCTION

As a part of a continuing research program on the environmental aspects of fuel conversion, the U. S. Environmental Protection Agency has sponsored a research project on coal gasification at North Carolina State University in the Department of Chemical Engineering. The facility used for this research is a small coal gasification-gas cleaning pilot plant. The overall objective of the project is to characterize the gaseous and condensed phase emissions from the gasification-gas cleaning process, and to determine how emission rates of various pollutants depend on adjustable process parameters.

A complete description of the facility and operating procedures is given by Ferrell et al., Vol I, (1980), and in abbreviated form by Felder et al. (1980). A schematic diagram of the Gasifier, the Acid Gas Removal System (AGRS), and other major components is shown in Figure 1.

In an initial series of runs on the gasifier, a pretreated Western Kentucky No. 11 coal was gasified with steam and oxygen. The results of this work are given by Ferrell et al., Vol II, (1981), and were presented at the EPA Symposium on Environmental Aspects of Fuel Conversion Technology V, held in St. Louis, Mo., September, 1980.

The second major study carried out on the facility was the steam-oxygen gasification of a New Mexico subbituminous coal (from the Navaho mine of the Utah International Co.) using refrigerated methanol as the AGRS solvent. This paper presents a brief summary of the gasifier operation using this coal, shows examples of analyses of some of the gasifier effluent streams, and presents a summary of the results of the operation of the AGRS using the gasifier make gas as feed.

SUMMARY OF GASIFIER OPERATION

The fluidized bed gasifier and raw gas cleaning system (cyclone, venturi scrubber, filters and heat exchanger) used for these studies was originally designed for the gasification of a devolatilized coal char with a very low volatile matter content. Extensive modification of the upper part of the gasifier, the venturi scrubber system, and the heat exchanger was required for operation with the high volatile matter New

Mexico coal. Table 1 shows an analysis of the char and coal used in studies to date. After modification, the system functioned well in providing a clean, dry gas to the acid gas removal system.

All of the experimental work so far has been carried out with the solid coal particles fed into the reactor several feet above the top of the fluidized bed. The particles are thus in contact with the hot product gases for several seconds before mixing into the fluidized bed, a mode of operation that tends to maximize the production of tars and other organic liquids from the coal. It is an excellent mode of operation for our present purpose since it produces relatively high concentrations of environmentally important elements and compounds.

TABLE 1
COAL AND CHAR ANALYSIS

	Coal Char	New Mexico Coal
Proximate Analysis		
Fixed Carbon	86.0	42.0
Volatile Matter	2.4	35.4
Moisture	0.9	10.5
Ash	10.7	22.6
Ultimate Analysis		
Carbon	83.8	52.5
Hydrogen	0.6	4.8
Oxygen	2.2	18.3
Nitrogen	0.1	1.2
Sulfur	2.6	0.6
Ash	10.7	22.6

A total of 15 gasifier runs were made covering a range of reactor parameters. For this series of runs, the average temperature of the fluidized bed was varied from about 1600°F to 1800°F, and the molar steam to carbon ratio was varied from about 1.0 to 2.0. The coal feed rate and the reactor pressure were kept nearly constant. Several of the first reactor runs were made with mixtures of coal and char, but all integrated runs reported on later were made with 100% coal. At the lower temperatures the production of methane and of tars and other hydrocarbons is maximized. As the temperature is increased, the make gas rate increases, the production of methane and other hydrocarbons decreases, and the concentration of CO_2 increases.

GASIFIER MODELING RESULTS

To aid in the formulation of gasifier performance correlations, a simple model has been developed which considers the gasification process to occur in three stages: instantaneous devolatilization of coal in a zone above the fluidized bed, instantaneous combustion of carbon at the

bottom of the bed, and steam-carbon gasification and water gas shift reaction in a single perfectly mixed isothermal stage. The model is significant in and of itself, but its particular importance to the project is that it enables the specification of gasifier conditions required to produce a feed to the acid gas removal system with a predetermined flow rate and composition.

In a previous report (Ferrell et al., 1981), the structure of the model was presented, and the ability of the model to correlate data on the gasification of a devolatilized bituminous coal was demonstrated. The model was subsequently extended to include the evolution of volatile gases in the pyrolysis stage of the gasification process, and used to fit the data from the present series of runs with the New Mexico subbituminous coal. The model takes as input the average reactor bed temperature and pressure, the bed dimensions, feed rates of coal, steam, oxygen, and nitrogen, solids holdup in the bed, and ultimate analysis of the feed coal, and calculates carbon conversion and make gas flow rate and composition. A complete description of the model in its present form will be given in an EPA report now in preparation. A lot of model predictions vs measured values of carbon conversion is shown in Figure 2. The reasonably close proximity of most points to the 45 degree line on this and similar plots for total make gas flow rate and individual species (CO, H_2, CO_2) emissions is gratifying in view of the simplicity of the model.

AGRS OPERATION AND RESULTS

Top feeding coal into the gasifier allows a substantial amount of devolatilization to take place before the coal enters the fluidized bed. While most commercial fluidized bed gasifiers will use a deep-bed injection method of feeding coal into the fluidized bed, it was decided not to modify our system in order to maximize the formation of tars, oils, and other hydrocarbons and to provide a more complete test of the AGRS.

It should also be noted that the relatively simple acid gas removal system used in this study lacks the complexity of the selective systems found in many physical absorption processes. These systems, which use more than one absorber and stripper, and often several flash tanks, separate sulfur gases from carbon dioxide before further processing of the acid gas. This is done to concentrate the sulfur gases before they are fed to a sulfur recovery unit, and to recover the CO_2 or vent the CO_2-rich stream to the atmosphere. While the AGRS used in this study could have been modified to emulate an existing selective absorption process, it was decided that data obtained from a relatively simple but well-characterized system would be of more use than data obtained from a fairly complex system, similar but not identical, to existing commercial systems. Through judicious use of computer simulation and engineering calculations, the data obtained from our system should be extrapolatable to more industrially significant situations.

Complete results from all runs carried out will be published in a forthcoming EPA report. Illustrative results from a single run will be presented here. Gas analyses from the six different locations shown in Figure 1 are given in Table 2. The paragraphs that follow summarize the principal conclusions derived from analyses of the run data.

TABLE 2
GAS ANALYSIS SUMMARY FOR AMI-57/GO-76

Species	Sample Train	PCS Tank	Sour Gas	Sweet Gas	Flash Gas	Acid Gas
H_2	31.60	31.11	31.29	42.38	15.58	0.00
CO_2	23.51	23.91	21.98	-----	25.99	64.74
C_2H_4	0.52	0.53	0.56	0.0242	1.28	1.54
C_2H_6	0.72	0.72	0.76	0.0164	1.92	2.13
H_2S	0.250	0.284	0.287	0.0048	0.090	0.66
COS	0.0078	0.0076	0.0076	0.0001	0.0041	0.027
N_2	19.36	19.61	19.93	26.79	19.27	23.06
CH_4	6.56	6.46	6.57	7.54	14.20	2.36
CO	17.29	17.47	17.92	23.35	21.55	1.80
Benzene	0.087	0.097	0.234	TRACE	0.0031	0.15
Toluene	0.031	0.034	0.534	0.0054	0.0033	0.030
Ethyl Benz.	0.0016	0.0017	0.0450	-----	-----	-----
Xylenes	0.0080	0.0094	0.1557	-----	-----	-----
Thiophene*	44	44	127	-----	-----	-----
CH_3SH*	16	29	28	TRACE	5	TRACE
C_2H_5SH*	TRACE	-----	8	-----	-----	-----
CS_2*	TRACE	3	TRACE	TRACE	TRACE	TRACE
Propylene*	1505	1521	1811	107	995	4640
Propane*	208	198	253	301	172	2203
Butane*	185	150	143	54	91	71
Methanol**	-----	-----	-----	-----	-----	3.68

*Parts per Million (volume) **Estimated

Acid Gas Removal

The primary function of the AGRS is to remove CO_2 and sulfur compounds from the gases produced during coal gasification. When using refrigerated methanol, the absorber also acts as an excellent trap for any other compound which condenses or disolves in the methanol at absorber conditions.

The run data show that for the range of conditions studied, the most significant factor in high acid gas removal efficiencies is stripping efficiency. With the use of more extreme operating conditions and "cleaner" methanol fed to the absorber, the levels of CO_2, COS and H_2S in the sweet gas can be reduced to acceptable levels. This is a particularly important point in the case of COS removal which poses

problems for many coal gas cleaning systems. The data show that refrigerated methanol is effective in removing COS and no unusual solubility characteristics were evident at moderate pressures and low liquid temperatures.

Trace Sulfur Compounds

There are several sulfur compounds besides H_2S and COS present in the gas fed to the AGRS which must be removed. Table 2 shows the distribution of several of these compounds in the AGRS. While there is some scatter in the analyses for methyl mercaptan, thiophene, CS_2, and ethyl mercaptan/dimethyl sulfide, it appears that in most runs they are removed to very low levels in the absorber.

A point of potential environmental significance is that while these compounds are removed to low levels, they are not completely accounted for in the flash and acid gas streams. This can be seen for methyl mercaptan and thiophene, which are present in relatively high levels in the feed gas. These compounds will accumulate in the recirculatory solvent and most likely eventually leave the system in one of three exit streams: sweet gas, flash gas, or acid gas. Because most sulfur recovery systems cannot treat mercaptans and thiophene, they will present emission problems if some additional method of treating these gases is not used. This can be a significant problem because the total sulfur from mercaptans, organic sulfides, CS_2, and thiophene is approximately half of the total sulfur associated with COS. If these compounds appear with the sweet gas, they are likely to affect adversely downstream methanation catalysts. The presence of these compounds in the sweet gas stream is also a problem if the gas is to be burned for immediate use because the sulfur in these compounds will be converted to SO_2.

In examining the results from all runs, there appears to be some pattern of trace sulfur species distribution. An increase in stripper temperature from $-5.6^{\circ}F$ to $48^{\circ}F$ resulted in substantially greater amounts of mercaptan and thiophene in the acid gas stream. CS_2 seems to distribute to all exit streams in most of the runs despite the differences in process conditions.

Perhaps the most significant finding here is that over a wide range of processing conditions, the presence of at least small amounts of several different sulfur species is to be expected in all AGRS exit streams, and provision must be made for handling the associated problems.

Aliphatic Hydrocarbons

As the amount of volatile matter present in a particular coal increases, the production of aliphatic, aromatic, and polynuclear aromatic compounds produced during gasification also increases. Over the range of conditions studied here, the most significant point to be made about the distribution of aliphatic hydrocarbons is their presence in significant quantities in the flash and acid gases. Although flashing of

the methanol down to atmospheric pressure prior to stripping would release most of the hydrocarbons, the CO_2-rich flash gas would still contain substantial amounts of several hydrocarbon species. This stream would require further processing before it could be vented.

In a run in which the gasifier was operated at a lower temperature to increase the production of hydrocarbons, the aliphatics (excluding methane) made up almost 4.5% of the acid gas stream and 3.5% of the flash gas stream. While staging the flashing operations may result in a better distribution of these compounds, the total product from the flashing and stripping operations must be either recovered as product, fed to a sulfur recovery unit, or vented to the atmosphere. Since it is unlikely that all of the aliphatic hydrocarbons will appear in the sweet gas stream, as evidenced by the data collected here, additional treatment will be necessary to prevent their eventual appearance in a vent stream.

There appears to be no unusual pattern of distribution of aliphatic hydrocarbons in the AGRS. The lighter hydrocarbons-- methane, ethylene, and ethane-- seem to distribute as would be indicated from an examination of their pure-component solubilities in methanol. The magnitude of their solubilities, however, are greater than would be expected from Henry's law, especially at the high pressures used in the absorber. This is evident from the lower than predicted levels of ethane and ethylene in the sweet gas in several of the runs.

Aromatic Hydrocarbons

Because large amounts of aromatic hydrocarbons are produced during coal gasification, the potential for environmental problems is great. These compounds, which range from benzene to polynuclear species of many forms, must be prevented from escaping from the gas cleaning process and their distribution throughout the gas cleaning system is of great concern.

The simpler aromatics, benzene, toluene, and xylene, typically make up 0.1% (by volume) of the gas stream entering the AGRS. (See Table 2.) Analyses performed for selected runs indicate that significant quantities of these compounds are found in the solvent leaving the stripper. Eventually these compounds would build up in the solvent to the point of saturation. If the solvent is not effectively purged of these compounds periodically, they would begin to appear in several of the process streams.

Methanol Analysis

In order to identify the various hydrocarbon species that accumulate in the methanol, samples of the methanol leaving the stripper were taken for several runs. These samples were then analyzed by gas chromatography/mass spectrometry. The compounds detected are shown in Table 3. The presence of several siloxanes and phthalates was probably related to some contamination of the sample during processing.

Results from these runs indicate that most of the compounds accumulating in the methanol are simple aromatics, primarily substituted benzenes. A few C_{10} and C_{11} isomers were identified, indicating that napthalene is probably present but at trace levels. The presence of trace amounts of C_{14} and C_{15} isomers were found in but they could not be better identified. These may be polynuclear aromatics but they were present in very small amounts relative to the simpler aromatics.

Samples of liquid condensing in the knockout tank downstream from the sour gas compressor were collected and analyzed by GC/MS. This condensate contains most of the heavier hydrocarbons fed to the AGRS. Results of these analyses are presented in Table 4, and show that the compounds identified are very similar to those found in the stripped methanol. Again, mostly simple aromatics were found. No polynuclear aromatics were present, which supports the findings of the earlier analyses.

Results from these analyses indicate that very little, if any, polynuclear aromatic compounds were present in the gas fed to the AGRS. This is a particularly important finding. Analyses of the water used to quench the gasifier product gas stream showed that a substantial amount of polynuclear aromatics were present. Evidently, scrubbing of the raw product gas with water effectively removes these compounds.

Although polynuclear aromatics are removed by the quenching process, substantial amounts of simpler aromatics will be present in the sour gas fed to the AGRS. The use of cold traps may remove some of these compounds but provision must be made to prevent their release to the atmosphere through vent streams or through the sulfur recovery unit. The accumulation of these compounds in the methanol further complicates the problem because of the increased likelihood of their distribution to a number of process streams. Achieving efficient solvent regeneration is, therefore, a key step in avoiding environmental problems.

SUMMARY

A cyclone, a cold water quench scrubber, and a refrigerated methanol absorber have been used to clean the make gas from the steam-oxygen gasification of a New Mexico subbituminous coal in a pilot-scale fluidized bed ractor. A model developed for the gasifier provides the capability of predicting the make gas amount and composition as a function of gasifier operating conditions. The methanol functioned effectively for acid gas removal. Removal of CO_2, COS, and H_2S to sufficiently low levels was achieved with proper choice of operating conditions and effective solvent regeneration.

TABLE 3

COMPOUNDS IDENTIFIED IN STRIPPER EXIT METHANOL

1. sat'd hydrocarbon	21. toluene	42. C_3 alkyl benzene
2. CO_2	22. methyl thiophene isomer	43. C_3 alkyl benzene
3. C_4H_8 isomer	23. C_8H_{16} isomer	44. $C_{10}H_{22}$ isomer
4. tetramethylsilane	24. C_8H_{16} isomer	45. $C_{10}H_{22}$ isomer
5. trichlorofluro-methane	25. C_8H_{16} isomer	46. C_4 alkyl benzene
6. C_5H_{10} isomer	26. C_8H_{16} isomer (trace)	47. $C_{10}H_{22}$ isomer
7. unknown	27. C_8H_{14} isomer (trace)	48. $C_{10}H_{20}$ isomer
8. Freon 113	28. hexamethyl cyclotrisiloxane	49. unknown hydrocarbon
9. cyclopentadiene	29. C_9H_{20} isomer	50. C_9H_{10}
10. C_6H_{12} isomer	30. C_9H_{18} isomer	51. C_9H_8 isomer
11. C_6H_{14} isomer	31. ethyl benzene	52. alkyl benzene isomer
12. C_6H_{10} isomer	32. xylene (M,P)	53. $C_{11}H_{24}$ isomer
13. benzene	33. styrene	54. $C_8H_{10}O$ isomer
14. C_7H_{14} isomer	34. xylene (O)	55. $C_{11}H_{24}$ isomer
15. C_7H_{16} isomer	35. C_9H_{18} isomer	56. $C_8H_{10}O$ isomer
16. C_7H_{16} isomer	36. C_9H_{20} isomer	57. unknown siloxane
17. C_7H_{12} isomer	37. C_3 alkyl benzene	58. unknown siloxane
18. C_7H_{12} isomer	38. $C_{10}H_{22}$ isomer	59. unknown siloxane
19. C_7H_{12} isomer	39. unknown hydrocarbon	60. $C_{14}H_{30}$ isomer
20. unknown hydrocarbon	40. unknown hydrocarbon	61. $C_{14}H_{30}$ isomer
	41. $C_{11}H_{24}$ isomer	62. unknown
		63. $C_{15}H_{32}$ isomer

TABLE 4

COMPOUNDS IDENTIFIED IN COMPRESSOR KNOCKOUT SAMPLE

1. 1-pentene	10. substituted benzene
2. hydrocarbon	11. C_8 hydrocarbon
3. benzene	12. C_9 hydrocarbon
4. hydrocarbon	13. propyl or ethyl methyl substituted benzene
5. Toluene	14. propyl or ethyl methyl substituted benzene
6. cyclo C4-C5	15. 1-decene
7. hydrocarbon	16. 2-propyl benzene
8. ethyl benzene	17. 1-ethyl-4-methyl benzene
9. dimethyl benzene	

The presence of several trace sulfur compounds--mercaptans, thiophenes, organic sulfides, and CS_2--complicates the gas cleaning process because these compounds were found to distribute among all exit streams from the AGRS. Since no provision is made to specifically treat these forms of sulfur, the possibility of their emission into the atmosphere exists and must be dealt with to avoid significant environmental problems.

A wide variety of aliphatic and aromatic hydrocarbons are present in the gas stream fed to the AGRS. The aliphatic hydrocarbons, ranging from methane to butane, cover a wide range of solubilities. Their presence in all AGRS streams must be anticipated to prevent their emission to the atmosphere.

While a wide range of simple aromatics were identified in the gas stream fed to the AGRS, essentially no polynuclear aromatic compounds were found. Apparently, the water quenching process effectively removes these compounds from the gasifier product gas. However, significant quantities of simple aromatics were found to accumulate in the recirculating methanol, indicating a potential for their eventual discharge to the atmosphere. Provision must be made to periodically purge the solvent of these compounds and/or remove them prior to the AGRS through cold traps.

REFERENCES

1. Ferrell, J. K., R. M. Felder, R. W. Rousseau, J. C. McCue, R. M. Kelly, and W. E. Willis, "Coal Gasification/Gas Cleanup Test Facility: Vol I. Description and Operation", EPA-600/7-80-046a, (1980).

2. Felder, R. M., R. M. Kelly, J. K. Ferrell, and R. W. Rousseau, "How Clean Gas is Made from Coal", Env. Science and Tech., Vol 14, 658, (1980).

3. Ferrell, J. K., , R. M. Felder, R. W. Rousseau, S. Ganesan, R. M. Kelly, J. C. McCue, and M. J. Purdy, "Coal Gasification/Gas Cleanup Test Facility: Vol II. Environmental Assesment of Operation with Devolatilized Bituminous Coal and Chilled Methanol", EPA, (1981).

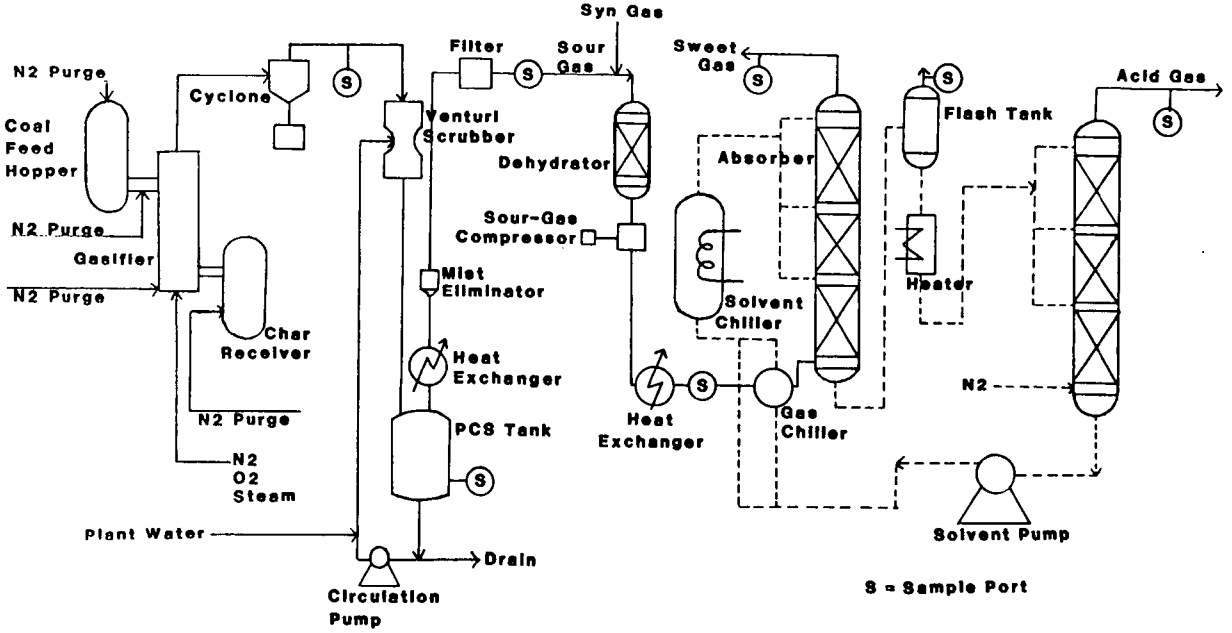

Figure 1

Pilot Plant Facility

Figure 2

Predicted vs. Experimental Carbon Conversion,
Gasification of New Mexico Coal

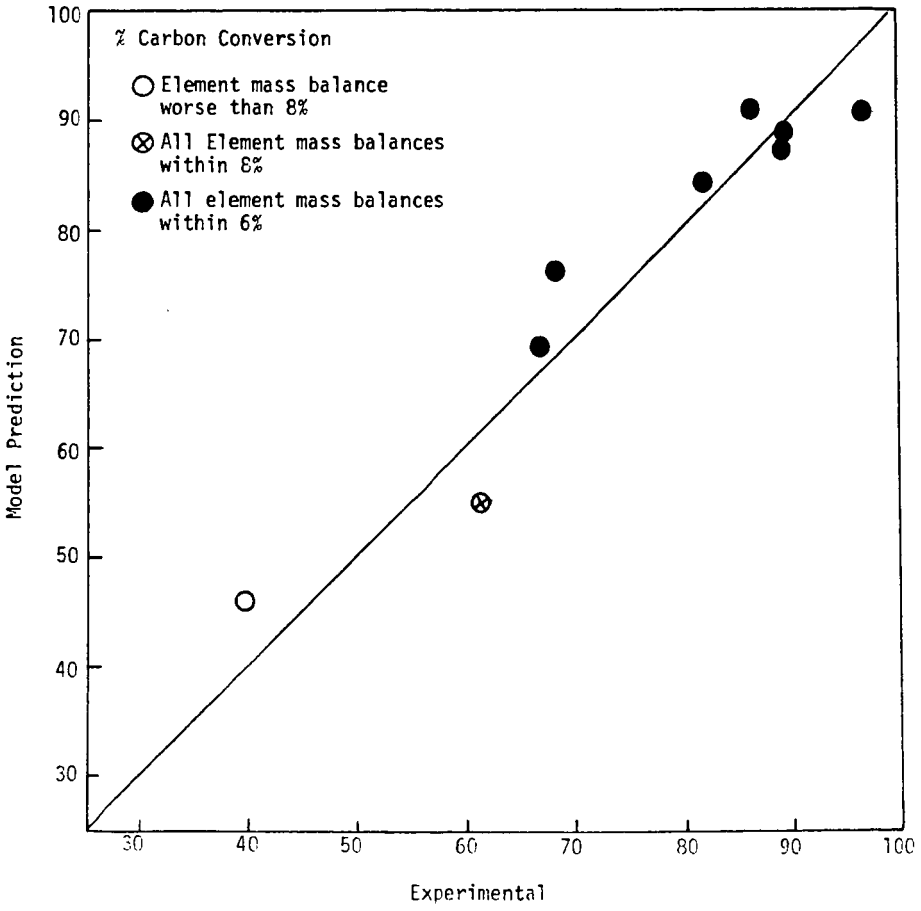

DIRECT METHANATION - A NEW METHOD OF CONVERTING SYNTHESIS GAS TO SUBSTITUTE NATURAL GAS

Howard S. Meyer, Vernon L. Hill, Ab Flowers

Gas Research Institute
8600 West Bryn Mawr Avenue
Chicago, Illinois 60631

John Happel, Miguel A. Hnatow

Catalysis Research Corporation
450 E. Edsall Boulevard
Palisades Park, NJ 07650

I. INTRODUCTION

The United States has vast resources of energy in the form of coal. One method of distributing this energy source to the consumer is to gasify the coal and distribute the gas through the existing natural gas pipeline distribution system. However, raw synthesis gas from a coal gasifier is not of sufficient purity and does not provide heating value suitable for use directly as substitute natural gas (SNG). The synthesis gas produced by a coal gasifier requires extensive purification and upgrading before it can be interchanged with natural gas. The current raw gas conversion systems were not specifically designed with the production of pipeline quality gas from coal in mind. Potentially, significant cost reductions could result from the development of an improved, integrated processing system.

As part of the strategic objective of improving reliability, operability, or reducing gas costs of coal gasification processes, the Gas Research Institute (GRI) is developing a new process for converting synthesis gas to SNG. The key to this process is the development of a sulfur-resistant, direct methanation catalyst. Preliminary cost estimates show that the direct methanation process could decrease capital costs by over 20% and operating costs by 10%, resulting in gas costs savings of about 15% over state-of-the-art methanation and combined shift-methanation processes.

II. METHANATION PROCESSES

A conventional gas processing system, as shown in Figure 1A, includes gas quench, water-gas shift, gas cooling, acid gas removal, methanation, dehydration, and compression. These clean-up processes produce separate streams that require further purification so that by-products, such as sulfur, phenols, ammonia, BTX, and tars, can be isolated for sale whenever possible. The gas quench utilizes oil and/or water to cool the raw gas and to remove particulates, tars, and oils, and other condensible components.

Water-gas shift (Equation 1) is required to adjust the H_2/CO ratio to over 3

$$CO + H_2O \rightleftharpoons H_2 + CO_2 \qquad 1)$$

as needed for methanation. Added steam reacts with the carbon monoxide to produce the required hydrogen. The use of new sulfur-insensitive shift catalysts show an economic advantage by allowing the shift process to be upstream of the gas cooling and acid gas removal systems. The acid gas removal system removes water, carbon dioxide, and sulfur-containing compounds. The current methanation process uses nickel-based catalysts for

converting (methanating) carbon monoxide and hydrogen to methane (Equation 2). After methanation, dehydration is required to remove the water formed during methanation; after which the gas is compressed to pipeline standards.

$$3H_2 + CO \rightleftharpoons CH_4 + H_2O \qquad 2)$$

Nickel catalysts have demonstrated their effectiveness for converting synthesis gas to methane. However, there are very strict process restrictions for successful use of nickel catalysts. Satisfying these restrictions can require process steps that are costly. A major restriction of nickel catalysts arises from their extreme sensitivity to poisoning by sulfur compounds that are always present in coal-derived synthesis gas. Although "sweet" pipeline gas can contain 4 ppm hydrogen sulfide (0.25 grains/100 scf), gas processed by nickel catalysts must be purified to 0.1 ppm sulfur to avoid irreversible poisoning of the catalyst. The nickel catalyst can also be irreversibly poisoned by carbon fouling, unless the hydrogen/carbon monoxide ratio of the input gas is maintained above 2.85 and/or excess steam is added. Nickel catalysts are also deactivated at high temperatures (above 950°F), such as those that can occur during the exothermic methantion reaction. Nickel catalysts cannot be exposed to oxygen after activation. They require special handling and pretreatment procedures to maintain reactivity.

Improvements to the conventional methanation process are those embodying combined shift-methanation, such as those developed by Conoco, R. M. Parsons, United Catalyst, ICI, and UOP. These processes utilize the water formed in methanation for water-gas shift. (Equations 1 and 2 simultaneously.) A combined shift-methanation process is shown in Figure 1B. Since nickel-based catalysts are used, removal of sulfur is required prior to shift-methanation. All the combined shift-methanation processes require steam addition for stoichiometry, temperature moderation, and/or to prevent carbon formation. An additional acid gas removal system is required downstream of the shift-methanation process to remove the high concentration of CO_2.

The direct methanation process being developed for GRI shows significant improvements over the conventional methanation and combined shift-methanation processes. The direct methanation process, shown in Figure 1C, methanates the raw gas directly using equal molar concentrations of carbon monoxide and hydrogen to form carbon dioxide and water. The chemistry of the process is such that steam is not needed either to suppress carbon formation or to drive the water-gas shift reaction. Although the overall reaction for combined shift-methanation is the same as for direct methanation (Equation 3), the mech-

$$2CO + 2H_2 \rightleftharpoons CH_4 + CO_2 \qquad 3)$$

anism appears different in that CO_2 is produced directly rather than by the water-gas shift, thus eliminating the high steam requirement. The process shows potential savings in steam usage and acid gas removal. Other process advantages are expanded upon in the remainder of the paper.

III. DIRECT METHANATION CATALYST DEVELOPMENT

Catalysis Research Corporation (CRC), located in Palisades Park, New Jersey, is responsible for iteratively developing novel catalyst formulations, performing scoping tests to evaluate the effectiveness of the formulations, and proposing process sequences that best utilize the advantages of the most promising catalysts. During the last six years, CRC has tested over 600 new catalyst formulations resulting in several compositions that have promise for application both in a conventional methanation process and in a new direct methanation process.

The catalyst development program for a sulfur-resistant methanation catalyst, from 1974-1978, lead to two patented catalyst formulations. In 1977, Patent 4,151,191 was issued to CRC for a cerium-molybdenum catalyst, designated as GRI Series 200 (GRI-C-284). In 1981, Patent 4,260,553 was issued to CRC for a cerium-molybdenum-aluminium catalyst, designated as GRI Series 300 (GRI-C-318). Both patents were assigned to GRI. These catalysts satisfied the original project objective of developing a sulfur-resistant methanation catalyst; however, they also lead to a new area of study.

In 1979, a second breakthrough was made in the CRC catalyst formulation work. A new family of catalysts, the GRI Series 400 and 500 catalysts, were developed that promote the direct methanation reaction (Equation 3) rather than the water-gas shift reaction (Equation 1). These catalysts provide the key to the new direct methanation process. The overall project objective was changed to reflect this breakthrough, and subsequential work concentrated on developing a direct methanation process.

The present series of catalysts are the most active catalysts yet developed. These catalysts show sufficiently high conversion and selectivity such that they can be used in a direct methanation process that involves no gas recycling and uses only a single acid gas removal system. They can operate with feed gases containing high levels of sulfur compounds and CO_2. Carbon formation has not been observed, even with H_2/CO ratios as low as 0.1 and with no steam addition, and the catalysts have high maximum operating temperatures. The catalyst are very easy to handle; they can be exposed to air at room temperature with no loss of activity, and therefore, they require little or no pretreatment.

IV. DIRECT METHANATION CATALYST CHARACTERIZATION

SRI International, located in Menlo Park, California, is responsible for characterizing the promising catalysts developed by CRC. The studies are intended to define the bulk and surface properties that affect the specific methanation activity, thermal stability, and deactivation resistance of these catalysts as an aid in further development and improvement. SRI has been involved with the Direct Methanation Project since 1977, but also has developed catalysts under contracts to the American Gas Association (A.G.A.) since 1972.

The direct methanation process requires a catalyst that selectively promotes the direct methanation reaction (Equation 3). Catalyst selectivity and activity can be strongly dependent upon both the composition and morphology of the catalyst. Development of basic methods to relate microcompositional and morphological properties of the catalyst to selectivity and activity is vitally important in the development of improved catalysts and gas processes for coal conversion plants. Work being performed by SRI is intended to refine measurement techniques suitable for understanding the observed behavior of the direct methanation catalysts.

In order to evaluate catalyst structure, SRI had to develop or improve new experimental techniques utilizing (1) x-ray photoelectron spectroscopy (XPS or ESCA), (2) scanning electron microscopy (SEM), and (3) BET surface area measurements to provide information on structural changes of catalysts. Dispersion and sintering stability studies have been performed using x-ray diffraction (XRD), SEM, and ESCA to define changes in the properties that control methanation activity. Solid state properties of the catalysts have been determined by a variety of surface science techniques.

Because of its nature, most of the work performed by SRI is proprietary; a general discussion of some aspects of the work follows. First, tests were

performed to study structural changes of the catalyst during methanation. This resulted in the discovery of a critical formulation variable that controls the specific methanation activity. Later, discovery of a correlation between methanation activity and surface acidity, as measured by quantitative absorption of a weak base (ammonia), simplified catalyst evaluation. Finally, a preliminary explanation of the mechanism by which the GRI Series 400 and 500 catalysts operate was developed.

V. DIRECT CATALYST METHANATION EVALUATION

The Institute of Gas Technology (IGT), located in Chicago, Illinois, is responsible for evaluating the promising catalyst formulations prepared by CRC using feed gases that simulate gasifier effuents and developing the process design data for promising catalysts in various processing sequences. The studies are intended to test the catalysts for longer times and at more severe and realistic conditions than the scoping tests performed by CRC. IGT has been involved with the Direct Methanation Project since 1978, but also has evaluated catalyst under contracts to A.G.A. since 1972.

The GRI Series 500 catalysts are the best methanation catalysts tested to date. They are capable of promoting the methanation reaction at temperatures from 600° to 1200°F, at all pressures from 200 to 1000 psig, at feed gas H_2/CO mole ratios from 3 down to 0.5, and in the presence of up to 3 mole % sulfur (H_2S, COS, CS_2, CH_3SH, C_2H_5SH, C_3H_7SH, and C_4H_4S). No carbon formation was detected under any of the above mentioned conditions. The presence of CO_2 in the feed retarded the total CO conversion but did not promote any other reactions. Hydrocarbon additions of up to 2 mole % C_6H_6, 0.05 mole % C_6H_5OH, and 0.3 mole % NH_3 did not poison or foul the catalysts. Life tests were conducted on the GRI Series 200 catalysts for more than 5000 hours, and ongoing life tests of the GRI Series 500 catalysts have extended for more than 2500 hours.

The promising catalysts were also tested in various processing sequences to provide process design data. IGT tested the effects of space velocity, temperature, pressure, and feed composition on the conversion of CO and H_2 to CH_4 and CO_2 by the direct methanation process. The feed gas simulated a gasifier effluent. The product composition of each reactor was used as the feed composition for each successive reactor stage, and runs at identical temperature and pressure were conducted. This approach generated information on the process variables at each reactor stage, provided input for process design, and served as a guideline for catalyst improvement.

Quench gases simulating those from the dry-bottom Lurgi, Slagging Lurgi, Westinghouse and HYGAS processes were tested. For cases where the H_2/CO ratio is less than 1, as in the Slagging Lurgi case at H_2/CO = 0.4, a preconditioning shift was required to increase the H_2/CO ratio to 1.1 to 1.3. The process steam requirements are therefore much lower than required for shifting the gas to 3 as needed for nickel methanation catalysts. The shift was performed with a CRC developed, GRI Series 300 catalyst and required only 16% steam in the feed gas to the methanation step, as shown in Figure 2. Typical data for a Slagging Lurgi flowsheet are shown in Figure 3 for the first reactor stage.

VI. DIRECT PROCESS METHANATION EVALUATION

C F Braun & Company, located in Alhambra, California, is the engineering/ construction firm responsible for developing conceptual processes from the design data collected by IGT and from the process sequences recommended by CRC. First-cut economic evaluations are then performed based on the conceptual process design. The conceptual process design work includes

preparing process flow diagrams and sizing equipment. Capital cost and operating requirements estimates are used in the economic evaluation to determine gas costs.

A preliminary economic evaluation was conducted in 1979, based on the use of a GRI Series 300 catalyst. The results indicated the concept would not be competitive because the design required CO_2 removal prior to methanation. However, CO_2 removal is not required with the use of the GRI Series 400 and 500 catalysts, because these catalysts have good activity in streams with a high CO_2 content.

A first-cut analysis of the direct methanation process for a Slagging Lurgi gasifier raw gas was just completed. The analysis compared a 250 billion Btu/day Slagging Lurgi gasification plant with a combined shift-methanation process to a plant designed around the direct methanation process. The design of the gasifier was not changed, but the overall downstream process, utilizing commercially available subsystems, was redesigned to best exploit the direct methanation process advantages. A simplified flowsheet, based on a GRI Series 500 catalyst, is shown in Figure 4.

The preliminary results show the direct methanation process could reduce capital costs over 20%, operating cost by 10%, and reduce the gas cost by about 15%. The savings are realized in reduced steam requirements and more efficient sulfur management processes specifically for this application. Further savings were anticipated when new subsystems are developed specifically for use with direct methanation.

VII. CONCLUSIONS

The current GRI project to develop a direct methanation process is making excellent technical progress. Direct methanation processes utilizing the CRC catalysts could potentially realize the following advantages over existing technology:

- Reduced plant investment, operating costs, and gas costs
- Effective hydrogen utilization
- One acid gas removal step
- Smaller acid gas removal feed stream
- Higher energy efficiency
- Sulfur tolerance
- Carbon fouling tolerance
- Lower process steam requirements
- Decreased heat exchange area

If the development continues to be successful, the direct methanation process will be pursued through the pilot plant scale to provide the technology base required for commercial application.

ACKNOWLEDGEMENT

The authors wish to acknowledge the contributions made by Dr. Henry Wise at SRI International, Mr. Anthony L. Lee at IGT, Dr. Roger Detman at C F Braun & Co. and their staffs for their contributions to the overall progress of this project.

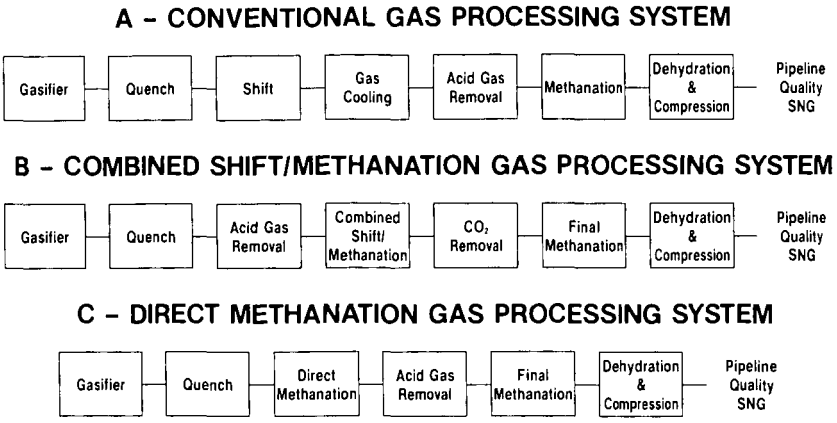

FIGURE 1. METHANATION PROCESSES

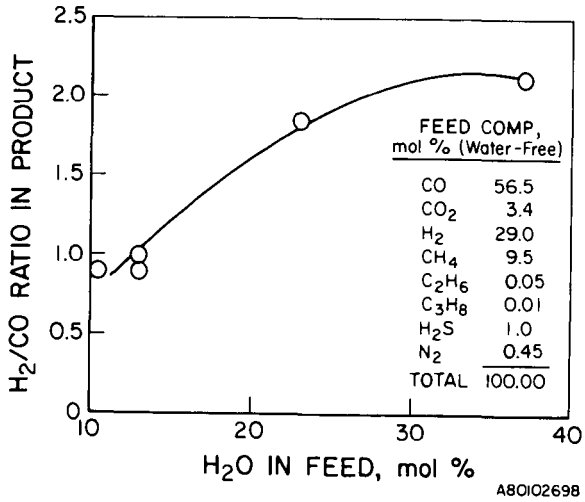

FIGURE 2. PRECONDITIONING SLAGGING LURGI RAW GASES (1000 psig, 580°F, 4500 SCF/hr-ft^3 GRI-C-318 Catalyst)

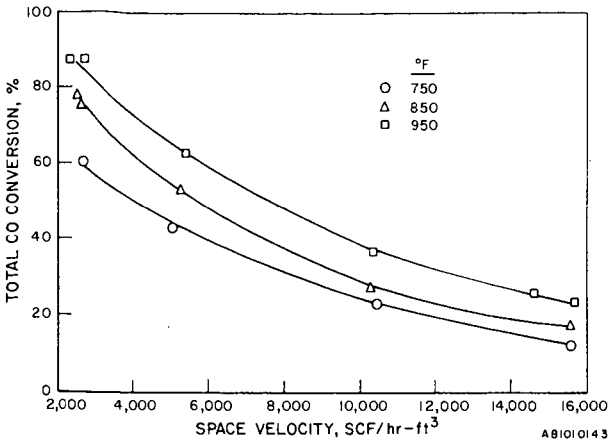

FEED COMPOSITION, mol %

CO	34.27
CO_2	14.43
H_2	37.02
CH_4	10.60
C_2H_6	0.34
C_3H_8	0.11
C_4H_{10}	0.05
H_2S	0.98
COS	0.02
N_2	0.33
H_2O	1.85
TOTAL	100.00

FIGURE 3. CO CONVERSION IN THE FIRST DIRECT METHANATION STAGE FOR SLAGGING LURGI RAW GASES (450 psig, GRI-C-525 Catalyst)

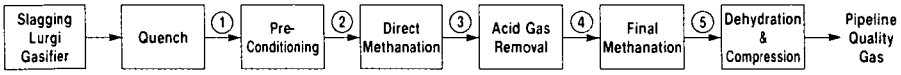

Gas Analysis, Vol %
(H_2O and N_2 Free Basis)

Stream / Component	1	2	3	4	5
CO	58.9	37.6	1.7	4.1	0.1
CO_2	6.5	19.1	56.1	0.7	0.8
H_2	25.9	35.8	6.7	16.1	4.7
CH_4	6.1	5.3	32.3	77.6	92.7
C_2^+	0.5	0.4	0.6	1.5	1.7
H_2S	2.1	1.8	2.6	0	0

FIGURE 4. CONCEPTUAL FLOWSHEET FOR DIRECT METHANATION OF SLAGGING LURGI RAW GASES

VARIATIONS IN THE INORGANIC CHEMISTRY OF COAL

W.S. Fyfe, B.I. Kronberg, Department of Geology, The University of Western Ontario, London, Canada

J. R. Brown, Energy Research Laboratories, Department of Energy, Mines and Resources, Ottawa, Canada

INTRODUCTION

The composition of coal reflects its complex physical and chemical history. Throughout coal genesis, from accumulation of plant debris and during subsequent coalification, solute species in ground waters are constantly exchanged with the porous and reducing carbonaceous debris. From existing geochemical data (e.g., Wedepohl, 1969; Kronberg et al., 1981), it appears that coal and coal-related materials (peat, lignite, etc.) may incorporate and accumulate a complex array of elements. To some extent coal deposits acts as gigantic carbon filters through which ground waters wash the products of rock leaching. Very little is known concerning the exact siting of trace elements in coal and these elements at times attain ore grade (e.g., U, Mo).

The modern large-scale (10^{15} g a^{-1}) burning of coal may have ramifications not only for the global carbon cycle but contingent on their fates during combustion, also for the global cycle of other elements concentrated in coal. For example the deposition over the past five decades of charcoal as well as several metals (Cr, Fe, Co, Ni, Cu, Zn, Cd, Sn and Pb) in Lake Michigan sediments correlates with variations (oil, coal, wood, installation of control devices) in fuel use (Goldberg et al., 1981). Associated with coal combustion is the accumulation of easily leachable ash. Other recent work (Chapelle, 1980) shows that some metals (Cr, Ni, Zn, Cd, Pb) sorbed onto surfaces of Fe-Al-O phases in ash are easily leached by percolating waters.

Here discussion is confined to the coal chemistry of the transition metals, some of which are known to play catalytic roles in coal combustion and to the coal chemistry of the halogens. The presence of F and Cl at the per cent levels in some coals is significant for combustion technologies (concerned with corrosion problems, etc.) and for problems related to atmospheric emissions.

EXPERIMENTAL

The analytical data reported here pertain to samples of raw coal, ash from coal, lignite and tar sand, as well as NBS standard reference coals and coal ash. The non-reference coals are bituminous coals from Western Canadian mines, hosted in Cretaceous formations. The lignites are from North Dakota and Ontario, and the tar sand from Fort McMurray, Alberta. The British Columbia coals (samples 2-6, Table 1) are from different seams in the same mine, as are the Alberta coals (samples 7-9). The sample numbers correspond to those appearing in more detailed analytical reports (Kronberg et al., 1981; Brown et al., 1981a, b). The analytical techniques employed in all these studies are spark source mass spectroscopy (SSMS) and electron spectroscopy for chemical analysis (ESCA).

SSMS is useful for surveying the concentrations of 60-70 elements in a single analysis. However, it is necessary to pre-ash or otherwise pre-treat samples containing substantial material of low mass number, which easily forms polyatomic positive ions. Coal, due to its high carbon content exemplifies this difficulty, and an unmanageable number of interferences appear in the mass spectral record of raw coal. In this study the samples of coals, lignites and tar sand were dry ashed for 4-6 hours at 600°C in a muffle furnace. Sample electrodes, prepared by mixing the ash with pure graphite (Taylor, 1965), were sparked in a JEOL mass spectrometer

(JMS-01BM-2). The mass spectra were recorded photographically and interpreted semi-quantitatively using USGS standards (Flanagan, 1973). With regard to the analysis of coals and other geological materials (soils, Mn nodules, rocks, volcanic ash, deep-sea sediments, etc.) the analytical uncertainty is within the variation encountered using normal sampling techniques.

ESCA is a spectroscopic surface sensitive technique by which the concentrations of all elements (except H) can be surveyed semi-quantitatively to a surface depth of 1-5 nm. Detection limits are $\simeq 10^{-9}$ g cm^{-2} of surface ($\simeq$0.1 bulk wt. %). Thus for geological materials, semi-quantitative information can be obtained for major elements and for surface concentrated minor and trace elements (Brown, 1978; Bancroft et al., 1979). There are several advantages of ESCA for coal analysis: (1) ESCA is non-destructive. (2) It is often possible to gather details on the in situ chemistry of elements (oxidation state, coordination number, etc.). (3) Both raw coal and coal ash may be analysed. Ashing effectively concentrates the mineral fraction in coal by an order of magnitude, permitting concentration measurement of additional elements. Surface concentration of elements (e.g., F, S) during combustion by surface sorption reactions may be monitored. (4) ESCA multi-element scans may be done quickly ($\sim$ 1 hour) and may be useful in fingerprinting coals.

ESCA spectra were recorded using a McPherson 26 spetrometer equipped with an aluminum anode operating at 200 watts. Details of the ESCA procedures used for this study are available elsewhere (Brown et al., 1981a, b).

RESULTS AND DISCUSSION

The concentrations, obtained by SSMS (Table 1), of transition metals and halogens for some North American coals and coal-related materials are compared (Table 2) to data available for coal from various sources and to crustal abundances. The chaotic concentration patterns for many elements are a reflection of the complexity of chemical and physical processes associated with coal formation. The extreme variation is possibly related to local ground water chemistry and to the local permeability of coal and enclosing strata. With respect to crustal abundances (CA), both the transition metal and halogen concentrations, range from strongly depleted (less than 10-fold CA) to strongly enriched (greater than 10-fold CA). The data from other sources include those from coal deposits on other continents, and the wide concentration ranges may be an expression of the type of Earth processes leading to coal deposition and formation.

Of the transition metals (Table 1) Sc, Y and Zr appear the least mobile. The variations in Nb concentrations are intriguing and Nb may be more mobile or may be hosted in phases distributed more unevenly. The variation in Ti concentrations is noteworthy, and chemical migration of Ti in association with coal diagenesis has been noted (Degens, 1958). Moreover, there is evidence for the chemical coupling of Ti (and Zr) compounds to enzymes and other biologically active macromolecules (Kennedy, 1979). Further, Taylor et al. (1981) have shown that Mg, Ca, Ti, Fe, Cu, Zn species in coal may be extracted by organic solvents.

Our knowledge of the sources of halogens and their mode of concentration in coal is vague. River and ground waters flowing into coal basins would contribute substantial amounts of Cl. It could be introduced by rain and aerosols either directly or transferred via the biosphere. The sources of Br and F are less certain. F could be added during deposition by the influx of fine-grained detrital minerals or volcanic ash. For example, fluorite (CaF_2) is observed in the ESCA scan of coal No. 8 (Table 3).

In the ESCA scans of raw coals (Table 3), the largest peaks correspond to the detection signals for carbon (C 1s) and oxygen (O 1s). Other elements detected included Al, Si, Ca, sometimes S, and in some samples substantial F and Cl. Large

variations, indicated by the number of counts per second during ESCA analysis, are attributed to chemical variations in coal surfaces. The differences in carbon peak positions were of interest especially in sample no. 8, for which the C 1s peak position is indicative of graphitic carbon and this scan also contains the largest F 1s signal.

Recently, an examination of raw coal macerals by XPS indicates that fisinite displays characteristics (C 1s binding energy 284.4 eV) essentially identical to pure graphite. It was also observed that the vitrinite fraction of a western Canadian coal sample was greatly enriched (> 1 wt. percentage) in an organically found fluorine species, $^{a}(CF_2)_n$ type.

In the ESCA scans of ashed coals (Table 4) many more elements (Na, Mg, Ti and Fe) appeared and the F 1s and S 2s peaks are enhanced. S appearing both as SO_4^{2-} and S^{2-} is likely associated with Fe as iron sulphide (pyrite), the outer shell oxidized to sulphate by combustion. The concentrations of Al, Ca, Ti and Fe in NBS reference ash (1633a) measured by ESCA (using the Si 2s peak as a reference) agree well with recommended values. In the ash, F and S surface concentrations are much greater than those observed in the bulk samples, and this could be evidence for preferential siting of these elements on ash surfaces. Cl was not detected on the ash surfaces by ESCA, in contrast to the high signals noted on raw coal surfaces, and Cl may be removed in the volatile phase during combustion.

CONCLUSION

The combined use of SSMS and ESCA results was successful in part in overcoming the unique analytical difficulties presented by the heterogeneous chemical and physical distribution of intimately combined inorganic and organic species in coal. These techniques and modifications of them are applicable to the study of the combustion chemistry of coal as well as to the assessment of the environmental impact of coal utilization.

REFERENCES

Babu, S.P. (Ed.) 1975. Trace elements in fuels. Adv. Chem. Ser. 141. Am. Chem. Soc., Washington, D.C. 214 pp.

Bancroft, G.M., Brown, J.R., and Fyfe, W.S. 1979. Advances in, and applications of, x-ray photoelectron spectroscopy (ESCA) in mineralogy and geochemistry. Chem. Geol. 25, 227-243.

Brown, J.R. 1979. Adsorption of metal ions by calcite and iron sulphides: A quantitative XPS study. Ph.D. thesis, University of Western Ontario, London, Ontario, 220 pp.

Brown, J.R., Kronberg, B.I., and Fyfe, W.S. 1981,a. Semi-quantitative ESCA examination of coal ash surfaces. FUEL 60: 439-446.

Brown, J.R., Kronberg, B.I., and Fyfe, W.S. 1981,b. An ESCA examination of coal and coal ash surfaces, In: Proceedings "Coal: Phoenix of the '80's" (ed. A.M. Al Taweel), 64th Canadian Chemical Conference, Halifax, N.S.

Chapelle, F.H. 1980. A proposed model for predicting trace metal composition of fly-ash leachates. Environ. Geol. 3(3): 117-122.

Degens, E.T. 1958. Geochemische Untersuchungen zur Faziesbestimmung im Ruhrkarbon und im Saarkarbon. Glückauf, Jg. 94, Essen.

Fairbridge, R.W. (ed.) 1972, Encyclopedia of geochemistry and environmental earth sciences series, Vol. IVA, Van Nostrand Reinhold, New York, 1321 pp.

Flanagan, F.J. 1973. 1972 values for international geochemical reference samples. Geochim. Cosmochim Acta 37: 1189-1200.

Goldberg, E.D., Hodge, V.F., Griffin, J.J., Koide, M. and Edgington, D.N. 1981. Impact of fossil fuel combustion on the sediments of Lake Michigan. Envir. Sci. & Tech. 15 (4): 466-471.

Goldschmidt, V.M. 1954. Geochemistry, Claredon press, Oxford 730 pp.

Kennedy, J.F., 1979. Transition-metal oxide chelates of carbohydrate-directed macromolecules. Chem. Soc. Rev. 8 (2) 221-257.

Kronberg, B.I., Brown, J.R., Fyfe, W.S., Peirce, M. and Winder, C.G. 1981. Distribtuions of trace elements in western Canadian coal ashes. FUEL 6D: 59-63.

Taylor, S.R. 1965. Geochemical analysis by spark sourc-mass spectrography. Geochim. Cosmochim. Acta 29: 1234-1261.

Taylor, L.T., Hausler, D.W. and Squires, A.M. 1981. Organically bound metals in a solvent-refined coal: metallograms for a Wyoming subbituminous coal. Science, 213, 644-646.

Wedepohl, K.H. 1969. Handbook of Geochemistry. Springer-verlag, Berlin.

TABLE 1 - CONCENTRATIONS ($\mu g\ g^{-1}$) OF SOME ELEMENTS IN ASH FROM COAL, LIGNITE AND TAR SAND (SSMS DATA)

Sample Element	Yukon coal	British Columbia coals					Alberta coals			North Dakota lignite	Athabasca Tar Sand	Ontario lignite coal ash	NBS Reference Materials		
	1	2	3	4	5	6	7	8	9	10	11	12	1633a	1632a coals	1635
F	50	>500	>500	150	>500	>500	500	500	30	>500	>500	500	>500	500	>500
Cl	5	5	5	2	5	15	>50	50	10	1	50	50	50	>50	50
Sc	30	100	100	100	30	30	30	30	3	15	10	30	100(40)[a]	30	10
Ti	1,000				1,000			300		3,000			8000		
V	15	40	150	150	15	40	40	40	10	1,250	13	130	400(300)	130	40
Cr	15	15	15	5	5	15	15	5	0.3	15	18	3	18(196)	18	6
Mn															
Fe	100,000				10,000			1000		200,000			94,000	11,000[b]	2200[b]
Co	40	13	13	13	130	40	40	13	3	130	1	10	12(46)	12	360
Ni	150	15	15	15	450	150	150	50	5	60	1	15	5(127)	5	5
Cu	180	60	180	60	180	180	60	60	60	180	2	20	50(118)	18	18
Zn	40	400	40	12	120	40	40	120	3	85	4	4	35(220)	35	12
Br	0.5	0.5	0.5	0.2	0.2	0.5	0.5	0.5	0.2	0.2	0.05	1	0.2	0.2	0.2
Y	40	40	40	40	120	120	120	120	5	60	1	35	35	35	35
Zr	200	200	200	200	200	200	200	200	60	200	5	20	60	60	200
Nb	4	40	13	40	40	40	40	13	2	13	1	5	13	13	13
Mo	3	3	3	3	30	30	3	3	5	200	1	4	10(30)	4	1
I	1	0.3	1	<0.3	1	0.3	<0.3	3	30	1	1	1	1	<0.3	0.3

a NBS reference values

b raw coal analysis

TABLE 2

ELEMENT	RANGE[a]	DATA FROM VARIOUS SOURCES[b,c,d,e]		CRUSTAL ABUNDANCE[f]
		coal	ash	
F	30->500	71-175		544
Cl	1->50	6-1000	186-3,000	126
Sc	3-100	3	10-1,000	25
Ti	300-8000	180-960	~30,000	10,500
V	10-1250	4-50	0.2-24,600	136
Cr	0.3-15	< 2-27	116-800	122
Mn		70-130	250-280	
Fe				
Co	3-130	3-25	10-39	29
Ni	5-450	4-100	5-80,000	99
Cu	60-180	3-180	15->500	68
Zn	3-400	20-200	160-10,000	76
Br	0.2-0.5	0.1-23	7-12	2.5
Y	5-120	3-25	100	31
Zr	60-200	10-300	115-5000	162
Nb	2-40	5-41		20
Mo	3-200	trace-3000	8-500	1.2
I	<0.3-30		142-587	0.46

[a]this study [b]Babu, 1975 [c]Goldscmidt, 1954 [d]Wedepohl, 1969 [e]Yudovich et al., 1972

[f]Fairbridge, 1972.

TABLE 3 - ESCA Chemical Analysis of Raw Coal Surfaces

Element (wt %) 15%	Raw Coal Samples[a]													
	N8S Standards				North American Coals									
	1632a		1635		1		5		8		10		12	
	ESCA	bulk[b]	ESCA	bulk[b]	ESCA	bulk[c]	ESCA	bulk[c]	ESCA	bulk[c]	ESCA	bulk[c]	ESCA	bulk[c]
Si	7.7	5.8	1.3	0.52	10.5	6.0	1.0	1.0	2.7	1.0	N.D.	2.0	4.1	N.A.
Al	5.20	3.1	0.8	0.30	10.6	2.0	2.5	2.0	7.4	1.0	1.2	2.0	3.4	N.A.
Fe	N.D.[d]	1.1	N.D.	0.22	N.D.	2.0	0.4	0.1	N.D.	0.50	0.9	1.0	1.D	N.A.
Ca	N.D.	0.24	1.5	0.54	N.D.	5.0	1.7	2.0	2.4	0.30	N.D.	0.5	1.7	N.A.
Ti	N.D.	0.15	N.D.	0.02	N.D.	0.1	N.D.	0.5	N.D.	0.1	0.9	0.3	N.D.	N.A.
S	N.D.	1.59	0.8	0.32	N.D.	2.0	N.D.	3.0	N.D.	2.0	3.1	3.0	N.D.	N.A.
F	1.25	N.A.[e]	1.4	N.A.	N.D.	N.A.	1.9	N.A.	3.8	N.A.	N.D.	N.A.	N.D.	N.A.
Cl	N.D.	0.08	N.D.	0.003	0.8	N.A.	1.1	N.A.	0.9	N.A.	1.5	N.A.	2.2	N.A.
N	1.2	1.27	1.5	1.0	0.3	N.A.	2.0	N.A.	1.4	N.A.	N.D.	N.A.	62.0	N.A.
C[f]	59.3	{86.7	73.8	{97.1	48.1	{82.9	74.0	{91.4	60.0	{95.1	71.8	{91.2	25.6	N.A.
O[g]	25.3		18.9		29.7		15.3		21.4		20.6			

[a]Surface concentrations are calculated from equation 1 using ESCA peak intensity ratios normalized to Si 2s except Sample No. 10, where Al 2s had to be used. Note the surface compositions have been calculated on a hydrogen free basis as hydrogen cannot be detected by ESCA.

[b]Accepted values from US N8S certificate of analysis (14)and/or reference (15).

[c]Bulk analysis by XRF and/or SSMS (4); note carbon and oxygen (a combined value) are determined by difference; coal 12 not analyzed.

[d]N.D. not detected. [e]N.A. not analyzed.

[f]Carbon content measured by ESCA includes a small sorbed portion (hydrocarbons) derived from the UHV system.

[g]Oxygen content measured includes a small portion of adsorbed oxygen due to handling in air prior to analysis.

TABLE 4 - ESCA Chemical Analysis of Coal Ash Surfaces

Element (wt %) 15%	Ashed Samples[a]											
	NBS Standard		North American Coal Ash									
	1633a		1		5		8		10		12	
	ESCA	bulk[b]	ESCA	bulk[c]	ESCA	bulk[c]	ESCA	bulk[c]	ESCA	bulk[c]	ESCA	bulk[c]
Si	16.9	22.8	10.9	10.0	21.5	25.0	2.8	3.0	5.1	10.0	4.6	5.3
Al	10.0	(14.0)	8.2	7.0	10.0	10.0	6.4	3.0	11.3	9.0	9.5	6.6
Fe	2.7	9.4	1.4	6.1	N.D.	1.0	1.1	0.1	4.2	10.0	8.0	5.4
Ca	2.2	1.1	5.8	10.0	0.9	0.5	2.9	0.1	5.1	4.0	9.8	25.7
Ti	1.3	(0.8)	1.5	0.1	2.5	1.0	0.6	0.03	0.6	0.3	N.D.	0.2
S[d]	4.2	[≥0.05]	1.87	N.D.	N.D.	N.D.	1.6 1.6	N.D.	3.74	N.D.	3.9	4.9
F	2.0	[≈0.05]	0.9	0.05	N.D.	N.D.	1.0	0.05	N.D.	0.05	N.D.	N.A.
Ba	N.D.	(0.15)	0.8	0.2	N.D.	0.06	1.5	0.6	N.D.	0.3	N.D.	N.A.
Mg	N.D.	0.50	0.9	5.0	N.D.	0.10	N.D.	N.D.	6.7	10.0	14.5	5.8
Na	N.D.	N.A.	N.D.	N.A.	N.D.	N.A.	N.D.	N.A.	3.2	N.A.	N.D.	0.7
C[e]	14.1	{51.14	40.5	{61.55	31.4	{62.34	66.5	{93.12	34.4	{56.35	28.1	{45.4
O[f]	46.6		27.3		33.7		14.0		25.7		21.7	

[a] Surface concentrations are calculated from equation 1 using XPS peak intensity ratios normalized to Si 2s.

[b] Accepted values from US NBS certificate of analysis (14); values in brackets listed but not certified, values in square brackets determined in concomitant SSMS study (4).

[c] Analysis by XRF and/or SSMS (4).

[d] Sulphur is present as the sulphate species (S^{6+}) except for ashed sample No. 8 where sulphide (S^{2-}) was also detected.

[e] As per Table 1; note some of this carbon is probably carbonaceous surface sited residue deposited during the coal ashing step.

[f] As per Table 1; some of this oxygen will be from oxygen species such as CO, CO_2, etc., associated with the carbonaceous coating (see e).